國 立 交 通 大 學

電信工程學系碩士班

碩士論文

適用於多輸入多輸出無線區域網路之適應性調變編碼及傳送模式選擇之跨層設計

Cross-Layer Design for Adaptive Modulation/Coding and Transmission Mode Selection over MIMO WLANs

研 究 生：楊松根　　Student: Sung-Kang Yang

指導教授：李大嵩 博士　　Advisor: Dr. Ta-Sung Lee

中 華 民 國 九 十 四 年 六 月

適用於多輸入多輸出無線區域網路之適應性調變編碼及傳送模式選擇之跨層設計

Cross-Layer Design for Adaptive Modulation/Coding and Transmission Mode Selection over MIMO WLANs

研 究 生：楊松根　　Student: Sung-Kang Yang

指導教授：李大嵩 博士　　Advisor: Dr. Ta-Sung Lee

國立交通大學

電信工程學系碩士班

碩士論文

A Thesis
Submitted to Institute of Communication Engineering
College of Electrical Engineering and Computer Science
National Chiao Tung University
in Partial Fulfillment of the Requirements
for the Degree of
Master of Science
in
Communication Engineering
June 2005
Hsinchu, Taiwan, Republic of China

中 華 民 國 九 十 四 年 六 月

適用於多輸入多輸出無線區域網路之適應性調變編碼及傳送模式選擇之跨層設計

學生：楊松根　　指導教授：李大嵩 博士

國立交通大學電信工程學系碩士班

摘要

多輸入多輸出(Multiple-Input Multiple-Output, MIMO)為使用多天線於傳送和接收端的可靠通訊技術，並被認為是符合第四代高速通訊需求的最佳方案之一。另一方面，正交分頻多工（Orthogonal Frequency Division Multiplexing, OFDM）為一種具高頻譜效益，並能有效克服多路徑衰落效應的調變技術。在本論文中，吾人針對 MIMO-OFDM 提出一種跨層設計之適應性收發架構，使其能夠隨時間動態地在頻率與空間通道上調整傳輸參數，如：調變階數、通道編碼以及傳輸能量，吾人更進一步的透過同時考慮實體層與媒體存取層之共同設計，將 MIMO 技術向上延伸至媒體存取層，依據不同的品質要求，進行調整及修正系統參數與選用適當的 MIMO 傳輸技術，適切調整及修正重傳次數、封包長度、傳輸功率、傳輸速率、調變型態等系統參數，以便充分地利用空間、時間以及頻率通道上的特性以維持系統的目標錯誤率，達到最佳的性能。此種架構的特色之一在於可視需要彈性地獲取多樣與多工兩種增益，且針對上層之需求根據通道狀況選擇適當之傳送模式與參數。另外，不同的通道環境會造成不同的多路徑衰落效應。基於此一觀點，吾人將探討結合智慧型天線與 MIMO 之通訊系統架構，針對不同的環境效應，選取最適合之傳輸技術。吾人將進一步針對 MIMO 提出一種適應性傳收架構，以便充分利用無線通道的特性。最後，吾人藉由電腦模擬驗證上述架構在室內無線環境中具有優異的傳輸表現。

Cross-Layer Design for Adaptive Modulation/Coding and Transmission Mode Selection over MIMO WLANs

Student: Sung-Kang Yang Advisor: Dr. Ta-Sung Lee

Institute of Communication Engineering

National Chiao Tung University

Abstract

Multiple-input multiple-output (MIMO) is a promising technique suited to the increasing demand for high-performance 4G broadband wireless communications with multiple antennas at both transmitter and receiver side. In this thesis, we consider a new wireless communication system combining MIMO and OFDM, called the MIMO-OFDM system. To fully exploit the channel properties in the space-time-frequency wireless channels, we propose an adaptive MIMO-OFDM transceiver architecture along with a designed loading procedure to dynamically adjust the transmission parameters such as modulation order, channel coding and transmit power over spatial and frequency channels, according to the instantaneous channel statistics, to meet the target BER. Such transceiver scheme enjoys both the diversity and multiplexing gain in a flexible manner. Furthermore, we evaluate different error control and adaptation mechanisms available at different layers, namely MAC retransmission strategy, physical-layer channel coding, modulation order, MIMO mode, and adaptive packetization strategies. Besides, In a wireless transmission environment, the transmitted signal is scattered by various environmental objects causing different multi-path fading effects. With this point of view, we here consider a wireless communication system combining smart antenna or MIMO techniques. Depending on the channel condition, the optimal transmission technique is selected to combat channel impairments. Finally, we evaluate the performance of the proposed systems, and confirm that they work well in a typical indoor environment.

Acknowledgement

I would like to express my deepest gratitude to my advisor, Dr. Ta-Sung Lee, for his enthusiastic guidance and great patience. I learn a lot from his positive attitude in many areas. Heartfelt thanks are also offered to all members in the Communication Signal Processing (CSP) Lab for their constant encouragement. Finally, I would like to show my sincere thanks to my parents for their invaluable love.

Contents

List of Figures

List of Tables

Acronym Glossary

4G	the fourth generation
AMC	adaptive modulation and coding
ARQ	automatic repeat request
AWGN	additive white Gaussian noise
BER	bit error rate
BPSK	binary phase shift keying
BLAST	Bell Lab Layered space time
BS	base station
CP	cyclic prefix
CIR	channel impulse response
CRC	cyclic redundancy check
CSI	channel state information
DFT	discrete Fourier transform
D-BLAST	diagonal Bell labs' layered space-time
EQ	equalizer
FDD	frequency division duplex
FFT	fast Fourier transform
ICI	intercarrier interference
IEEE	institute of electrical and electronics engineers
IFFT	inverse fast Fourier transforms
ISI	intersymbol interference
LA	link adaptation
LOS	line of sight
MAC	medium access control layer
MIMO	multiple-input multiple-output

ML	maximum likelihood
MMSE	minimum mean square error
MRC	maximal ratio combining
MS	mobile station
MUX	multiplex
OFDM	orthogonal frequency division multiplexing
OSIC	ordered successive interference cancellation
PHY	physical layer
PER	packet error rate
QAM	quadrature amplitude modulation
QoS	quality of service
QPSK	quaternary phase shift keying
RF	radio frequency
RX	receiver
SD	spatial diversity
SM	spatial multiplexing
SNR	signal-to-noise ratio
SIC	successive interference cancellation
STC	space-time coding
STBC	space-time block coding
STTC	space-time trellis coding
TDD	time division duplex
TX	transmitter
V-BLAST	vertical Bell laboratory layered space-time
ZF	zero forcing

Notations

b_i	rate at the ith transmit antenna
C	transmission code words matrix
f_d	Doppler frequency
E_b	bit energy
E_s	symbol energy
$h_t^{i,j}$	channel gain between the jth transmit and ith receive antenna at time t
$H[k]$	channel frequency response on the kth subcarrier
M	modulation order
N_c	number of subcarriers (FFT/IFFT size)
N_{cp}	number of guard interval samples
N_t	number of transmit antenna
N_r	number of receive antenna
N_0	noise power spectrum density
p_n	path metric associated with the nth information bit
P_{budget}	power budget
q	antenna state
r_t^i	received data at the ith transmit at time t
S	set of signal constellation
s_t^j	transmitted signal form the jth transmit at time t
$\mathbf{T}$	set of switching levels
T_s	symbol duration
T_{sample}	sampling period
$d[k]$	input symbol on the kth subcarrier
$r[k]$	received data on the kth subcarrier
$\eta[k]$	additive white noise vector on the kth subcarrier
$\mathbf{w}_j$	weighting vector for the jth layer

η_t^i	additive white noise at the *i*th receive antenna at time *t*
σ_n^2	noise power
ε_{error}	target BER
γ	instantaneous SNR
τ_{rms}	root mean squared excess delay spread
ρ	average SNR at each receive antenna
λ	eigenvalue

Chapter 1

Introduction

Next generation broadband wireless communication systems are expected to provide users with multimedia services such as high-speed Internet access, wireless television, and mobile computing, etc. The rapid growing demand for these services is driving the wireless communication technology towards higher data rates, higher mobility and higher carrier frequency. However, the physical limitation of the wireless channel, typically subject to both time-selective and frequency-selective fading that are induced by carrier phase/frequency drifts, Doppler shifts and multipath propagation, presents a fundamental challenge for reliable communications. On the other hand, the limited availability of bandwidth promotes an emerging issue of high spectral efficiency. Hence, recent research efforts are carried out to develop efficient coding and modulation schemes along with sophisticated signal processing algorithms to improve the quality and spectral efficiency of wireless communication links [17][23]. Some popular examples include smart antennas, in particular multiple-input multiple-output (MIMO) technology [1]-[6], coded multicarrier modulation, adaptive modulation [7]-[10], and link-level retransmission techniques [24].

MIMO systems can be defined as follows: Given an arbitrary wireless system, we consider a link for which the transmitter side as well as the receiver side is equipped with multiple antennas. Such setup is illustrated in Fig. 2.1. The signals on the transmit

antennas at one end and the receive antennas at the other end are “co-processed” in such a way that the quality (Bit Error Rate or BER) or the data rate (bits/sec) of the communication link is improved. A core idea in MIMO systems is the space-time signal processing in which time is complemented with the spatial dimension inherent in the use of multiple spatially distributed antennas. A key feature of MIMO systems is to efficiently exploit the multipath, rather than mitigate it, to achieve the signal decorrelation necessary for separating the co-channel signals. Specifically, the multipath phenomenon presents itself as a source of diversity that takes advantage of random fading.

Orthogonal frequency division multiplexing (OFDM) is a multipath-friendly mechanism that treats the whole transmission band as a set of adjacent narrow sub-bands. This property leads OFDM to be chosen over a single-carrier solution to avoid using a complicated equalizer, which is usually a heavy burden in a wideband communication receiver. Moreover, with proper coding and interleaving across frequencies, multipath turns into an OFDM system advantage by yielding frequency diversity. OFDM can be implemented efficiently by using the Fast Fourier Transforms (FFTs) at the transmitter and receiver. At the receiver, FFT reduces the channel response into a multiplicative constant on a tone-by-tone basis.

In 1996, a new wireless communication scheme based on combination of the concepts of MIMO and OFDM was proposed [35]. Since then, MIMO-OFDM becomes an emerging research topic. The signaling scheme and receiver design are categorized into two categories: spatial multiplexing (SM) and spatial diversity (SD) schemes. In the former system, different data streams are transmitted from different antennas simultaneously and detected based on their unique spatial signature at the receiver. This implies the creation of parallel spatial channels to maximize the data rate. In the latter, the space-time coding (STC) [11]-[14] technique is designed for use with multiple

transmit antennas. ST codes introduce temporal and spatial correlation into signals by sending the same information through different paths, thus multiple independently faded replicas of the data symbols can be coherently combined to average the fading gains. From this point of view, fading can in fact be beneficial through increasing the degrees of freedom available for communication. Both SM and SD are looking at maximizing spectrum efficiency of the transmission system, but just in different ways. In this combination, multipath remains an advantage for MIMO-OFDM since frequency selectivity caused by multipath improves the rank distribution of the channel matrices across frequency tones and thereby increases capacity. Besides, by admitting the equivalence or independence between sub-channels (each corresponds to a particular transmit antenna, frequency tone and time slot) introduced by MIMO and OFDM, different ST coding schemes can be applied to MIMO-OFDM to fit different transmission environments.

To meet the ever growing bandwidth needs of enterprise and home networks, as well as those of Wireless LAN (WLAN) hot spots, IEEE is creating a task force to develop a standard that will raise the effective throughput of WLAN up to 100-300 Mbps. The higher-speed standard, IEEE 802.11n is expected to adopt the MIMO-OFDM scheme as its transmission platform. Although the data rate of a MIMO-OFDM system can be increased drastically, the number of system parameters that need to be estimated in either the initial link set-up stage or the regular transmission stage increases as well. In principle, the MIMO technologies can provide not only the antenna gain for interference suppression, but also various point-to-point link profits for covering wider service regions and improving various Quality of Services (QoS). High-speed data service in WLANs through MIMO largely relies on rich-scattering and reliable background channel conditions. The radio environment inside a network, however, may be time-varying, and within which high-speed

transmission may lead to high frame error rates. To sustain good link services, adaptive modulation techniques are proposed to dynamically adjust transmission parameters based on the near instantaneous channel state information (CSI) [9][10] to ease channel impairments. Also, most wireless communication transceivers have built-in modules for supporting Physical (PHY) layer data processing and Medium Access Control (MAC) layer resource management. As a result, cross-layer processing that exploits the joint resource for more efficient PHY layer designs and more effective MAC protocol setups will become an important issue. In this thesis, we will attempt to develop an adaptive wireless transceiver that can take advantages of the existing system jointly to effectively exploit the available degrees of freedom in the wireless communication systems. Besides, an adaptive wireless transceiver which employ smart antenna and special multiplexing techniques is proposed to overcome the wireless channel impairments.

This thesis is organized as follows. In Chapter 2, we describe the general data model and channel capacity of a MIMO communication link. Some existing transmit diversity, spatial multiplexing and beamforming techniques are also presented to provide a preliminary overview. In Chapter 3, an adaptive modulation concepts and bit loading procedure suited to the V-BLAST based MIMO-OFDM system are introduced. In Chapter 4, we develop the cross-layer design by combining AMC at physical layer with several MAC protection strategies. In Chapter 5, the optimal space-time processing technique for a specific channel condition is discussed from the point-of-view of ergodic capacity. Finally, Chapter 6 gives concluding remarks of this thesis and leads the way to some potential future works.

Chapter 2

MIMO Technique Overview

Multiple antennas can be used for increasing the amount of diversity or the number of degrees of freedom in the wireless communication systems. In this chapter, we introduce the basic ideas and key features of the MIMO systems.

2.1 Transmit/Receive Diversity

In wireless communications systems, diversity techniques are widely used to reduce the effects of multipath fading and improve the reliability of transmission without increasing the transmitted power or sacrificing the bandwidth. Diversity techniques are classified into time, frequency and space diversity. In this section, we focus on space diversity that is also called antenna diversity. And it can classify space diversity into two categories: receive diversity and transmit diversity.

2.1.1 Receive Diversity

The use of multiple antennas at the receiver, which is referred to as receive diversity, is well known. In essence, multiple copies of the transmitted stream are received, which can be efficiently combined using appropriate signal processing

algorithms. This technique is aimed to provide an AWGN-like channel where the outage probability is driven to zero as the number of antennas increases. There are several ways to combine the received signals, such as switch combining, selection combining, equal gain combining, and maximal ratio combining (MRC).

In the MRC, the outputs of the N_r receive antennas are linearly combined so as to maximize the instantaneous SNR. The coefficients that yield the maximum SNR can be found from the optimization theory. Consider a $1 \times N_r$ transmission scheme and denote the received data at the lth receive antenna as

$$r_l = h_l s + \eta_l \tag{2.1}$$

where h_l denotes the channel gain from the transmit antenna to lth receive antenna, and η_l is the independent noise samples of power σ^2. Further, we assume perfect channel estimation the receive side. Finally, the transmitted signal power is normalized to be 1. The MRC is achieved by using the linear combination

$$y = \sum_{l=1}^{N_r} w_l^* r_l = \sum_{l=1}^{N_r} w_l^* h_l s + \sum_{l=1}^{N_r} w_l^* \eta_l \tag{2.2}$$

prior to detection. The noise power after MRC is given by

$$\varsigma_\eta = \sigma^2 \sum_{l=1}^{N_r} |w_l|^2 \tag{2.3}$$

while the instantaneous signal power is

$$\sum_{l=1}^{N_r} |w_l^* h_l|^2 \tag{2.4}$$

The ratio of these two quantities

$$\gamma = \frac{\sum_{l=1}^{N_r} |w_l^* h_l|^2}{\sigma^2 \sum_{l=1}^{N_r} |w_l|^2} \tag{2.5}$$

can be maximized by applying the Cauchy-Schwartz inequality defined as

$$\sum_{l=1}^{N_r}\left|a_l^* b_l\right|^2 \le \sum_{l=1}^{N_r}\left|a_l\right|^2 \sum_{l=1}^{N_r}\left|b_l\right|^2 \tag{2.6}$$

where the equality in Equation 2.6 is obtained for $w_l = h_l$ for all l, which provides the weighting coefficients for MRC. Hence, the heavily faded antennas, which are less reliable, are counted less than the less faded antennas, which are more reliable, and vice versa. The SNR provided by MRC is given by

$$r_{\mathrm{MRC}} = \frac{1}{\sigma^2}\sum_{l=1}^{N_r}\left|w_l\right|^2 \tag{2.7}$$

Noting that $\left|w_l\right|^2/\sigma^2$ is the post-processing SNR for the lth receive antenna, Equation 2.7 is just the sum of the SNRs for each receive antenna, which means r_{MRC} can be large even when the individual SNRs are small. It can also be proved that the MRC is the optimal combining technique in the sense of MMSE [40].

2.1.2 Transmit Diversity

In some applications, especially when the power consumption and size constraint are the major concerns, multiple antennas at the receiver may be impractical. This leads us to the use of multiple transmit antennas. Previous work on transmit diversity can be classified into three broad categories: Schemes using feedback, schemes with feedforward or training information but no feedback, and blind scheme. Here, we only concentrate on the space-time codes (STC), which belong to the second category. Space-time codes introduce temporal and spatial correlations into signals transmitted from different antennas, so as to provide diversity at the receiver, and/or coding gain over an uncoded system without sacrificing the bandwidth.

2.2 Spatial Multiplexing: Concept and Technique

Spatial multiplexing (SM) is a technique that yields an increased bit rate by using multiple antennas at both end of the wireless link [1]-[3]. This increase comes at no extra bandwidth and power consumption. However, such a technique calls for an efficient way to map the transmit signals to individual antenna elements. At the receiver, the individual data streams are separated and demultiplexed to yield the original transmitted signals, as illustrated in Figure 2.2. The separation is made possible by the fact that the rich multipath contributes to lower correlation between MIMO channel coefficients, and hence creates a desirable coefficient matrix condition (i.e., full rank and low condition number) to resolve N_t unknowns from a linear system of N_r equations. In the following, we will introduce two SM schemes: D-BLAST and V-BLAST.

2.2.1 Diagonal Bell Labs' Layered Space-Time

The Layered Space-Time processing concept was first introduced by Foschini [1] at Bell Labs. The first version, D-BLAST, utilizes multiple antenna arrays at both the transmitter and receiver, and an elegant diagonally-layered coding structure in which code blocks are dispersed across diagonals in space-time. The encoding and decoding procedures are described as follows:

- Encoding:

Considering a system equipped with N_t transmit and N_r receive antennas, the encoder applies the space-time codes to the input to generate a semi-infinite matrix $\boldsymbol{C}$ of N_t rows to be transmitted. Figure 2.5 shows the encoding scheme, where c_τ^k,

representing an element in the *k*th row and τth column of ***C***, is transmitted by the *k*th transmit antenna at time τ. The data received at time τ by the *l*th receive antenna is r_τ^l, which contains a superposition of c_τ^k, $k=1,2,\ldots,N_t$, and an AWGN noise component. Each subsequence is encoded using a conventional 1-D constituent code with low decoding complexity.

- Decoding:

At any instance τ, the received datum vector is $\mathbf{r}_\tau = \mathbf{H}_\tau \mathbf{c}_\tau + \boldsymbol{\eta}_\tau$ (refer to Section 2.1). The decoding task is to determine $\mathbf{c}_\tau = \left[c_\tau^1, c_\tau^2, ..., c_\tau^{N_t}\right]^T$ with the only available information being $\mathbf{r}_\tau$ and $\mathbf{H}_\tau$. The D-BLAST uses a repeated process of interference suppression, symbol detection and interference cancellation for decoding all symbols, $c_\tau^{N_t}, c_\tau^{N_t-1}, ..., c_\tau^1$. Such decoding process could be expressed in a general form:

Let the QR decomposition of $\mathbf{H}_\tau$ be $\mathbf{Q}_\tau \mathbf{R}_\tau$, where $\mathbf{Q}_\tau$ is an $N_r \times N_r$ unitary matrix and $\mathbf{R}_\tau$ is an $N_r \times N_t$ upper triangular matrix. We modify the received data to get

$$\begin{aligned}\mathbf{y}_\tau &= \mathbf{Q}_\tau^H \mathbf{r}_\tau = \mathbf{Q}_\tau^H \mathbf{H}_\tau \mathbf{c}_\tau + \mathbf{Q}_\tau^H \boldsymbol{\eta}_\tau = \underbrace{\mathbf{Q}_\tau^H \mathbf{Q}_\tau}_{\mathbf{I}_{N_r}} \mathbf{R}_\tau \mathbf{c}_\tau + \underbrace{\mathbf{Q}_\tau^H \boldsymbol{\eta}_\tau}_{\tilde{\boldsymbol{\eta}}_\tau} \\ &= \mathbf{R}_\tau \mathbf{c}_\tau + \tilde{\boldsymbol{\eta}}_\tau\end{aligned} \tag{2.8}$$

where

$$\mathbf{y}_\tau = \begin{bmatrix} y_\tau^1 \\ y_\tau^2 \\ \vdots \\ y_\tau^{N_r} \end{bmatrix}, \mathbf{R}_\tau = \begin{bmatrix} r_\tau^{1,1} & r_\tau^{1,2} & \cdots & r_\tau^{1,N_t} \\ 0 & r_\tau^{2,2} & \cdots & r_\tau^{2,N_t} \\ 0 & 0 & \ddots & \vdots \\ \vdots & 0 & \ddots & r_\tau^{N_t,N_t} \\ 0 & \ddots & \ddots & 0 \\ 0 & 0 & \ddots & \vdots \\ 0 & 0 & \cdots & 0 \end{bmatrix}, \tilde{\boldsymbol{\eta}}_\tau = \begin{bmatrix} \tilde{\eta}_\tau^1 \\ \tilde{\eta}_\tau^2 \\ \vdots \\ \tilde{\eta}_\tau^{N_r} \end{bmatrix} \tag{2.9}$$

Since $\mathbf{R}_\tau$ is upper triangular,

$$y_\tau^k = r_\tau^{k,k} c_\tau^k + \tilde{\eta}_\tau^k + \{\text{contribution from } c_\tau^{k+1}, c_\tau^{k+2}, ..., c_\tau^{N_t}\} \tag{2.10}$$

Now, we can figure out that the interference from c^l, $l < k \le N_t$, are first suppressed in y^k and the residual interference terms in Equation 2.10 can be cancelled by the available decisions $\hat{c}_\tau^{k+1}, \hat{c}_\tau^{k+2}, \ldots, \hat{c}_\tau^{N_t}$. Assuming all these decisions are correct, the present decision variable is

$$\tilde{c}_\tau^k = r_\tau^{k,k} c_\tau^k + \tilde{\eta}_\tau^k, \quad k = 1, 2, \ldots, N_t \tag{2.11}$$

The relationship between c^k and $\tilde{c}^k$ in Equation 2.11 can be interpreted as the input and output of a SISO channel with the channel power gain $\left|r^{k,k}\right|^2$ and AWGN. The channel power gain $\left|r^{k,k}\right|^2$ are independently chi-squared distributed with $2\times(N_r-k+1)$ degrees of freedom. Moreover, if there are no decision feedback errors, we can treat the kth row of the $\boldsymbol{C}$ matrix as transmitted over a $(N_t, N_r)=(1, N_r-k+1)$ system without interference from the other rows and all fades are i.i.d.

Figure 2.6 shows typical decoding steps (suppression, detection, decoding and cancellation) performed in a D-BLAST system. The receiver generates decisions for the first diagonal of $\boldsymbol{C}$, $\hat{c}_1^1, \hat{c}_2^2, \ldots, \hat{c}_{N_t}^{N_t}$. Based on these decisions, the diagonal is decoded and fed back to remove the contribution of this diagonal from the received data. The receiver continues to decode the next diagonal and so on. The encoded substreams share a balanced presence over all paths to the receiver, so none of the individual substreams is subject to the worst path.

2.2.2 Vertical Bell Labs' Layered Space-Time

The diagonal approach suffers from certain implementation complexities that make it inappropriate for initial implementation. Therefore, Foschini proposed another low-complexity version of detecting the symbols transmitted synchronously over

antennas, that is, V-BLAST [3]. The "V" here stands for the vertical vector mapping process, which differs from the diagonal form in D-BLAST. In V-BLAST, no inter-substream coding, or coding of any kind, is required, though conventional coding of the individual substreams may certainly be applied. In [4], a vertical-and-horizontal coding structure along with iterative detection and decoding (IDD) was promoted and showed to significantly improve the performance with limited complexity.

Figures 2.5 and 2.7 displays the typical encoding and decoding steps in V-BLAST. The decoding process can also be interpreted via the general form (QR decomposition) as mentioned in decoding D-BLAST. In each step *I*, the signals from all but one transmit antenna are eliminated using interference suppression and cancellation with already detected signals. Following the data model in D-BLAST, at a given time instant τ, let $\tilde{\mathbf{H}}^{i=1} = \mathbf{H}_\tau$ and $\tilde{\mathbf{r}}^{i=1} = \mathbf{r}_\tau$ at the first decoding step. In each step *i*, the nulling matrix $\mathbf{G}^i$ is calculated as the pseudo-inverse of $\tilde{\mathbf{H}}^i$

$$\begin{aligned}\mathbf{G}^i &= (\tilde{\mathbf{H}}^i)^+ \\ &= \left((\tilde{\mathbf{H}}^i)^H \tilde{\mathbf{H}}^i\right)^{-1} (\tilde{\mathbf{H}}^i)^H\end{aligned} \tag{2.12}$$

Each row of $\mathbf{G}^i$ can be used to null all but the *i*th desired signal. Instead of choosing an arbitrary layer to be detected first, it was suggested to start with the layer showing the biggest post-detection SNR to efficiently reduce the error propagation effect [3]. This corresponds to choosing the row of $\mathbf{G}^i$ with the minimum norm and defining the corresponding row, $\mathbf{w}_{k_i}^T$, as the nulling vector at this step:

$$k_i = \underset{j \notin \{k_1,\ldots,k_{i-1}\}}{\arg\min} \| (\mathbf{G}^i)_j \|^2 \tag{2.13}$$

$$\mathbf{w}_{k_i} = (\mathbf{G}^i)_{k_i}^T \tag{2.14}$$

Multiplying $\mathbf{w}_{k_i}$ with the vector of received data $\tilde{\mathbf{r}}^i$ suppresses all layers but the one

transmitted from antenna k_i and we get a soft decision value

$$\overline{c}_\tau^{\,k_i} = \mathbf{w}_{k_i}^T \tilde{\mathbf{r}}_\tau^i \tag{2.15}$$

Now the k_i th layer can be detected within the constellation set *S* that we use:

$$\hat{c}_\tau^{\,k_i} = \arg\min_{\tilde{x}\in S} \| \tilde{c} - \overline{c}_\tau^{k_i} \|^2 \tag{2.16}$$

As soon as one layer is detected, we can improve the detection performance for the subsequent layers by subtracting the part of the detected signal from the received vector,

$$\tilde{\mathbf{r}}_\tau^{i+1} = \tilde{\mathbf{r}}_\tau^i - \hat{c}_\tau^{\,k_i} \left(\tilde{\mathbf{H}}^i\right)^{k_i} \tag{2.17}$$

where $\left(\tilde{\mathbf{H}}^i\right)^{k_i}$ denotes the k_ith column of $\tilde{\mathbf{H}}^i$. After canceling out the signal from the k_ith transmit antenna, the channel matrix is reduced to

$$\tilde{\mathbf{H}}^{i+1} = \left(\tilde{\mathbf{H}}^i\right)^{\overline{k_i}} \tag{2.18}$$

where the notation $\left(\tilde{\mathbf{H}}^i\right)^{\overline{k_i}}$ denotes the matrix obtained by zeroing columns $k_1, k_2, ..., k_i$ of $\tilde{\mathbf{H}}^i$. Since we decrease the number of layers to be nulled out in the next step by one, the diversity gain is increased by one at each step (from (N_r–N_t+i) to (N_r–N_t+i+1)). This can be proven by the Cauchy-Schwartz inequality [3]. The full Zero-Forcing V-BLAST detection algorithm can be summarized as follows:

Initialization:

$i \leftarrow 1$

$\mathbf{G}^1 = \left(\tilde{\mathbf{H}}^1\right)^+$

$k_1 = \arg\min_j \| (\mathbf{G}^1)_j \|^2$

Recursion:

$$\mathbf{w}_{k_i} = (\mathbf{G}^i)^T_{k_i}$$

$$\overline{c}^{k_i} = \mathbf{w}^T_{k_i} \tilde{\mathbf{r}}^i$$

$\hat{c}^{k_i} = Q(\overline{c}^{k_i})$, $Q(\cdot)$ denotes the slicing operation

$$\mathbf{r}^{i+1} = \mathbf{r}^i - \hat{c}^{k_i} (\tilde{\mathbf{H}}^i)^{k_i}$$

$$\tilde{\mathbf{H}}^{i+1} = \left(\tilde{\mathbf{H}}^i\right)^{\overline{k_i}}$$

$$\mathbf{G}^{i+1} = \left(\tilde{\mathbf{H}}^{i+1}\right)^{+}$$

$$k_{i+1} = \arg \min_{j \notin \{k_1, \cdots k_i\}} \| (\mathbf{G}^{i+1})_j \|^2$$

$$i \leftarrow i+1$$

The post-processing SNR for the k_ith detected component of **c** is

$$\rho_{k_i} = \frac{<| c^{k_i} |^2>}{\sigma^2 \| \mathbf{w}_{k_i} \|^2} \tag{2.19}$$

where the expectation value in the numerator is taken over the constellation set S.

Another way to improve detection performance especially for mid-range SNR values is to replace the ZF nulling matrix by the more powerful MMSE one [3]:

$$\mathbf{G}^i = \left((\tilde{\mathbf{H}}^i)^H \tilde{\mathbf{H}}^i + \frac{1}{SNR} \mathbf{I} \right)^{-1} (\tilde{\mathbf{H}}^i)^H \tag{2.20}$$

In this case, in additional to nulling out the interference, the noise level on the channel is taken into account. Thus, the SNR has to be estimated at the receiver. Figure 2.7 shows the typical decoding procedure in V-BLAST.

The D-BLAST code blocks are organized along diagonals in space-time. It is this coding that leads to D-BLAST's higher spectral efficiencies for a given number of transmit and receive antennas.

2.3 Review of OFDM

OFDM can be regarded as either a modulation or a multiplexing technique. The basic concept of OFDM is to split a high rate data stream into a number of lower rate streams that are transmitted simultaneously over subcarriers. In order to eliminate the effect of inter-symbol interference (ISI), a guard time is appended to each OFDM symbol. The guard time is chosen to be larger than the maximum delay spread such that the current OFDM symbol never hears the interference from the previous one. However, this method will cause the inter-carrier interference (ICI) due to the loss of orthogonality between subcarriers. To solve this problem, OFDM symbols are cyclically extended in the guard time to introduce cyclic prefix (CP). This ensures that the delayed replicas of an OFDM symbol always have an integer number of cycles within the FFT interval. As a result, CP resolves both ISI and ICI problems caused by multipath, as long as the delay spread of channel is smaller than the length of CP. Besides, adding CP makes the transmitted OFDM symbol appear periodic, and the linear convolution process of the transmitted OFDM symbols (containing CP) with channel impulse response will be translated into a circular convolution one. According to discrete-time linear system theory, this circular convolution is equivalent to multiplying the frequency response of the OFDM symbol with the channel's frequency response. This property can be demonstrated as follows:

Assuming that the channel length is smaller than N_{cp} (number of samples in CP), we can express the received datum vector $\mathbf{y}$ as

$$\mathbf{y} = \mathbf{H}\mathbf{x} + \boldsymbol{\eta}$$

$$\underbrace{\begin{bmatrix} y_{N_c-1} \\ \vdots \\ y_0 \end{bmatrix}}_{\mathbf{y}} = \underbrace{\begin{bmatrix} h_0 & h_1 & \cdots & h_{N_{cp}} & 0 & \cdots & 0 \\ 0 & h_0 & h_1 & \cdots & h_{N_{cp}} & 0 & \vdots \\ 0 & 0 & \ddots & \ddots & \cdots & \ddots & 0 \\ 0 & \cdots & 0 & h_0 & h_1 & \cdots & h_{N_{cp}} \end{bmatrix}}_{\mathbf{H}} \underbrace{\begin{bmatrix} x_{N_c-1} \\ \vdots \\ x_0 \\ x_{-1} \\ \vdots \\ x_{-N_{cp}} \end{bmatrix}}_{\mathbf{x}} + \underbrace{\begin{bmatrix} \eta_{N_c-1} \\ \vdots \\ \eta_0 \end{bmatrix}}_{\boldsymbol{\eta}} \tag{2.21}$$

When we use SVD, we have

$$\mathbf{H} = \mathbf{F}\boldsymbol{\Lambda}\mathbf{M}^H \tag{2.22}$$

where $\mathbf{F}\mathbf{F}^H = \mathbf{I}$ and $\mathbf{M}\mathbf{M}^H = \mathbf{I}$. If we let $\mathbf{x} = \mathbf{M}\mathbf{X}$ and $\mathbf{Y} = \mathbf{F}^H\mathbf{y}$, then we can get

$$\mathbf{Y} = \mathbf{F}^H\mathbf{y} = \mathbf{F}^H(\mathbf{H}\mathbf{x} + \boldsymbol{\eta}) = \mathbf{F}^H\mathbf{H}\mathbf{M}\mathbf{X} + \underbrace{\mathbf{N}}_{\mathbf{F}^H\boldsymbol{\eta}} = \boldsymbol{\Lambda}\mathbf{X} + \mathbf{N} \tag{2.23}$$

It is interesting to note that when the guard period contains a CP, that is, $x_{-i} = x_{N-i}$ for $i = 1, \ldots, N_{cp}$, Equation 2.21 can be rewritten in a more compact matrix form

$$\begin{bmatrix} y_{N_c-1} \\ \vdots \\ y_0 \end{bmatrix} = \begin{bmatrix} h_0 & h_1 & \cdots & h_{N_{cp}} & 0 & \cdots & 0 \\ 0 & h_0 & h_1 & \cdots & h_{N_{cp}} & \ddots & 0 \\ \vdots & \ddots & \ddots & \ddots & \ddots & \ddots & \vdots \\ 0 & \cdots & 0 & h_0 & h_1 & \cdots & h_{N_{cp}} \\ h_{N_{cp}} & 0 & \cdots & 0 & h_0 & \cdots & h_{N_{cp}-1} \\ \vdots & \ddots & \ddots & \ddots & \ddots & \ddots & \vdots \\ h_1 & \cdots & h_{N_{cp}} & 0 & \cdots & 0 & h_0 \end{bmatrix} \begin{bmatrix} x_{N_c-1} \\ \vdots \\ x_0 \end{bmatrix} + \begin{bmatrix} \eta_{N_c-1} \\ \vdots \\ \eta_0 \end{bmatrix} \tag{2.24}$$

And $\mathbf{H}$ becomes the so called "circulant matrix" and has the property that $\mathbf{H} = \mathbf{Q}^H\boldsymbol{\Lambda}\mathbf{Q}$, where $\mathbf{Q}$ is a DFT matrix with *kl*th entry as

$$\mathbf{Q}_{kl} = \frac{1}{\sqrt{N_c}} e^{-j2\pi\frac{kl}{N_c}} \tag{2.25}$$

And the transformed symbol is $\mathbf{x} = \mathbf{Q}^H\mathbf{X}$ (IDFT of $\mathbf{x}$). Thus $\mathbf{X}$ can be interpreted as symbols in the frequency domain. At the receiver, we have the received data $\mathbf{y}$ being transformed to $\mathbf{Y}$

$$\begin{aligned}\mathbf{Y} &= \mathbf{Q}^H\mathbf{y} = \mathbf{Q}^H(\mathbf{Hx}+\boldsymbol{\eta}) \\ &= \underbrace{\mathbf{Q}^H\mathbf{HQ}^H}_{\boldsymbol{\Lambda}}\mathbf{X} + \underbrace{\mathbf{Q}^H\boldsymbol{\eta}}_{\mathbf{N}} \\ &= \boldsymbol{\Lambda}\mathbf{X}+\mathbf{N}\end{aligned} \tag{2.26}$$

Now, we can realize that by using CP, the OFDM modulation is equivalent to multiplying the frequency domain signals of the OFDM symbol (that is, **X**) with the channel's frequency response $\boldsymbol{\Lambda}$.

Broadband transmission over multipath channels usually exhibits frequency selective fading. Since data rate requirements can be expected to increase even further in the future, this effect is likely to amplify. In OFDM, frequency diversity can be realized through coding and interleaving across subcarriers. Because information bits are separated over many subcarriers, the impairment of fading occurring at particular frequency tones can be mitigated. As a consequence, in the coded OFDM systems the presence of frequency selective fading actually saves the frequency tones at fading. Depending on the coding rate and interleaving death, gains can be achieved at locations experiencing significant delay spread.

It can be concluded that OFDM is a powerful modulation technique that increases bandwidth efficiency and simplifies the removal of distortion due to a multipath channel. Advances in fast Fourier transform (FFT) algorithm enable OFDM to be efficiently implemented in hardware, even for a large number of subcarriers. The key advantages of OFDM transmission are summarized as follows:

1. OFDM deals with multipath delay channels in an efficient way. The implementation complexity is significantly lower than that of a single carrier system with an equalizer.
2. OFDM has a long symbol period (compared to an equal data-rate single-carrier system) that allows OFDM to be more robust against impulse noise.
3. OFDM supports dynamic bit loading that enable different subcarriers to use

different modulation modes depending on the channel characteristic or the noise level. Therefore, improved performance can be achieved in this systematic way.

2.4 V-BLAST Based OFDM

Due to the scarcity of radio spectrum, high spectral efficiency becomes a must-have requirement that encourages modern wireless modems toward this trend. An evolution of the V-BLAST supporting OFDM modulation seems to be a solution that can dramatically increase the capacity of wireless radio links with no additional power and bandwidth consumption. The core idea in such scheme is that with the aid of OFDM, the whole detection problem in MIMO-OFDM would be translated into N_c parallel sub-problems.

In the transmitter, as shown in Figure 2.8, a traditional 1-D channel encoder is used to encode the information bits. These coded bits are then mapped on the symbols of constellation adopted for each subcarrier. At a given time slot n, $N_c \times N_t$ bit streams $\{c_i[n,k]: k = 0,1,\ldots N_c\}$ for $i = 1,2\ldots, N_t$ are fed to the IFFT at the ith transmit antenna on the kth subcarrier to generate the nth transmitted OFDM symbols from the ith transmit antenna.

At the receiver side, as shown in Figure 2.9, receive antennas 1~N_r will receive the radiate signal from transmit antennas 1~N_t, where the V-BLAST requires $N_r \geq N_t$ to ensure its proper working. The received data at each receive antenna will then pass through a FFT with the removal of the CP. The FFT output, at the receive antenna j, is a set of N_c signals, one for each frequency subcarrier, expressed as

$$r_j[n,k] = \sum_{i=1}^{N_t} H_{j,i}[n,k]c_i[n,k] + \eta_j[n,k] \qquad \forall k = 1,2,...,N_c \tag{2.27}$$

where $H_{i,j}[n,k]$ is the flat fading coefficient representing the channel gain form the

transmit antenna i to the receive antenna j at frequency k, and $\eta_j[n,k]$ denotes the additive complex Gaussian noise at the receiver antenna j and frequency k with two-sided power spectral density $N_0/2$ per dimension and uncorrelated for different n's, k's, and j's.

2.5 MIMO Beamforming: Concept and Technique

Traditionally, the intelligence of the multiantenna system is located in the weight selection algorithm. Simple linear combining can offer a more reliable communications link in the presence of adverse propagation conditions such as multipath fading and interference. Beamforming is a key technique in smart antenna and increases the average SNR. In the following, we will introduce two schemes: beamforming and eigenbeamforming.

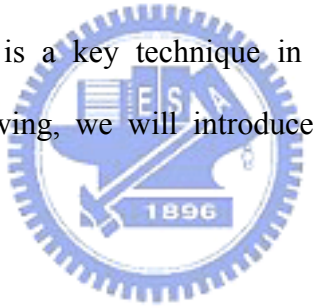

2.5.1 Generic Beamforming

As a feedback channel from the receiver to the transmitter can be obtained, beamforming can be utilized to maximize the receiver SNR and provide array gain [42]. With beamforming technique applied to both the transmitter and receiver, the beamformer output of the receiver is given by

$$\hat{s} = \mathbf{w}_R^H \left(\mathbf{H}\mathbf{w}_T s + \mathbf{n} \right) = \mathbf{w}_R^H \mathbf{H}\mathbf{w}_T s + \mathbf{w}_R^H \mathbf{n} \tag{2.39}$$

where $\mathbf{w}_R$ and $\mathbf{w}_T$ denote the weight vectors of transmitter and receiver, respectively, $\mathbf{x} = \mathbf{w}_T s$ is the transmitted signal vector, and $\mathbf{n}$ is Gaussian noise. This can be

illustrated by Figure 2.10. If $\mathbf{w}_R$ and $\mathbf{w}_T$ are chosen as the dominant left and right singular vectors associated with the channel matrix **H**, the beamformer output can be rewritten as

$$\hat{s} = \lambda_1^{1/2} s + \mathbf{w}_R^* \mathbf{n} \tag{2.40}$$

where λ_1 is the largest eigenvalue of the matrix $\mathbf{H}\mathbf{H}^H$. According to Equation 2.40, the corresponding SNR is

$$\mathrm{SNR}_{\mathrm{BF}} = \frac{P_T}{\sigma_n^2} \lambda_1 \tag{2.41}$$

where P_T is the total transmitted power.

2.5.1 Eigenbeamforming Technique

The eigenbeamforming is an attractive method for downlink [43]. It can provide good diversity gains with less amount of feedbacks due to the short-term selection of eigenmode. Eigenbeamforming is particularly suitable for spatially correlation channels, and is easily applied to the spatial downlink channel. This is because that the spatial downlink channel possesses a higher spatial correlation and few dominant eigenmodes, in which each eigenmode can be considered as an uncorrelated path to the mobile station [44]. In a cellular system, the signal can be spatially selectively transmitted with only few directions due to the vanish of local scatters around the antenna array of the base station. This makes the eigenbeamforming effectively. Consider a system with M_T transmit antennas at the base station and M_R receive antennas at the mobile station. The received signal vector at the mobile station is given by

$$\mathbf{y}(t) = \sqrt{\gamma}\mathbf{H}(t)\,\mathbf{w}(t)\,s(t) + \mathbf{n}(t) \tag{2.42}$$

where γ is the input SNR, $\mathbf{H}(t)$ is the channel matrix, and $\mathbf{w}(t)$ is the beamforming weight vector. Assume that beamforming vector is normalized to one, i.e., $\|\mathbf{w}(t)\|^2 = 1$. The instantaneous SNR at the receiver is written as

$$\gamma_{rec} = \gamma \mathbf{w}^H(t)\,\mathbf{H}^H(t)\,\mathbf{H}(t)\,\mathbf{w}(t) \tag{2.43}$$

This suggests that the optimal weight vector, maximizing the instantaneous SNR, can be obtained as follows:

$$\mathbf{w}_{opt}(t) = \arg\max_{\|\mathbf{w}\|^2=1} \mathbf{w}^H(t)\mathbf{R}_{\mathbf{H}}(t)\,\mathbf{w}(t) \tag{2.44}$$

where $\mathbf{R}_{\mathbf{H}}(t) = \mathbf{H}^H(t)\,\mathbf{H}(t)$. The corresponding solution is the dominant eigenvector associated with the largest eigenvalue of the matrix $\mathbf{R}_{\mathbf{H}}(t)$. Note that since the channel information must be sent to the base station, this method is called close-loop beamforming. Suppose that the instantaneous channel matrix is not available. Assume that the beamforming vector is time-invariant (or very slowly varying). The beamforming vector can be obtained by maximizing the mean SNR as follows:

$$\begin{aligned} \mathbf{w}_{ms} &= \arg\max_{\|\mathbf{w}\|^2\le 1} E\left[\gamma_{rec}(t)\right] \\ &= \arg\max_{\|\mathbf{w}\|^2\le 1} \mathbf{w}^H \mathbf{R}_{\mathbf{H}} \mathbf{w} \end{aligned} \tag{2.45}$$

where $\mathbf{R}_{\mathbf{H}} = E\left[\mathbf{R}_{\mathbf{H}}(t)\right]$. The beamforming that uses $\mathbf{w}_{ms}$ is called the blind beamforming that can be employed in CDMA system with lower mobile speed.

2.6 Computer Simulations

In this section, we simulate the V-BLAST performance both for the ideal and realistic case. We define the relation between SNR and E_b/N_0 at each receive antenna as follows:

$$\text{SNR} = \frac{\text{signal power}}{\text{noise power}} = \frac{\frac{E_s}{T_s}}{N_0 B} = \frac{\frac{E_b \cdot N_t \cdot M}{T_s}}{N_0 \frac{1}{T_s}} = \frac{E_b}{N_0} \cdot (N_t \cdot M) \tag{2.46}$$

where E_s is the symbol energy, T_s is the symbol duration, B is the system bandwidth and M is the modulation order. Throughout the following simulations, the system transmit power is normalized to 1, and hence the noise power corresponding to a specific E_b/N_0 is generated by

$$\text{noise power} = \frac{N_0}{E_b \cdot N_t \cdot M} \tag{2.47}$$

Figure 2.10 shows the BER performance of the (N_t, N_r) = (4, 4) ZF V-BLAST system with ideal detection and cancellation. It is obvious that in the ideal case, the diversity gain increases as the number of effective transmit antennas decreases. However, as shown in Figure 2.11, the realistic V-BLAST system suffers from error propagation and hence the diversity gain degrades. In Figure 2.12, we compare two equal rate V-BLAST systems. It is interesting to see that the system with fewer transmit antennas will outperform the one with more transmit antennas in the BER performance. This phenomenon hints that given a MIMO channel and some transmit power budget, we can improve the MIMO system performance by simply adjusting transmission parameters at no cost of transmission rate. So, it strongly motivates us involve the concept of adaptive modulation in MIMO, which will be described in Chapter 3.

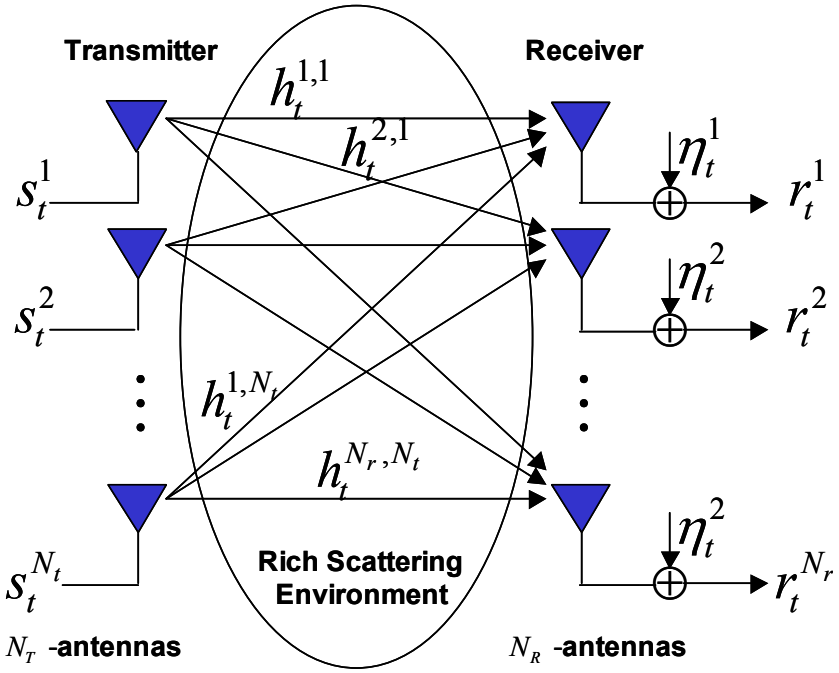

Figure 2.1: Diagram of a MIMO wireless transmission system.

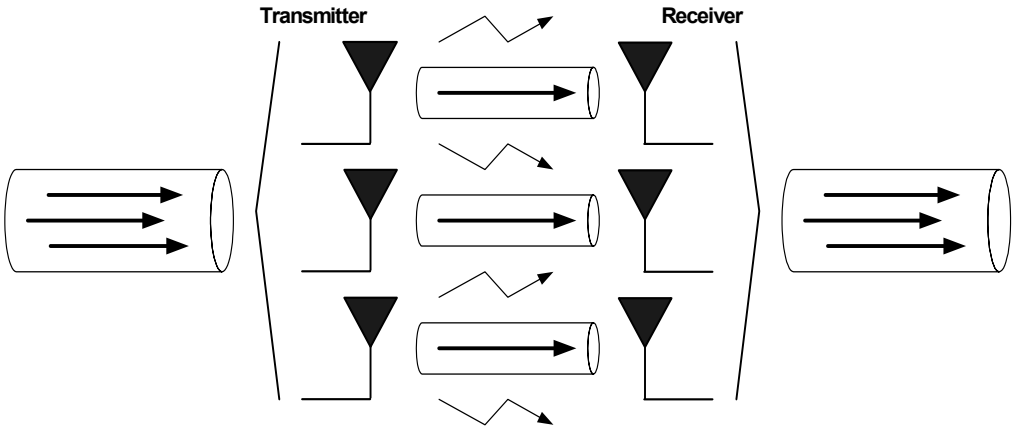

Figure 2.2: An illustration of a spatial multiplexing system.

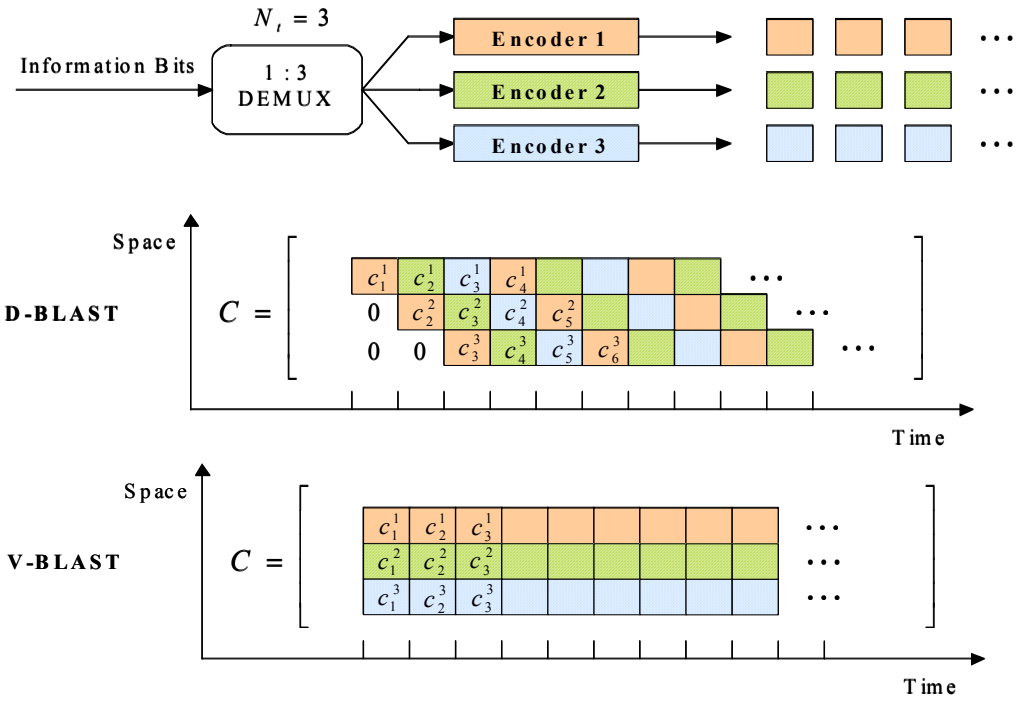

Figure 2.4: Diagonal and Vertical Layered Space-Time encoding with $N_t = 3$.

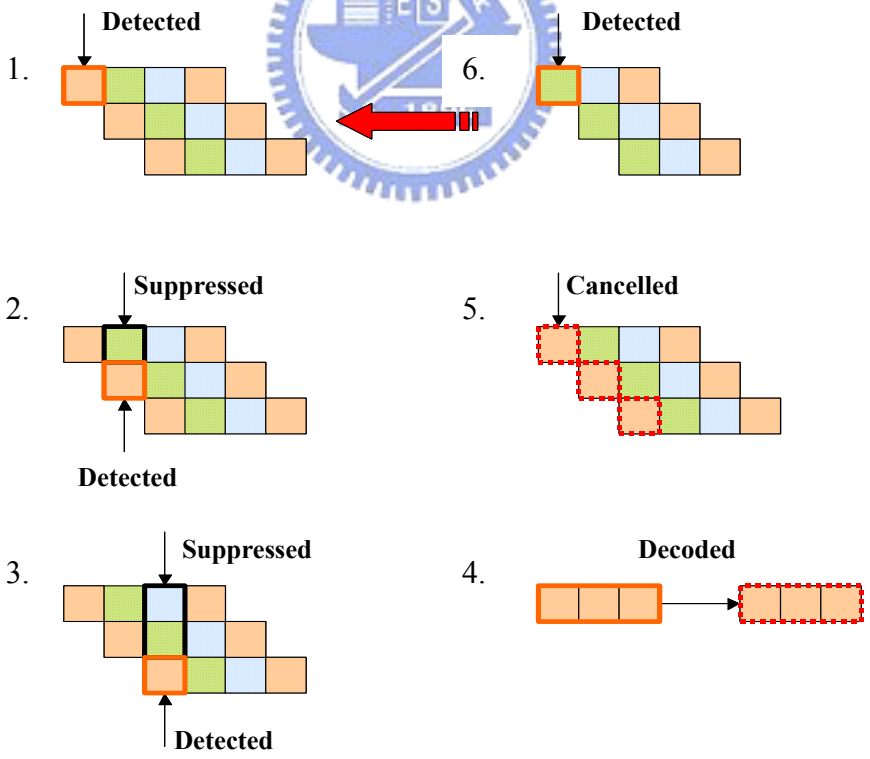

Figure 2.5: Diagonal Layered Space-Time decoding with $N_t = 3$.

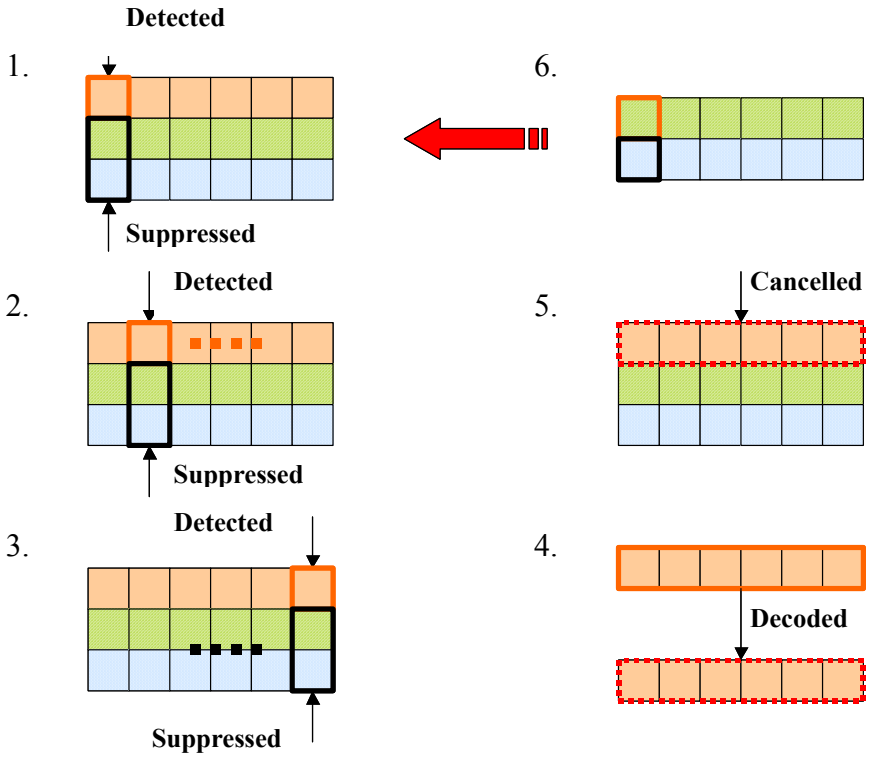

Figure 2.6: Vertical Layered Space-Time decoding with $N_t = 3$.

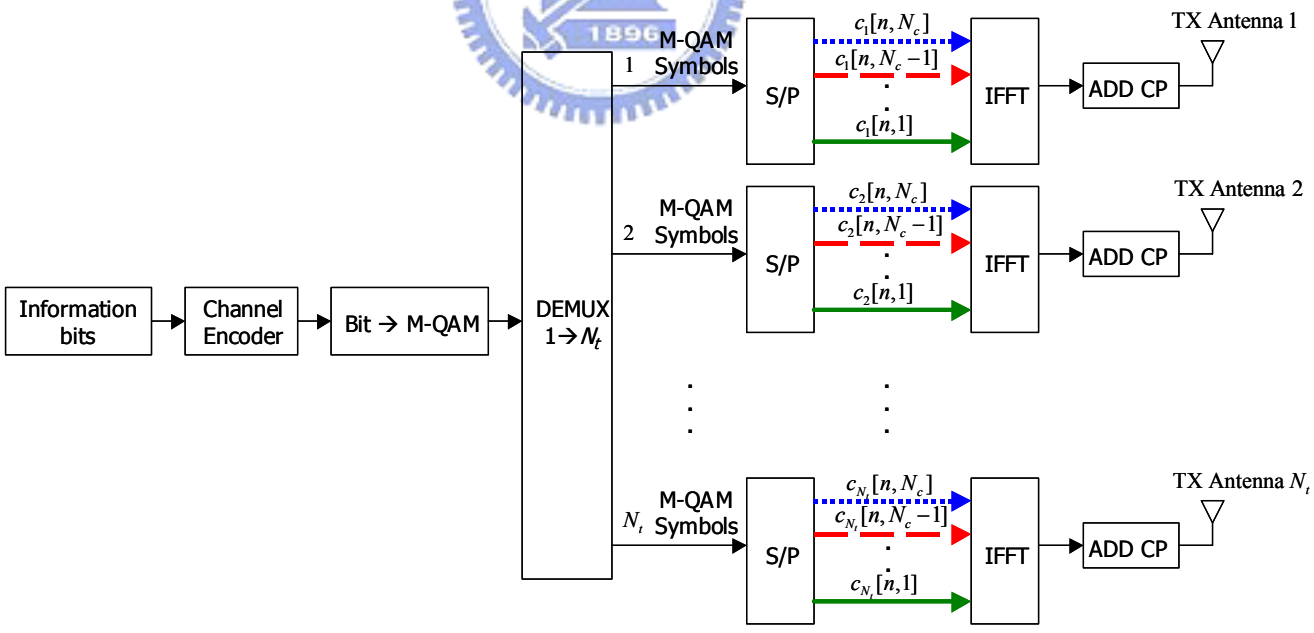

Figure 2.7: V-BLAST based MIMO-OFDM transmitter architecture.

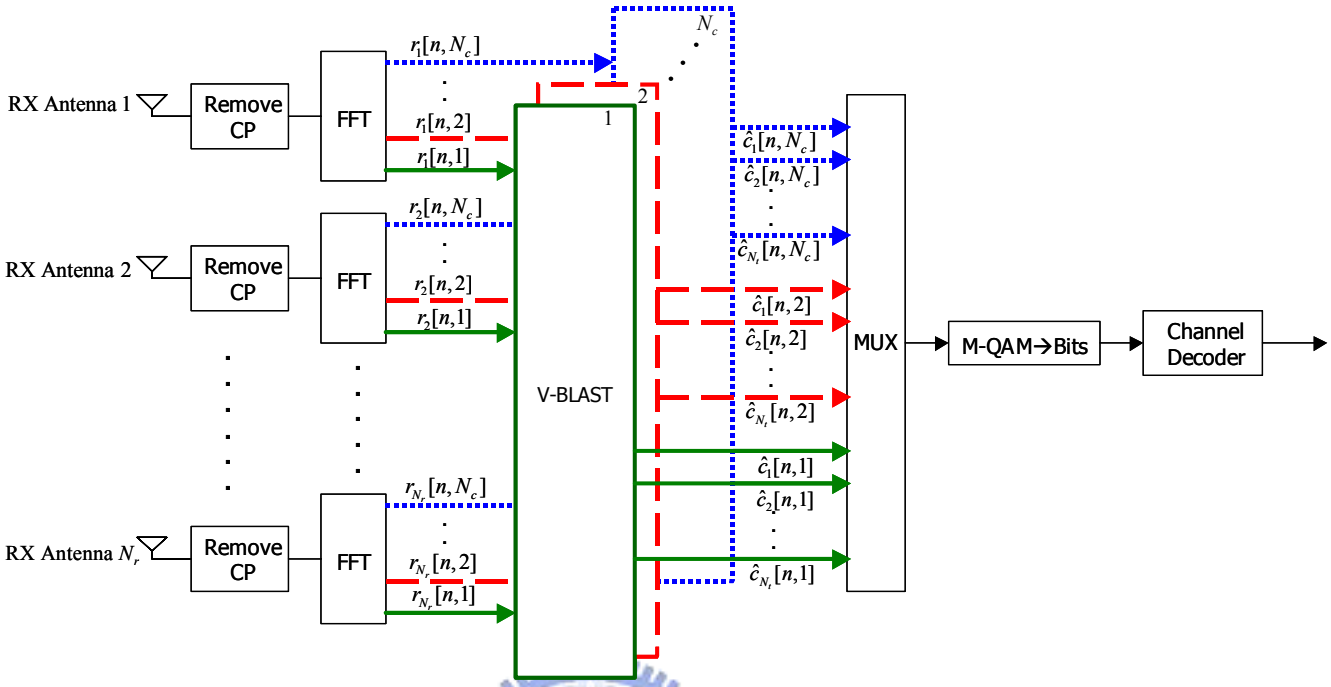

Figure 2.8: V-BLAST based MIMO-OFDM receiver architecture.

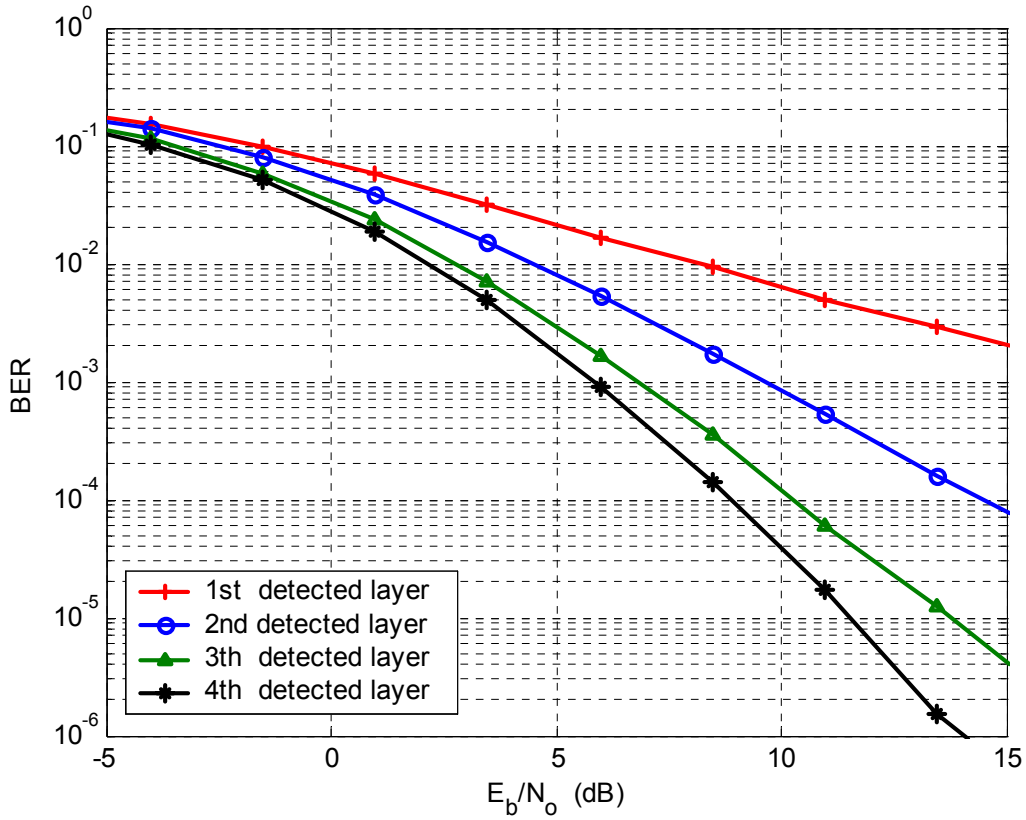

Figure 2.10: ZF V-BLAST performance with ideal detection and cancellation. QPSK modulation is used. $(Nt, N_r) = (4, 4)$.

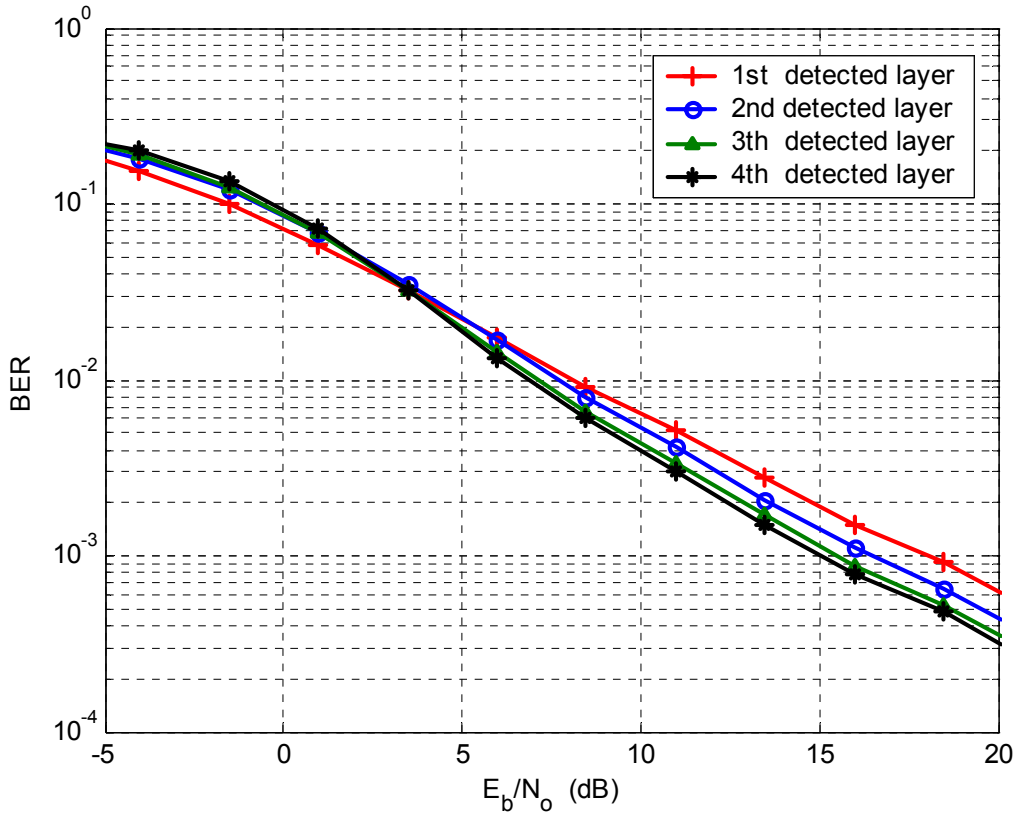

Figure 2.11: ZF V-BLAST performance with error propagation. $(N_t, N_r) = (4, 4)$. QPSK modulation is used.

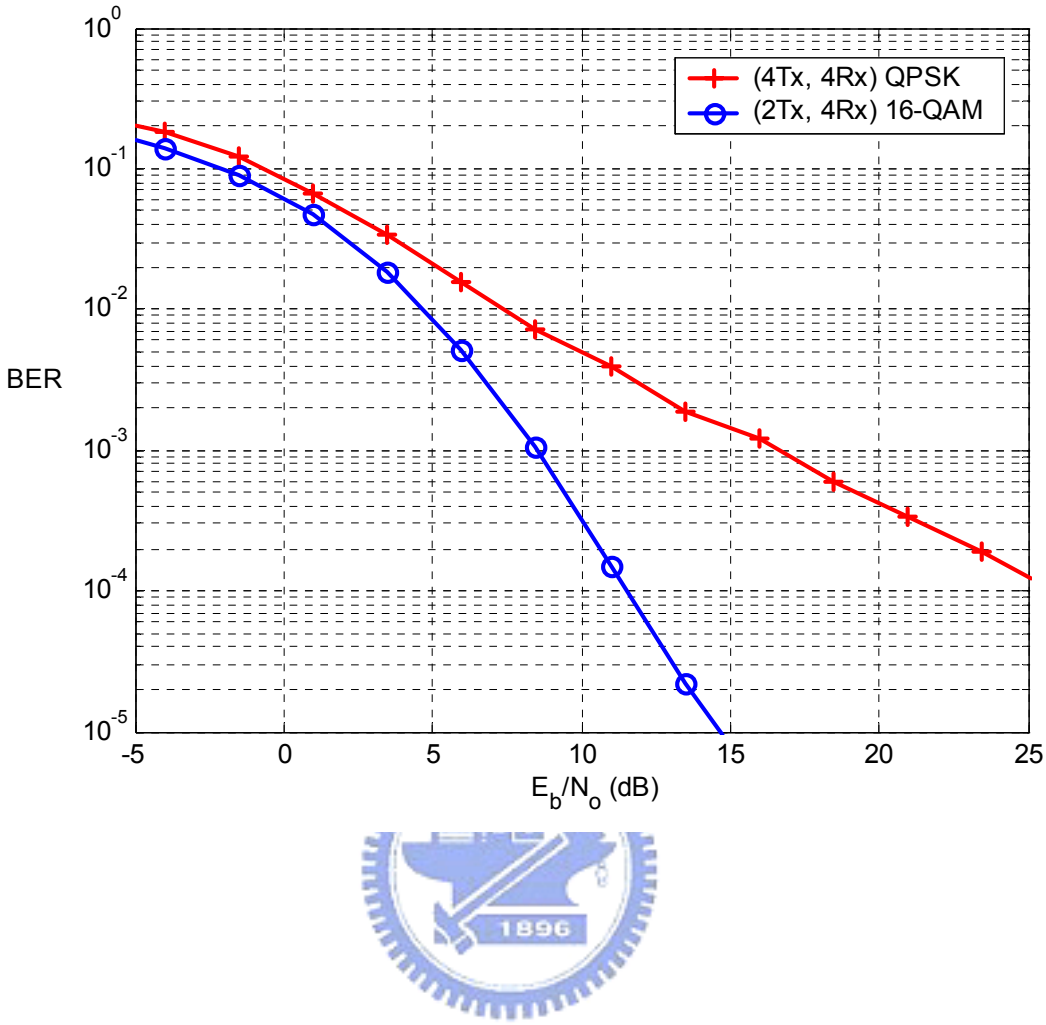

Figure 2.12: Comparison of ZF V-BLAST (N_t, N_r) = (4, 4) with QPSK modulation and (N_t, N_r) = (2, 4) with 16-QAM modulation.

Chapter 3

Adaptive Modulation Assisted MIMO-OFDM Systems

The combined application of MIMO and OFDM (MIMO-OFDM) yields a noticeable physical layer capable of meeting the requirements for 4G broadband wireless systems [17]. Thanks to OFDM, which is characterized by possessing multi-channels over frequencies, the signal processing techniques involved in MIMO-OFDM could be borrowed from the sophisticated space-time ones by admitting the virtual equivalence between time and frequency in some particular scenarios.

From the analysis of MIMO channel capacity, we figure out that the waterfilling distribution of power over channels with different SNR values achieves the optimal transmission scheme [34]. However, while the waterfilling distribution will indeed yield the optimal solution, it is difficult to compute, and also assumes infinite granularity in the constellation size, which is not practically realizable.

In this chapter, we introduce a practical adaptive loading procedure for MIMO-OFDM that uses the V-BLAST as both its channel quality indicator and detection algorithm. Bit and power are allocated in a manner to fix the total transmission power while maximizing the data rate and yet still maintaining a target system performance.

3.1 Adaptive Modulation

Wireless communication channels typically exhibit time-variant quality fluctuations and hence conventional fixed-mode modems usually suffer from bursts of error (see Figure 3.4 to get the idea). This defect could be somewhat mitigated if the system was designed to provide a high link margin, that is, determine transmission parameters based on the worst-case channel conditions to render the immunity against channel impairments. However, it results in insufficient utilization of the full channel capacity. An efficient approach of avoiding these detrimental effects is to dynamically adjust transmission parameters based on the near instantaneous channel quality information. In general, the following steps have to be taken to react to the change in channel condition for an adaptive wireless transceiver.

1. Channel quality estimation: If the communication between the two stations is bi-directional and the channel can be considered reciprocal, then each station can estimate the channel quality on the basis of received symbols, and adapt the parameters of the local transmitter to this estimation in an open-loop manner.
2. Choice of the appropriate parameters for the next transmission: The transmitter has to select the appropriate modulation mode for each sub-channel based on the prediction of the channel quality for the next timeslot.
3. Signaling of the employed parameters: The receiver has to be informed, as to which demodulator parameters to employ for the received packet. This information can be either conveyed by the transmitted signal itself, at the cost of a loss of effective data throughput, or estimated by a blind detection mechanism at the receiver.

3.2 SNR Based Switching Levels

In [7], several metrics that may be used as CSI were surveyed. Among those, SNR-based and Error-based CSI are the most commonly used ones. Typically, SNR or SINR could be available from the physical layer by exploiting power measurement in slots without intended transmit data. Approximate BERs are sometimes available via packet error rates (PERs), which are normally extracted from the cyclic redundancy check (CRC) at the link layer. These two types of CSI come with their pros and cons. SNR-based CSI offers the flexibility to adapt the modes on a very fast basis; however, it relies on the computation of switching thresholds that may be inaccurate. The accuracy of the threshold mechanism increases by taking into account higher order statistics of the SNR than just the mean. Error based CSI captures accurate performance of the modes; however, this accuracy is reached only after a substantial amount of traffic is observed. An important topic of current research is to combine all types of CSI together to yield accuracy and robustness over a wide range of channels, adaptation rates, and traffic conditions [7].

The first attempt to finding optimum switching levels that are capable of satisfying various transmission integrity requirements was mad by Webb and Steele [10]. They used the BER curves of each constituent modulation mode, obtained from simulations over an AWGN channel, to find the SNR value, where each modulation mode satisfies the target BER requirement. This intuitive concept of determining the switching levels has been widely used since then. By using this regime, the instantaneous BER always remains below a certain threshold BER ε_{error}. In order to satisfy this constraint, the first modulation mode should be "no transmission". In this case, the set of switching levels **T** (in dB) is given by

$$\mathbf{T} = \left\{ t_0 = -\infty,\ t_k \mid \varepsilon_{m_k}(t_k) = \varepsilon_{error},\ \forall k \geq 1 \right\} \tag{3.1}$$

where $\varepsilon_{m_k}(\gamma)$ is the BER of the m_k-ary constituent modulation mode over the AWGN channel when the instantaneous SNR, used as the channel quality measure, is γ. We use 7-mode AQAM, i.e. No TX, BPSK, QPSK, 8-QAM, 16-QAM, 32-QAM, and 64-QAM as constituent modulation modes. Their signal constellation diagrams and BER curves are depicted in Figure 3.5 and Figure 3.6. Throughout the following discussions, we will follow this method and concentrate on the case of $\varepsilon_{error} = 0.0001$, which is commonly required for low-BER data transmission systems. A set of switching thresholds according to Figure 3.6 is given in Table 3.2, which is independent of the underlying fading and the average SNR.

3.3 Adaptive MIMO-OFDM Systems

In a system with multiple antennas at the transmitter and/or receiver, the SNR not only varies over time and frequency but also depends on a number of parameters including the way the transmitting signals are mapped and weighted onto the transmit antennas, the processing techniques used at the receiver, and some propagation related parameters such as the pairwise antenna correlation. In this section, we consider a space-time-frequency scheme, that is V-BLAST based MIMO-OFDM as describe before, and develop a practical LA procedure that integrate temporal, spatial, and spectral components together.

Our problem is to assign bits and power to each sub-channel to maximize data rate for some given power budget and a target BER. The main feature of our approach is to separate the joint space-frequency problem into two separated ones by treating each OFDM tone as a narrow band MIMO. We demonstrate by computer simulations that the V-BLAST based MIMO-OFDM system works well to satisfy the system target BER even in the low SNR scenarios at the cost of degrading transmission rate.

Seeing that a discrete rate set should be used in a practical communication system, a loading criterion for discrete rate is required instead of using the water-filling solution derived by maximizing Shannon capacity. However, a close form solution for optimal discrete rate and power control could not be found and an exhaustive search over the set of rates and powers is too complicated to be conducted in a real time. Hence, some bit loading algorithms were proposed to obtain an optimal (or near optimal) solution [25]-[27]. On account of simplicity and capability, when applying bit loading in the MIMO-OFDM system, we promote that Campllo's loading criteria [27] could be somewhat modified and extended to the V-BLAST based adaptive MIMO-OFDM system with reasonable computation complexity.

The joint space-frequency bit loading problem should be taken apart into two separated sub-problems for the following reasons:

1. The active sub-channels should be predetermined before a full search over $N_c \times N_t$ sub-channels to avoid the unpredictable manner introduced by the V-BLAST detection algorithm.
2. By taking the joint loading problems apart into two smaller ones, the sorting complexity is significantly reduced.

Hence, at the first stage, the loading algorithm is applied to each subcarrier to obtain an optimal bit and power allocation over its N_t spatial channels. At the second stage, the same loading algorithm is processed over those active sub-channels surviving from the first stage (at most $N_t \times N_c$). The two-stages procedure are described as follows:

Stage 1:

For each sub-band k (containing N_t spatial channels), our allocation problem could be stated as follows:

$$\max \sum_{i=1}^{N_t} b_i[k] \quad \text{subject to} \quad \begin{cases} \sum_{i=1}^{N_t} P_i[k] \le P_{budget} \\ \varepsilon_i[k] \le \varepsilon_{error} \quad \forall i \end{cases} \tag{3.2}$$

where $b_i[k]$, $P_i[k]$, and $\varepsilon_i[k]$ are the rate (in bits/symbol), allocated power, and error probability, respectively, of the *i*th transmit antenna at the *k*th subcarrier, ε_{error} is the target BER, and P_{budget} is the total power constraint (P_{budget} is normalized to 1 in our simulation to guarantee a fair comparison between systems equipped with different transmit antennas). In general, *b* should be restricted to an integer number when the practicability is under consideration. However, if we define *b* as information rate, a system using a specified channel encoder along with different puncturing rate will make *b* equivalent to some fraction numbers. For example, if we use a convolution encoder to encode a sequence of source bits and puncture output bits to rate 3/4, and then modulate them by using QPSK, *b* will be equivalent to 3/2. To facilitate our descriptions, we start with the case without channel coding.

A. Initialization

1. Set *q*, defined as the state of the N_t transmit antennas according to their active modes, to be $2^{N_t} - 1$ at the first iteration. To realize what *q* denotes, we give an example. Assuming that four antennas are available at the transmitter side, if we select three of them, e.g. the 1st, 2nd, and 4th antennas to be active, the state *q* will become 13, which is the result of converting the corresponding active-mode vector [1, 1, 0, 1] to a decimal number. Let $\text{Rate} = 0$ and $P_{residual\_final} = P_{budget}$.

2. Load equal power on those $N_{t,active}[k]$ active transmit antennas such that

$$P_{i\_active}[k] = \frac{P_{budget}}{N_{t\_active}[k]} \quad \forall 1 \le i\_active \le N_{t,active} \tag{3.3}$$

3. Calculate the post-processing SNR of each active layer

$$\rho_{i\_active}[k] = \frac{P_{i\_active}[k]}{\sigma^2 \,\|\, \mathbf{w}_{i\_active}[k] \,\|^2} \tag{3.4}$$

4. Clip the power of each layer and thereby reduce its SNR to fit the nearest threshold below it (assumed to be t_k in Equation 3.1) by consulting the threshold table, and collect the residual power

$$P_{i\_active}[k] \leftarrow \frac{P_{i\_active}[k] \times 10^{(t_k/10)}}{\rho_{i\_active}[k]} \tag{3.5}$$

$$P_{residual}[k] = P_{budget} - \sum_{i=1}^{N_{t,active}[k]} P_{i,active}[k] \tag{3.6}$$

B. Power-Tighten

1. Since this step is valid for all subcarriers, we drop the index k for the following expressions. Let $\Delta p_i(b_i)$ be the power required for ith layer to increase rate from $b_i - 1$ to b_i. $\Delta p_i(b_i)$ is defined as

$$\Delta p_i(b_i) = \begin{cases} P_i \times 10^{\frac{\left(t_{b_i} - t_{b_i-1}\right)}{10}} - P_i, b_i > 1 \\ 10^{\frac{t_{b_i}}{10}} \qquad\qquad\qquad , b_i = 1 \end{cases} \tag{3.7}$$

We construct a power increment table containing $\Delta p_i(b_i + 1)$ and $\Delta p_i(b_i)$ $\forall\, 1 \le i \le N_{t,active}$ to record the least amount of power needed to step from current transmission mode into the next higher-rate mode.

2. Following the principle: A bit distribution is said to be Power-tighten if

$$0 \le P_{budget} - \sum_{i=1}^{N_t} P_i \le \min_{1 \le i \le N} [\Delta p_i(b_i + 1)] \tag{3.8}$$

3. $m = \arg\left\{ \min_{1 \le i \le N_{t,active}} [\Delta p_i(b_i + 1)] \right\}$

4. While $p_{residual} > \Delta p_m(b_m + 1)$

(a) $P_m \leftarrow P_m + \Delta p_m(b_m + 1)$

(b) $p_{residual} \leftarrow [p_{residual} - \Delta p_m(b_m + 1)]$

(c) $b_m \leftarrow b_m + 1$

(d) $m = \arg\left\{\min_{1 \le i \le N_{t,active}} [\Delta p_i(b_i + 1)]\right\}$

C. Power-Efficientizing

1. Following the principle: A distribution is said to be efficient if

$$\max_i [\Delta p_i(b_i)] \le \min_i [\Delta p_i(b_i + 1)] \tag{3.9}$$

2. $m = \arg\left\{\min_{1 \le i \le N_{t,active}} [\Delta p_i(b_i + 1)]\right\}$, and $n = \arg\left\{\max_{1 \le i \le N_{t,active}} [\Delta p_i(b_i)]\right\}$

3. If $n = m$

(a) $l = \arg\left\{\min_{1 \le i \ne m \le N_{t,active}} [\Delta p_i(b_i + 1)]\right\}$, and $j = \arg\left\{\max_{1 \le i \ne n \le N_{t,active}} [\Delta p_i(b_i)]\right\}$

(b) if $\Delta p_n(b_n) - \Delta p_l(b_l + 1) > \Delta p_j(b_j) - \Delta p_m(b_m + 1)$; $m \leftarrow l$

else $n \leftarrow j$

4. While $\Delta p_n(b_n) > \Delta p_m(b_m + 1)$

(a) $b_m \leftarrow b_m + 1$, $b_n \leftarrow b_n - 1$

(b) $P_m \leftarrow P_m + \Delta p_m(b_m + 1)$, $P_n \leftarrow P_n - \Delta p_n(b_n)$

(c) $p_{residual} \leftarrow [p_{residual} + \Delta p_n(b_n) - \Delta p_m(b_m + 1)]$

(d) $n \leftarrow \arg\left\{\max_{1 \le i \le N_{t,active}} [\Delta p_i(b_i)]\right\}$; $m \leftarrow \arg\left\{\min_{1 \le i \le N_{t,active}} [\Delta p_i(b_i + 1)]\right\}$

(e) If $n = m$

i. $l = \arg\left\{\min_{1 \le i \ne m \le N_{t,active}} [\Delta p_i(b_i + 1)]\right\}$, and $j = \arg\left\{\max_{1 \le i \ne n \le N_{t,active}} [\Delta p_i(b_i)]\right\}$

ii. if $\Delta p_n(b_n) - \Delta p_l(b_l + 1) > \Delta p_j(b_j) - \Delta p_m(b_m + 1)$; $m \leftarrow l$

else $n \leftarrow j$

Since it makes no sense to add and remove one bit in the same channel at the same time, the case $n = m$ should be discarded in (e) to avoid this contradiction.

D. Comparing and Recording

1. If (all the predetermined active layers remain surviving)

If $\sum_{i=1}^{N_t} b_i \geq \text{Rate}$

If $P_{residual} > P_{residual\_final}$

$\text{Rate} = \sum_{i=1}^{N_t} b_i$; $P_{residual\_final} = P_{residual}$

else $q \leftarrow q - 1$

else $q \leftarrow q - 1$

else $q \leftarrow q - 1$

In this stage, we do an exhaustive search to determine which transmit antennas should be active to support the optimal bit and power allocation for every subcarrier. Therefore, given a subcarrier, we should examine $2^{N_t} - 1$ possible combinations, which seem to be a time-consuming task. Fortunately, the needed effort can be eased due to the causality between every possible combination. For example, given a subcarrier, if we assume that the procedure starts with searching the antenna state [1, 1, 1, 1] and finally converges to the state [1, 0, 1, 0], then the following search starts with the antenna state [1, 0, 1, 0] will lead to the same result, thus can be omitted.

Stage 2:

In this stage, the algorithms *B* and *C* are reused for those sub-channels (both frequency and spatial channels) surviving from the first stage to further exhaust the total residual power, that is $\sum_{k=1}^{N_c} P_{residual}[k]$, to get a rate enhancement.

B. Power-Tighten

$$0 \le N_c \cdot P_{budget} - \sum_{i=1}^{N_t} \sum_{k=1}^{N_c} P_i[k] \le \min_{1 \le i \le N_t; 1 \le k \le N_c} [\Delta p_i[k](b_i[k]+1)] \tag{3.10}$$

C. Power-Efficientizing

$$\max_{i;k}[p_i[k](b_i[k])] \le \min_{i;k}[p_i[k](b_i[k]+1)] \tag{3.11}$$

3.4 Computer Simulations

In this section, computer simulations are conducted to evaluate the performance of the V-BLAST based adaptive MIMO-OFDM system. Throughout the simulation, we only deal with the discrete time signal processing in the baseband, hence pulse-shaping and matched-filtering are removed from consideration for simulation simplicity. Also, channel estimation and timing synchronization are assumed to be perfect. Table 3.3 lists all parameters used in our simulation. The configuration we consider here is a MIMO-OFDM system with a bandwidth of 20 MHz and 64 subcarriers. The set of QAM constellation used in the simulation is {0, 2, 4, 8, 16, 32, and 64}, i.e. $\Delta b = 1$. Each link in MIMO is modeled as an exponential decay Rayleigh fading channel with $\tau_{rms} = 50\ ns$.

Firstly, a look-up table that contains the SNR threshold values of each modulation mode should be established. These threshold values could be obtained from Figure 3.6 by consulting each BER curve to find the corresponding SNR value that meets the BER requirement (10^{-4} in our simulations).

Figure 3.10 shows the selection probability of each modulation mode at different SNRs. It's obvious that higher order modulation modes are preferred as the average channel SNR increases. In the low SNR scenario, the adaptive loading procedure forces

some of transmit antennas to be blocked frequently to avoid inefficient or unreliable transmission in order to meet the target BER requirement.

In Figure 3.11, we record the unutilized power ratio after the two-stage loading procedure to give an insight into the system. It can be found that in both the low (< 2 dB) and high (> 30 dB) SNR environments, much power remains unused. This is because that at low SNR, most sub-channels suffer from ill conditions so that they are turned off to save power. On the other hand, at high SNR, most sub-channels are fully loaded with little power consumption, hence there is extra power remaining. The residual power could be effectively used to achieve a higher performance margin by uniformly assigning them to those active sub-channels. In Figure 3.12, we see a significant BER improvement benefiting from the residual power at high SNRs.

3.5 Summary

In this Chapter, we introduce an adaptive MIMO-OFDM system to present a new viewpoint in which SM and SD are complementary rather than competing approaches. For instance, users closer to the transmitter are more likely to experience channel conditions preferring SM, assuming that scattering remains rich enough. For channels less suitable for SM, then the system will instead use SD. The flexibility in switching between SM and SD is realized by the use of adaptive modulation. In this system, the SD comes from the fact of more receive antennas than transmit antennas, under which the bit loading procedure can be deployed by excluding ill transmit antennas. In this case, more diversity gain could be extracted from the V-BLAST scheme. Moreover, by adjusting the transmission parameters to prevent ill-conditioned sub-channels from dominating the system performance, an indirect form of diversity is also drawn.

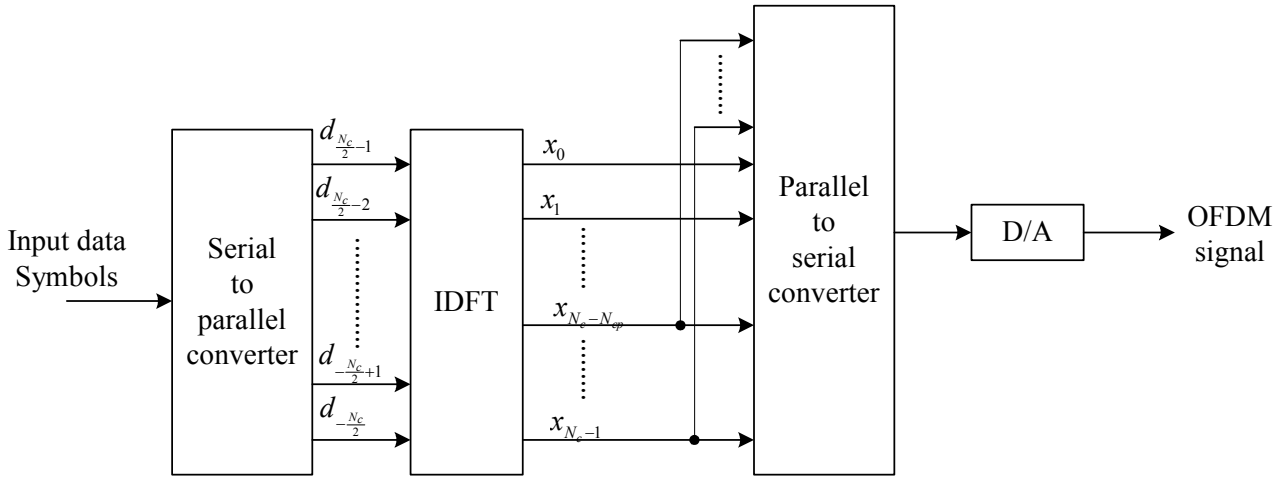

Figure 3.1: A digital implementation of appending cyclic prefix into OFDM signal in the transmitter.

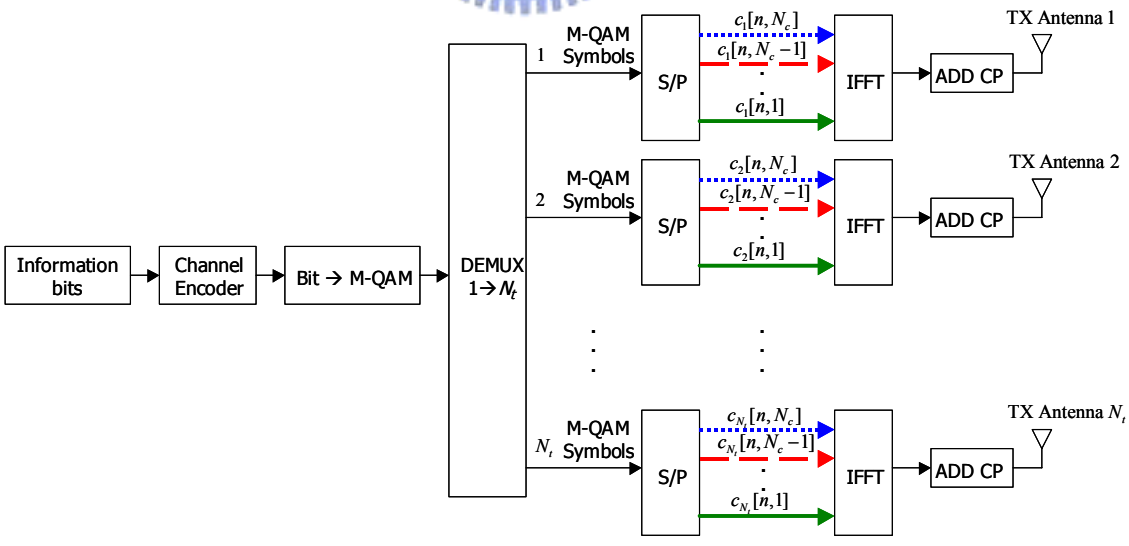

Figure 3.2: V-BLAST based MIMO-OFDM transmitter architecture.

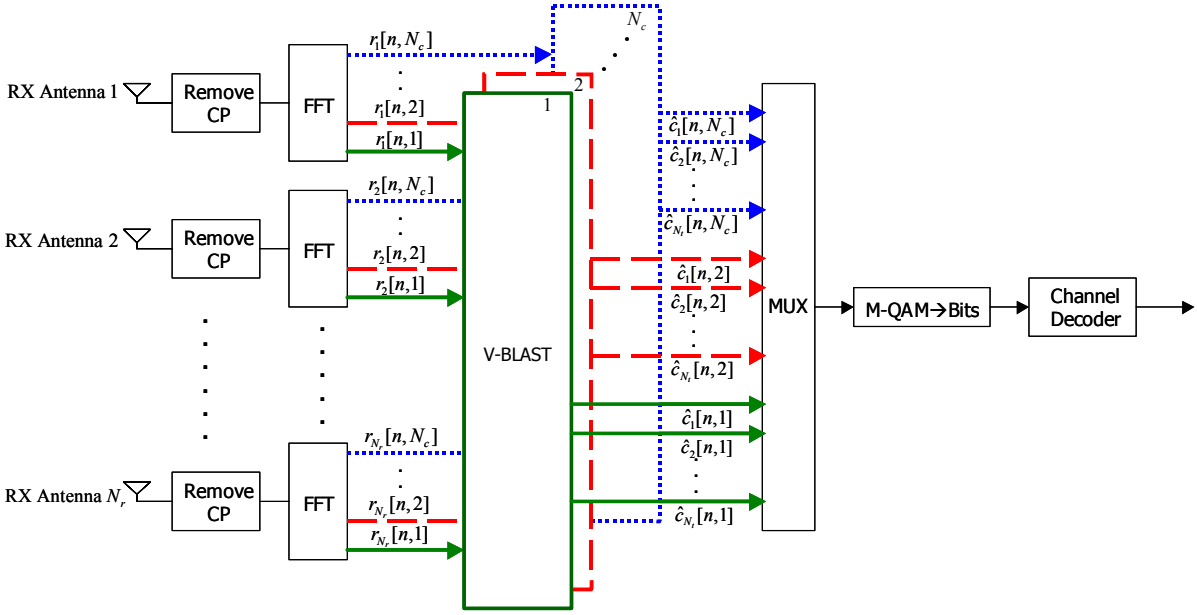

Figure 3.3: V-BLAST based MIMO-OFDM receiver architecture.

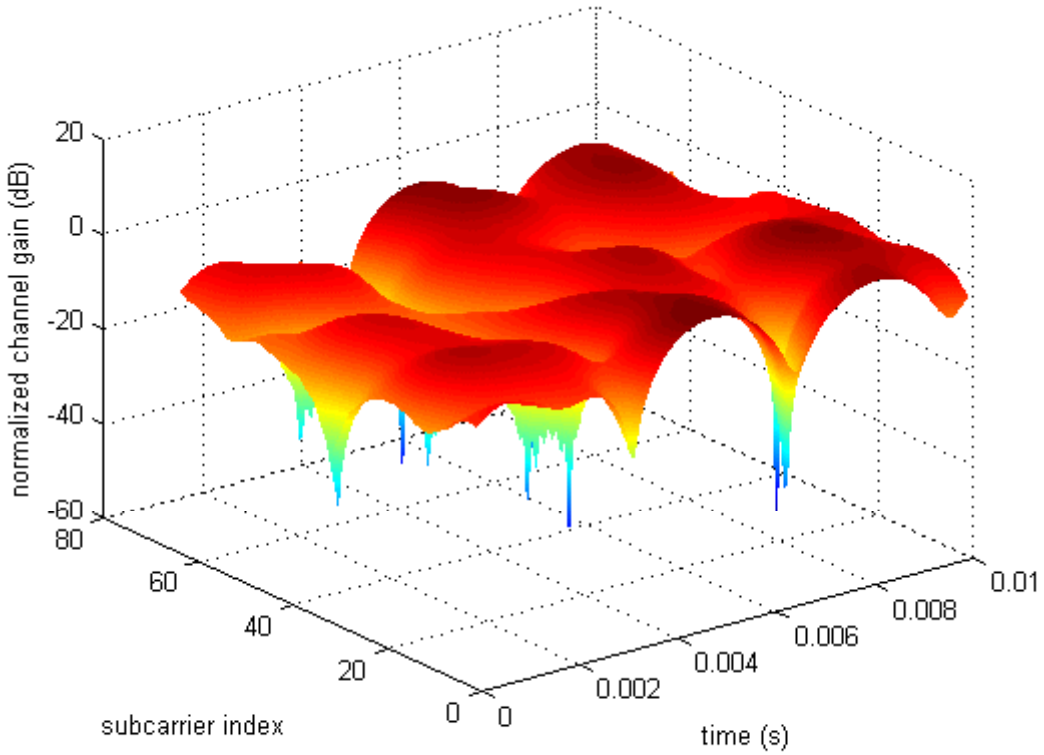

Figure 3.4: A typical time and frequency selective fading channel. (By assuming an exponential decay channel model with $\tau_{rms} = 50\ ns$ and a speed of 15 m/s at 5 GHz).

BPSK

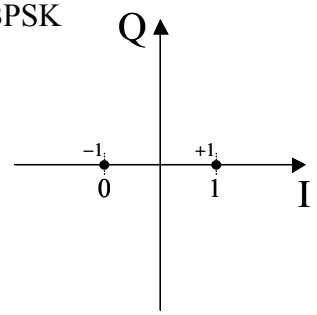

QPSK

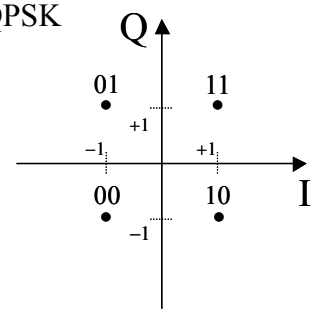

8-QAM

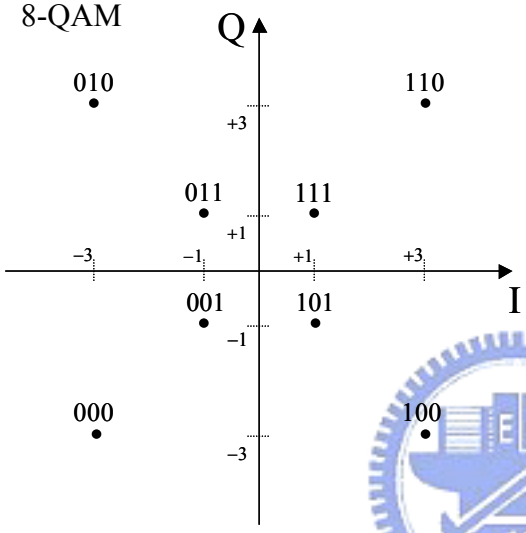

16-QAM

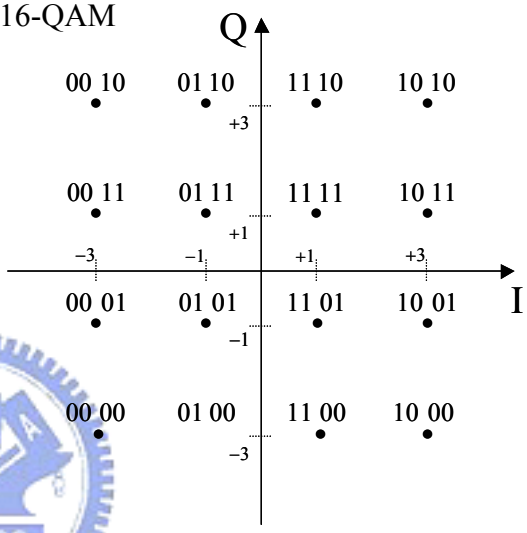

32-QAM

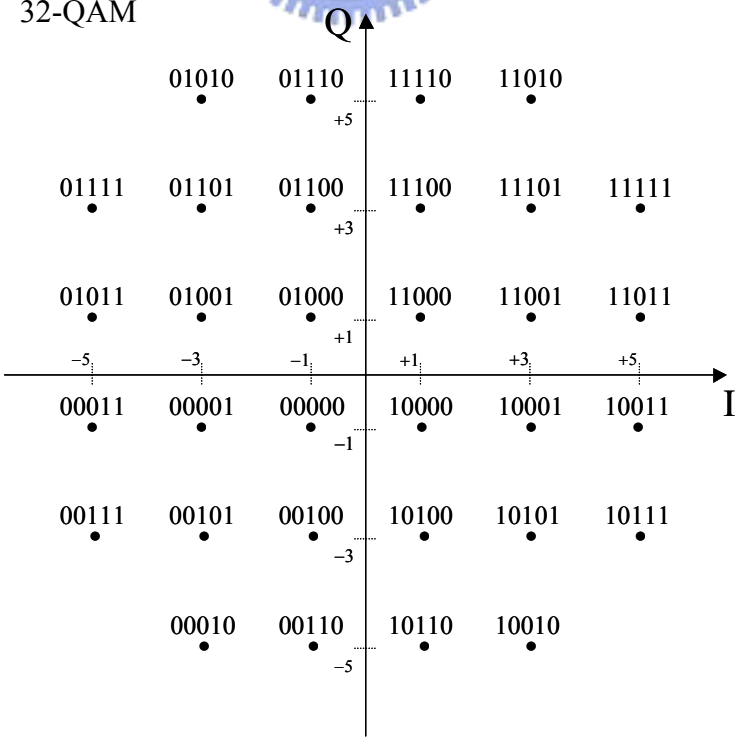

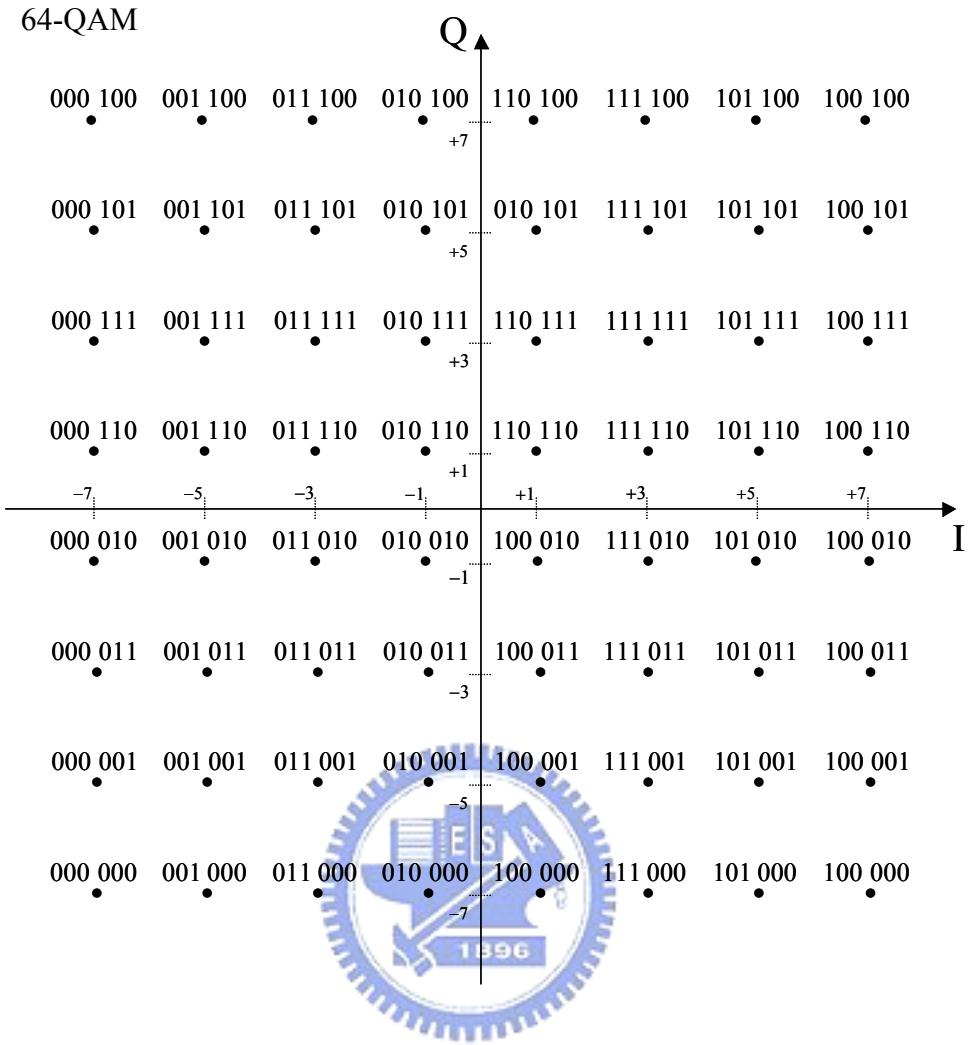

Figure 3.5: BPSK, QPSK, 8-QAM, 16-QAM, 32-QAM, and 64-QAM constellation diagrams.

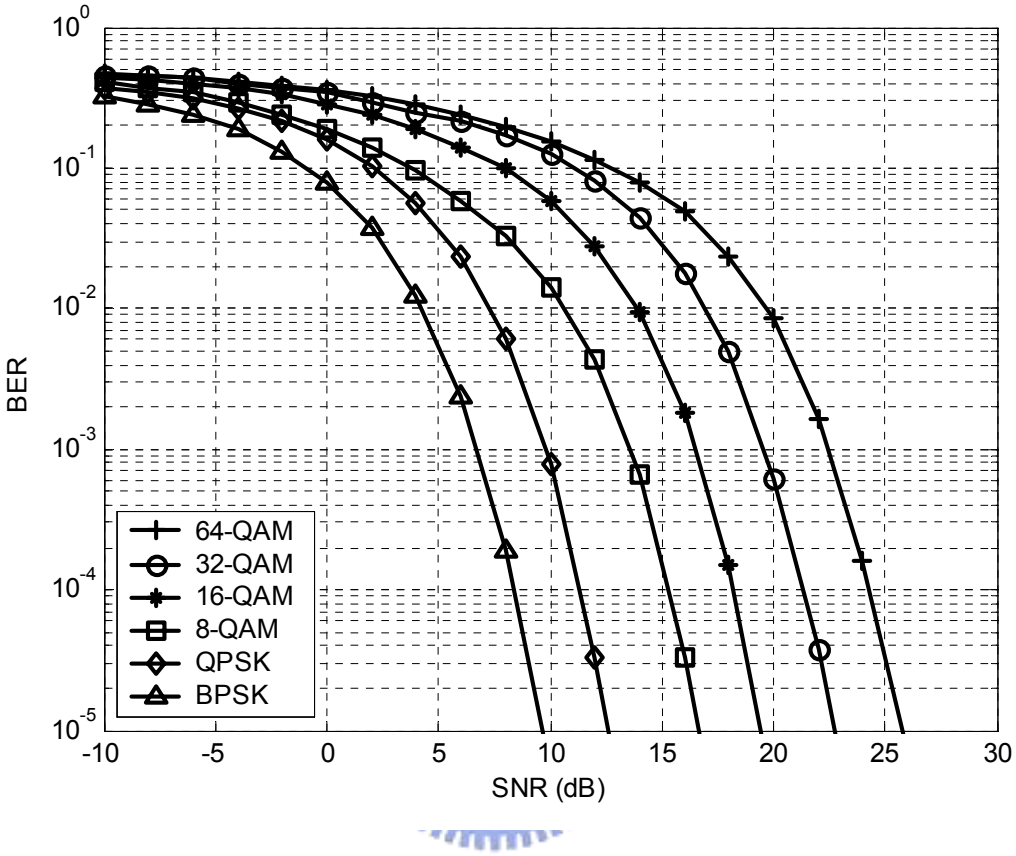

Figure 3.6: The average BER of various M-QAM modulation schemes over AWGN channel.

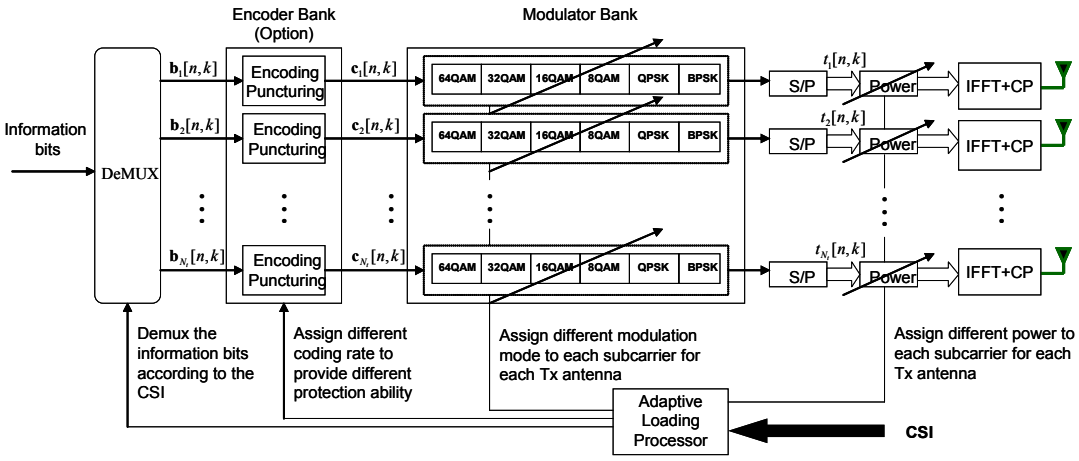

Figure 3.7: V-BLAST based adaptive MIMO-OFDM system transmitter architecture.

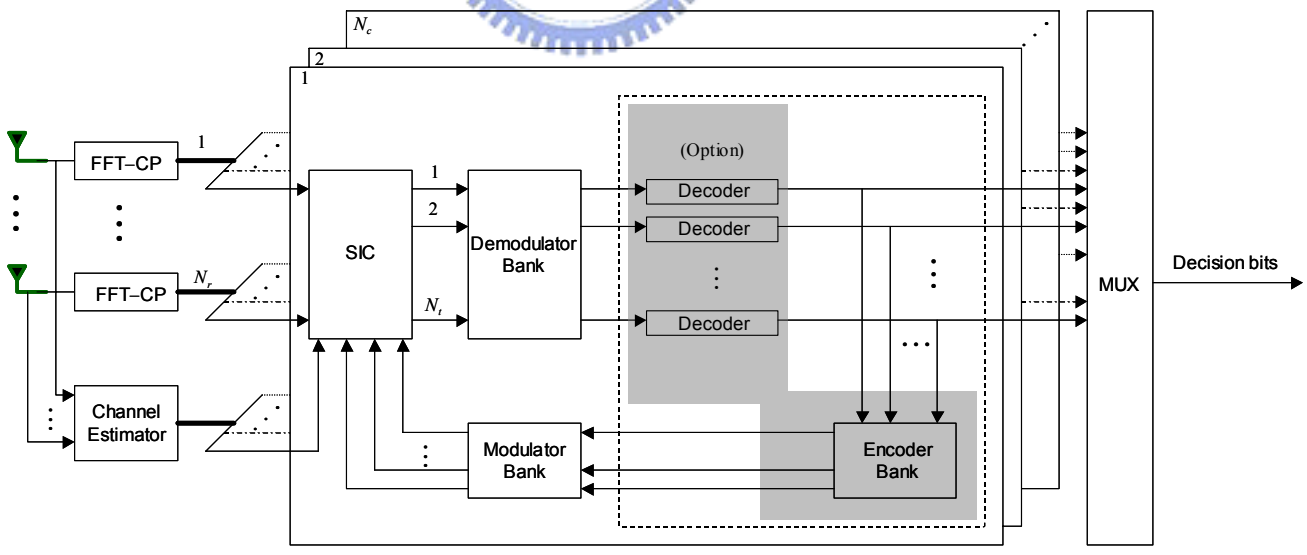

Figure 3.8: V-BLAST based adaptive MIMO-OFDM system receiver architecture.

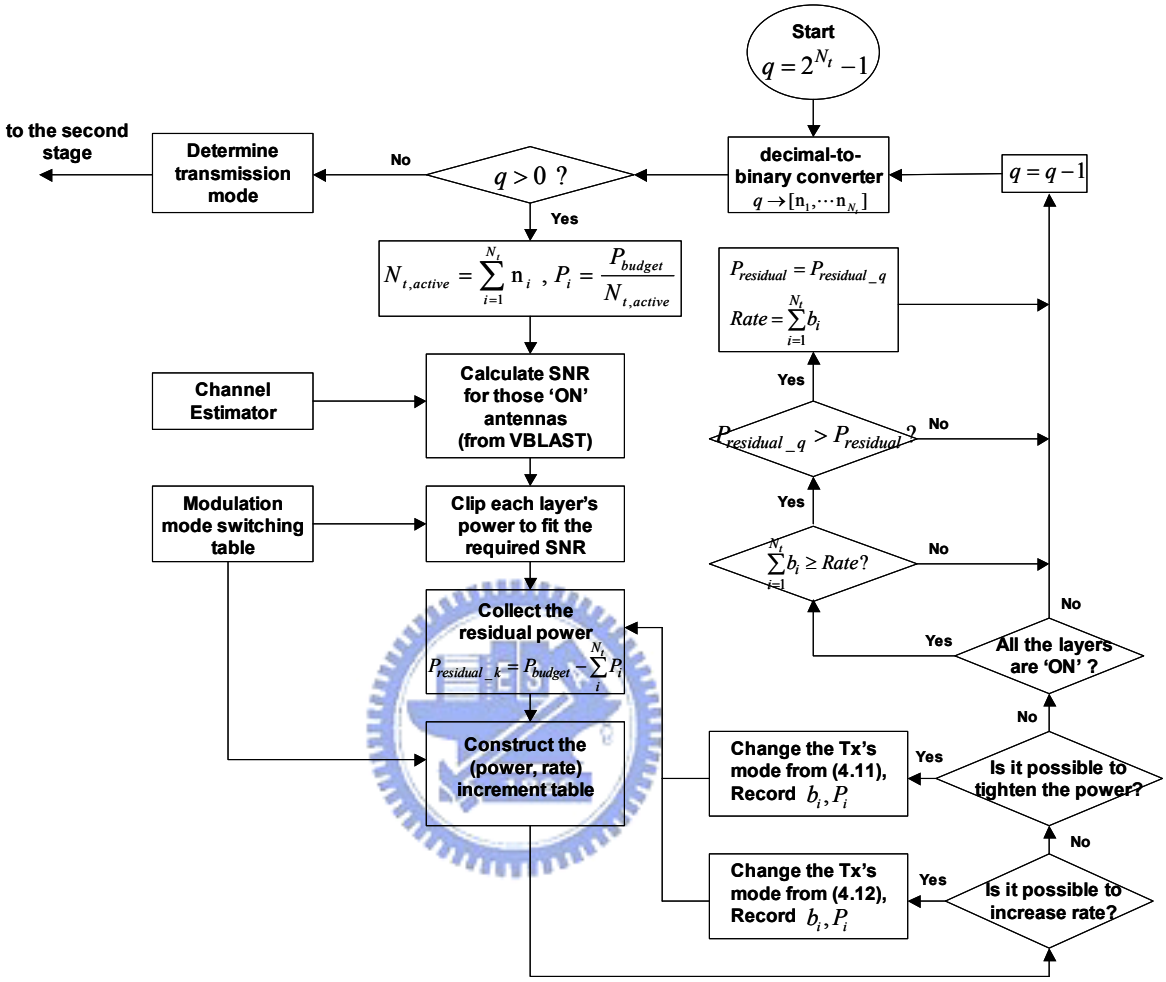

Figure 3.9: The first stage bit loading procedure flow chart.

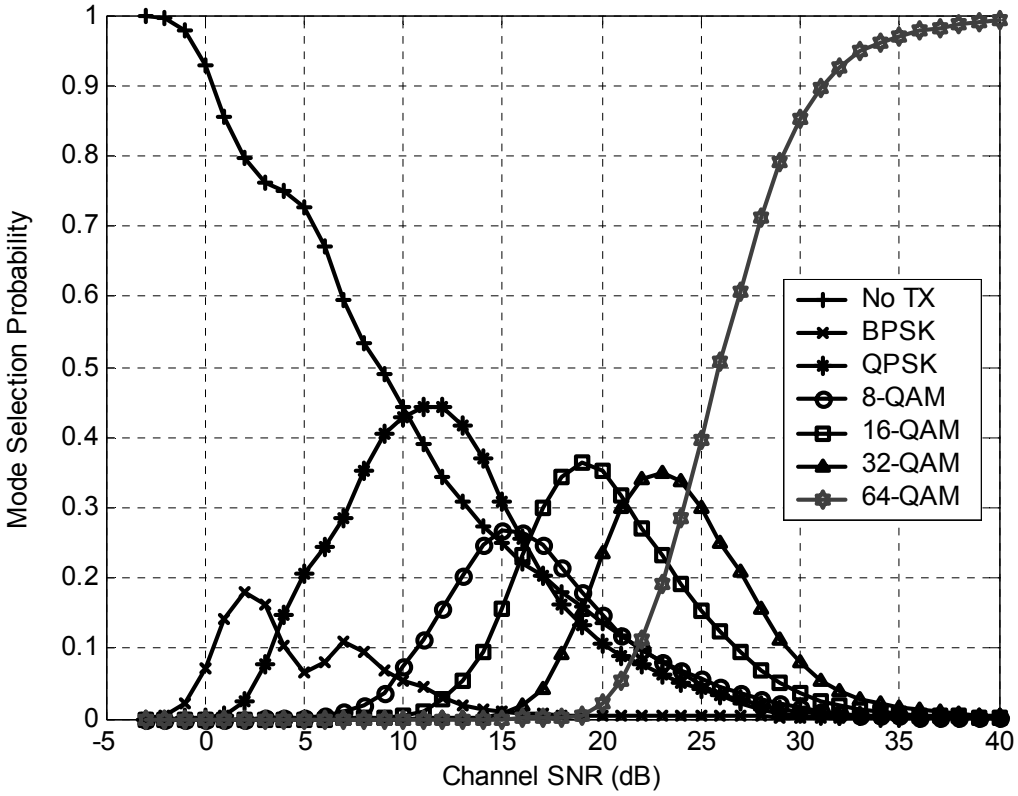

Figure 3.10: Simulated probabilities of each modulation mode utilized by the ZF V-BLAST based adaptive MIMO-OFDM system (with space loading) in the exponentially decay Rayleigh fading channel with τ_{rms} =50 *n*s. $f_d = 0$ Hz. $(N_t, N_r) = (4,4)$. Other simulation parameters are listed in Table 3.3.

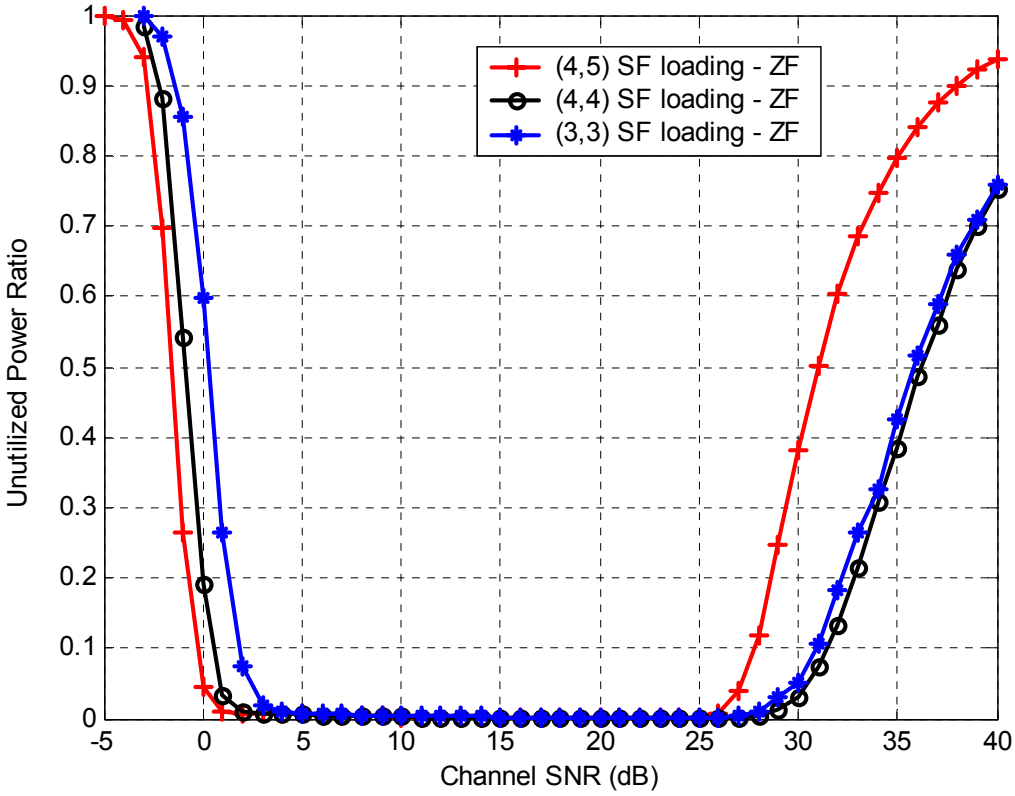

Figure 3.11: Unutilized power ratio in the V-BLAST based adaptive MIMO-OFDM system (with space-time loading) at different channel SNRs. Exponential decay Rayleigh fading channel with $\tau_{rms} = 50\ ns$. $f_d = 0$ Hz . $(N_t, N_r) = (4,5),\ (4,4)$, and $(3,3)$. Other parameters are listed in Table 3.3.

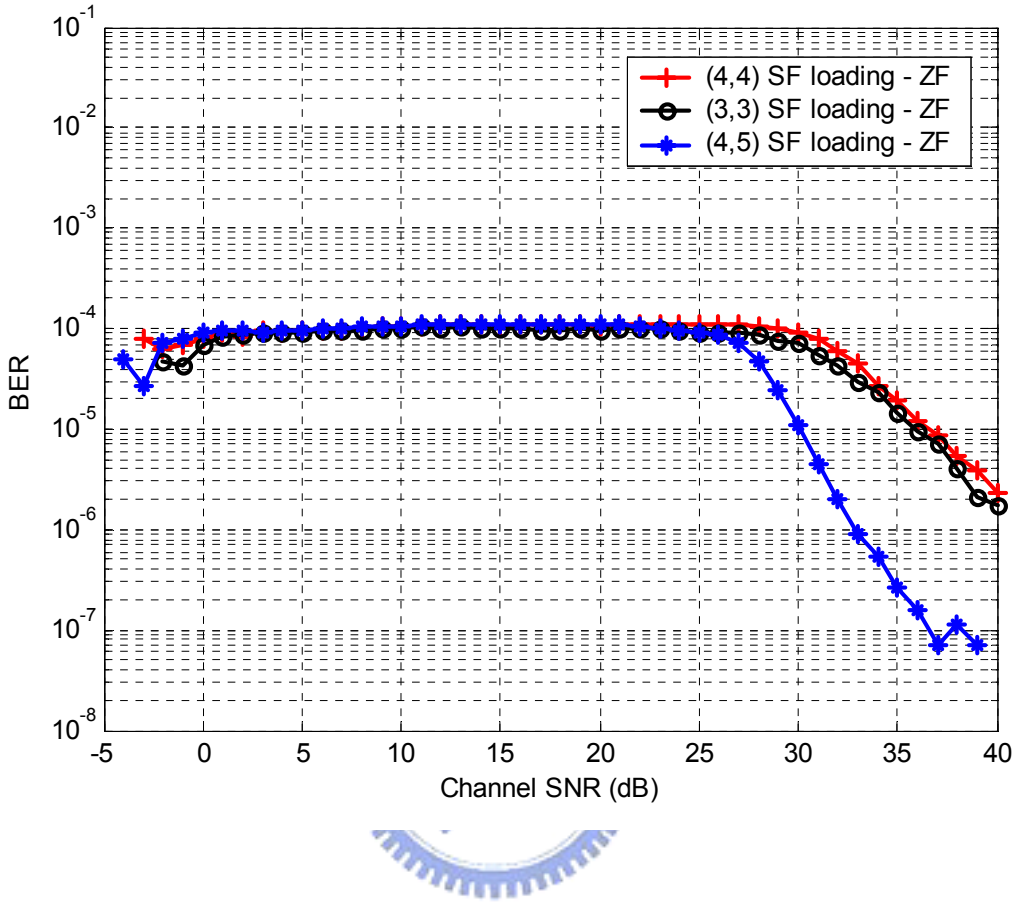

Figure 3.12: BER versus average channel SNR for the ZF V-BLAST based adaptive MIMO-OFDM system (with space-frequency loading) in an exponential decay Rayleigh fading channel with $\tau_{rms} = 50\ ns$. $f_d = 0$ Hz . $(N_t, N_r) = (4,5),\ (4,4)$, and $(3,3)$. Other parameters are listed in Table 3.3.

Table 3.1: Simulation parameters of the V-BLAST based OFDM system.

Number of transmit/receive antennas	3/3, 4/4, and 4/5
Carrier frequency	5 GHz
Modulation	QPSK
Number of FFT points	64
Guard interval	16 samples
Channel model	Exponential decay Rayleigh fading
Delay spread	$\tau_{rms} = 50$ ns
Bandwidth	20 MHz

Table 3.2: SNR threshold table for various M-QAM at the target BER=10^{-4}.

	No TX	BPSK	QPSK	8-QAM	16-QAM	32-QAM	64-QAM
S	$-\infty$	8.41	11.37	15.51	18.53	21.63	24.82

Table 3.3:Simulation parameters for the proposed V-BLAST based adaptive MIMO-OFDM system.

Number of transmit/receive antennas	3/3, 4/4, 4/5
Carrier frequency	5 GHz
Bandwidth	20 MHz
Number of carriers, FFT size	64
OFDM symbol duration	3.2 μ s
Guard interval	0.8 μ s
M-QAM available	0,1,2,3,4,5,6
Number of OFDM symbols in a packet	120
Channel model	Exponential delay profile, $\tau_{rms} = 50$ ns

Chapter 4

Cross-Layer Protection Strategies for AMC Over IEEE 802.11 MIMO WLANs

The evolution of the communications space will rely on the design of next generation wireless communication systems based on a whole new concept of fast, reconfigurable networks, supporting features such as high data rates, quality of service (QoS), adaptability to varying channel conditions, and integration of a number of wireless access technologies, depending on the exploitation of new resources such as cross-layer and contextual information. The system performance of future wireless networks will be enhanced by cross-layer joint design between physical layer and MAC layer.

In this chapter, instead of considering AMC at the physical layer and several protection strategies at the MAC layer separately, we pursue a cross-layer design that combines these two layers judiciously to maximize spectral efficiency, or throughput, under prescribed delay and error performance constraints. We also evaluate different error control and adaptation mechanisms available in the different layers for transmission, namely MAC retransmission strategy, modulation order, channel coding and adaptive packetization strategies.

4.1 The Concept of Cross Layer Design

The system performance of future wireless networks will be enhanced by cross-layer joint design between multiple protocol layers [32]. To this end, current research efforts focus on identifying the most promising approaches, and the requirements and challenges associated with their incorporation in future wireless systems design. In order to allow wireless communication transceivers to operate in a multi-parametric continuously changing environment, reconfigurable adaptive techniques to adjust the transmit parameters of transceivers and achieve the best performance need to be devised. Reconfigurability in smart antenna (a special form of MIMO) transceivers can be viewed as the capability of intelligent switching between transceiver architectures with varying performance in a certain parameter of interest. One example could be the design of an algorithm that exploits the fundamental trade-off between spatial diversity and multiplexing in MIMO channels. Novel approaches have been proposed recently that achieve reconfigurability by introducing parameterization in the transceiver design with respect to the parameters against which reconfiguration is to be performed, such as antenna correlation and CSI reliability [32][36].

The system performance can be enhanced by interacting with the higher layers of the open systems interconnection model of the International Standards Organization (OSI/ISO) protocol stack. Smart antenna techniques can be developed combining parameters in the physical, link (medium access control, MAC; data link control, DLC; scheduling, etc.), and network layers (radio resource management, routing, transport, etc.); that is, in a cross-layer fashion rather than attempting to optimize the designs in isolation from one another. A layer-isolated approach often proves inefficient when the performance evaluation takes into account higher layers. Furthermore, layer-isolated

approaches can prevent the physical layer innovations from being incorporated in the standardization effort and eventually adopted in the implementation phase. The information to be exchanged among the functionalities residing in different OSI layers can be classified as follows [36]:

- **CSI**, that is, estimates for channel impulse response, location information, vehicle speed, signal strength, interference level, and so on.
- **QoS-related parameters** including delay, throughput, bit error rate (BER), packet error rate (PER) measurements, and so on.
- **Physical layer resources** including spatial processing schemes, number of antenna elements, battery depletion level, and so on

It is also important to carefully consider the cross-layer optimization criteria. In practical systems, the link quality when employing smart antenna techniques is determined not only by the performance of data detection methods, but also by the specific coding scheme being used, the MAC/DLC functionalities adopted in the link layer, or even the performance of protocols in the higher layers of the protocol stack. Thus, all these blocks should optimally be designed to achieve the highest possible overall system throughput including all links instead of the highest data rate for a single link [36].

4.2 System Overview

4.2.1 Review of IEEE 802.11 MAC

The DCF provides the basic asynchronous and contention based shared access to the medium. It is a distributed scheme for ad-hoc networks and is based on CSMA/CA. CSMA/CA is also known as ‘Listen before Talk’ [16]. Before a station starts a transmission, it shall sense the wireless medium to determine if another station is

transmitting. If the medium is sensed as idle, the transmission may proceed. If the medium is as sensed busy, the station shall defer until the end of the current transmission. DCF describes two techniques for transmission. The basic scheme is mandatory and is known as a two-way handshaking technique. It is characterized by the immediate transmission of a positive acknowledgment (ACK) by the receiver if the current packet has been successfully received. The second scheme is optional and is known as a four-way handshaking technique. The transmitting station uses a Ready to Send (RTS) notice to inform the receiver and to reserve the channel. The receiver shall then reply by acknowledging with a Clear to Send (CTS). After the reception of the CTS, the transmission shall proceed. As in the basic scheme, the receiver shall also immediately acknowledge the transmitted data packet if successfully received. If the CTS is not received by the source, it is assumed that a collision has occurred and the RTS transmission is rescheduled. With this scheme, collision may only occur on the first RTS frame. The RTS/CTS scheme also enhances the system performance by reducing the duration of collisions when long packets are transmitted. The IEEE 802.11 MAC uses Inter Frame Space (IFS) timing to control the access to the channel. Each station is allowed to transmit only if it has sensed the medium to be idle for at least a Distributed IFS (DIFS). In addition, it shall also wait for a random back-off after DIFS, prior to attempting to transmit. The time duration between the reception of data and the transmission of an acknowledgment is called the Short IFS (SIFS). Figure 4.1 (a) shows the cycle of the basic access mechanism for a successful transmission. After this cycle, all the stations may contend again for access to the medium [16].

Figure 4.1 (b) shows the cycle of the RTS/CTS access mechanism for a successful transmission. The contention for the medium is similar. RTS and CTS frames are now introduced at SIFS intervals. Note that IFS timings do not depend on the access scheme but depend only on the PHY. However, SIFS is always smaller than DIFS in order to

prevent any other station trying to access the medium. Thus, priority is given to the current transmitting station. Collisions are unable to occur as a result of the inability of another station to detect the medium as being idle for a DIFS until the end of the ACK. The back-off time following the DIFS is slotted and a station is allowed to transmit only at the beginning of each slot. DCF uses an exponential back-off scheme to determine the random back-off timing. The back-off time is determined by:

$$\text{Backoff Time} = \text{Backoff Counter} \times \text{Slot Time} \tag{4.1}$$

where the back-off counter is uniformly and randomly chosen in the range [0, W - 1]. W is called the Contention Window. The back-off counter is decremented when the medium is sensed as idle and then frozen if the medium is sensed as busy. The counter is resumed when the medium is sensed as idle again after DIFS. Transmission may proceed when the counter has reached zero. After sensing the medium as idle for a DIFS time, Tx A and Tx B randomly set their back-off counter to 4 and 7 respectively. The back-off (BO) counters are decremented until either Tx A or Tx B becomes zero. BO(A) reaches zero when BO(B) is equal to 3, and consequently Tx A starts transmitting data whilst Tx B freezes its counter. Once the transmission cycle is finished, Tx A and Tx B restart sensing the medium. Tx B shall reactivate its BO(B) that was frozen at 3, whereas Tx A uses a new one (BO(A) = 5). The contention window W depends on the number of failed transmissions for the current frame. A transmission is considered as failed when a collision has occurred, i.e. when the back-off counters of two or more stations reach zero at the same time. W is initially set to $CW_{\min}$ for the first transmission attempt. After each failed transmission, W is doubled up to [16]:

$$CW_{\max} = 2^m \times (CW_{\min} + 1) - 1 \tag{4.2}$$

where m is called the maximum back-off stage. Once it reaches $CW_{\max}$, it remains at this value until it is reset. W is reset to $CW_{\min}$ after each successful transmission. The

value of W is then:

$$W = 2^i \times (CW_{\min} + 1) - 1 \qquad if \;\; 0 \le i \le m \tag{4.3}$$

$$W = CW_{\max} \qquad m \le i \tag{4.4}$$

where i represents the number of unsuccessful attempts. Similarto IFS timings, the contention window parameters are PHY dependent. The average back-off defines the back-off duration for 'lightly loaded networks', i.e. when each station has access to the channel after the first back-off attempt. Upon this assumption, the contention window length is therefore $CW_{\min}$. The average back-off duration is then:

$$\text{Average Backoff} = \text{Slot Time} \times \frac{CW_{\min}}{2} \tag{4.5}$$

From Figures 4.1 (a) and 4.1 (b), we can see that a successful cycle duration with the basic and RTS/CTS schemes are:

$$T_{\text{success}}^{\text{basic}} = \text{DIFS} + \text{Backoff} + \text{Data} + \text{SIFS} + \text{Ack} \tag{4.6}$$

$$T_{\text{success}}^{\text{rts}} = \text{DIFS} + \text{Backoff} + \text{RTS} + \text{CTS} + \text{Data} + 3 \times \text{SIFS} + \text{Ack} \tag{4.7}$$

If collisions occur, then these two equations are transformed into:

$$T_{\text{collision}}^{\text{basic}} = \text{DIFS} + \text{Backoff} + \text{Data} \tag{4.8}$$

$$T_{\text{collision}}^{\text{rts}} = \text{DIFS} + \text{Backoff} + \text{RTS} \tag{4.9}$$

In the case of the IEEE 802.11 PHY, ACK, RTS and CTS frames are transmitted with mode 1. The duration of data is mode dependent as well as packet length dependent. The total throughput for both schemes is then given by:

$$\text{Throughput} = \frac{\text{Transmitted Data}}{\text{Transmission Cycle Duration}} \tag{4.10}$$

4.2.2 IEEE 802.11n Draft Overview

The TGn Sync team has worked as a technical group for many months to develop a TGn proposal, recognizing that whatever decisions were made had to ultimately

survive the TGn process and therefore be based solely on technical merit.

The PHY techniques used to achieve the higher data rates involve a MIMO evolution of 802.11 OFDM PHY with spatial division multiplexing of spatial streams, and wider bandwidth options. Additionally, optional enhancements include advanced FEC coding techniques (Reed-Solomon and LDPC), transmit beamforming with negligible additional cost in the receiving client device, shortened guard interval and up to 7/8 coding. The TGn Sync proposal also offers seamless interoperability with 802.11 legacy devices. This interoperability is achieved with an enhanced 802.11 preamble design and efficient PHY and MAC level mechanisms, which also provide robustness and cost-effectiveness.

4.2.2.1 MIMO-OFDM PHY Specification

With the aim to increase the maximum PHY layer data rate, TGn Sync have introduced two primary techniques that are mandatory in proposal:

- Transmission of Multiple Spatial Streams via Multiple Transmit Antennas.
- Extended Bandwidth signaling. 20MHz channelization shall be mandatory worldwide.

Due to the susceptibility of a wireless link to multipath fading, especially in a MIMO channel, the proposal introduces two optional techniques for improving the robustness of the link between the transmitter and the receiver, with the aim to keep the client configuration low-cost and low-power:

- Transmitter beamforming, with the understanding that Access Points will be able to support more than 2 antennas, while the client stations would be restricted to 2 antennas.
- Advanced channel coding. Our proposal includes LDPC as an option. LDPC codes

exhibit a larger minimum free distance compared to the existing 802.11a convolutional code, and hence are able to better exploit the frequency and spatial diversity in the channel.

Besides spatial multiplexing, there are four other options for increasing data rate: (a) increasing the channel bandwidth, (b) increasing the constellation size, (c) increasing the coding rate, and (d) reducing the guard interval (GI) overhead.

The proposal focuses upon using spatial multiplexing and bandwidth expansion as the primary means for increasing the physical layer data rates. This is because both spatial multiplexing and channel bandwidth increase data rate by integer increments, whereas the rest of the techniques increase the data rate by fractional increments. The basic mandatory configuration in the PHY proposal for throughput enhancement is 2 spatial streams across a 20MHz channel bandwidth. The transmitter data path is shown in Figure 4.1 (c).

4.2.2.2 Support for Advanced Techniques

In basic mandatory 20/40MHz MIMO mode, the number of data streams created by the spatial parser in Figure 4.1 (c) is the same as the number of transmit antennas. In this basic configuration, each spatial stream is mapped to exactly one transmit antenna.

If Channel State Information (CSI) is available at the transmitter, we can perform spatial "shaping" using a steering matrix for each sub-carrier, as shown in Figure 4.1 (d). In SVD style MIMO, the steering matrix is obtained via singular value decomposition (SVD) of the physical channel transfer function matrix, **H**. In SVD-MIMO, each spatial stream is "transmitted" on a "singular vector" obtained from the SVD of **H**. We can further perform spatial water-filling by selecting an optimum power level, modulation level, and coding rate for each spatial stream.

The proposal introduces two classes of transmit beamforming: basic beamforming with MIMO (BF-MIMO), and advanced beamforming with MIMO (ABF-MIMO). In basic transmit beamforming, only spatial steering is performed. Support for basic beamforming is mandatory in a receiver since there is minimal implemenation overhead. In advanced beamforming, each spatial stream may have a unique MCS and a unique power level. The proposal also support bi-directional beamforming in the ABF-MIMO mode.

4.2.3 System Architecture of Proposed System

Figures 4.4 and 4.5 shows the system architecture of the proposed V-BLAST based adaptive MIMO-OFDM system. It consists of a joint adaptive modulation and coding module at the physical layer, and link adaptation module at the MAC layer.

At the physical layer, we have $N_c \times N_t$ sub-channels, where N_c is the number of subcarriers and N_t is the number of spatial channels per subcarrier. For a given time slot n, $N_c \times N_t$ bit streams, $\{\mathbf{b}_i[n,k]: k = 0,1,\ldots N_c\}$ for $i = 1,2\ldots, N_t$, are encoded separately in different puncturing rates into $N_c \times N_t$ coded bit streams, $\{\mathbf{c}_i[n,k]: k = 0,1,\ldots N_c\}$ for $i = 1,2\ldots, N_t$, respectively, and then modulated into QAM symbols, $\{t_i[n,k]: k = 0,1,\ldots N_c\}$ for $i = 1,2\ldots, N_t$, where the length of $\mathbf{b}_i[n,k]$, coding rate of $\mathbf{c}_i[n,k]$, and the modulation level of $t_i[n,k]$ are informed by the adaptive loading processor at the transmitter after receiving the CSI (either from the channel estimator or feedback signaling). Eventually, the *n*th OFDM symbols at the *i*th transmit antenna is generated by passing $\{t_i[n,k]: k = 0,1,\ldots N_c\}$ through an IFFT. A CP will be added before transmission to reduce the effect of ISI and ICI.

At the receiver, receive antennas $1 \sim N_r$ will receive the radiated signal from transmit antennas $1 \sim N_t$ and $N_r \geq N_t$ is assumed. The received data at each receive

antenna will then pass through a FFT with the removal of the CP. We can express the FFT output signal as

$$r_j[n,k] = \sum_{i=1}^{N_t} H_{i,j}[n,k]t_i[n,k] + \eta_j[n,k] \qquad \forall j = 1,2,...,N_r \tag{4.11}$$

where $\eta_j[n,k]$ denotes the additive complex Gaussian noise at the *j*th receive antenna, and assumed to be zero-mean with two-sided power spectral density $N_0/2$ per dimension and uncorrelated for different n's, k's, or j's. $H_{i,j}[n,k]$ denotes the channel frequency response for the *k*th subcarrier at time n, corresponding to the *i*th transmit and *j*th receive antenna.

These spectrally mixed data at the receiver are further processed by the V-BLAST algorithm as described before except that the modulation order used in each sub-channel are not fixed. Moreover, recall that the original V-LABST has to obey an ordering strategy in executing the cancellation process to ease the error propagation effects. But due to the use of adaptive modulation, the ordering becomes an unnecessary step because those ill channels are assigned more robust transmission modes to eliminate error bursts. In this way, the traditional interleaving techniques can be omitted as well. Besides, we assume that multiple transmission modes are available. Based on CSI acquired at the receiver, the AMC selector determines the modulation-coding pair (mode), which is sent back to the transmitter through a feedback channel. The AMC controller then updates the transmission mode at the transmitter. The decoded bit streams are mapped to packets, which are pushed upwards to the MAC layer.

The processing unit at the MAC layer is a packet, which comprises multiple information bits. On the other hand, the processing unit at the physical layer is a frame, which is a collection of multiple transmitted symbols. The detailed packet and frame

structures used in this thesis will be shown in Figure 4.6.

We next list the operating assumptions adopted in this thesis.

1. Perfect channel state information (CSI) is available at the receiver using training-based channel estimation. The corresponding mode selection is fed back to the transmitter without error and latency. The assumption that the feedback channel is error free and has no latency, could be at least approximately satisfied by using a fast feedback link with powerful error control for feedback information.
2. Error detection based on CRC is perfect, provided that sufficiently reliable error detection CRC codes. For flat fading channels, the channel quality can be captured by a single parameter, namely the received SNR.
3. At the physical layer, we deal with frame by frame transmissions, where each frame contains a fixed number of symbols. Each frame at the physical layer may contain multiple packets from the MAC layer. The packet and frame structures are depicted in Figure 4.6.

4.3 Throughput Efficiency and Delay Analysis

Here, we analyze the throughput efficiency and delay performance of the 802.11 DCF mode with RS code and a MAC retransmission limit. The throughput is defined as the ratio of the useful data, which is received to the total transmission time. Therefore, we take into account the overhead incurred due to use of the channel coding, retransmissions, and headers associated with different protocol layers. For the analysis, we have made the following assumptions:

1. The packets length = L_a bytes and these packets are not fragmented in any of the lower layers.
2. The overhead of the higher layer protocols, like RTP, UDP, and IP is 0 bytes. The

average frame transmission cycle computed in the following section accounts for the MAC and PHY overhead. The MAC layer retransmission limit is set to *R*.

4.3.1 Average Frame Transmission Cycle

In this section, we analyze the average transmission cycle of a MAC frame under different conditions [15][32]. This is used later in the computation of the throughput with FEC. Assuming that a packet with *L*-byte payload is transmitted using PHY mode *m*, the probability of a successful transmission is given by (see Figure 4.1 (c))

$$P_{\text{good\_cycle}}(L,\gamma,m) = \left[1 - P_{e,data}(L,\gamma,m)\right] \cdot \left[1 - P_{e,ack}(\gamma,m)\right] \tag{4.12}$$

where $P_{e,ack}$ is the CF-ACK error probability, m is modulation order, γ is wireless channel condition, and $P_{e,data}$ is the data packet error probability. These can be calculated from the corresponding packet sizes and the BER. The average transmission cycle for a successful cycle $T_{\text{good},i}(L)$, where neither the data packet nor the CF-ACK is in error, can be obtained from the timing intervals given in Figure 4.1 (d). Similarly, the average transmission cycle for a fail cycle $T_{\text{bad},i}(L)$, in a cycle where either the data packet or the CF-ACK packet is in error can be computed from the timing intervals given in Figure 4.1 (d). The average transmission cycle for a packet with an *L*-byte payload, given that the transmission is successful with the retransmission limit of *R*, can be obtained as follows:

$$D_{\text{av,succ}}(L,R) = \sum_{i=0}^{R} P\left[n \mid \text{succ}\right](L,\gamma,m) \cdot \left[iT_{\text{bad},i}(L) + T_{\text{good},i}(L)\right] \tag{4.13}$$

where the probability of a successful frame delivery within the retry limit can then be calculated by

$$P_{\text{succ}}(L,\gamma,m) = 1 - \prod_{i=1}^{R}\left[1 - P_{\text{good\_cycle}}(L,\gamma,m_i)\right] \tag{4.14}$$

and the condition probability that the data frame is successfully delivered at the *n*th transmission is given by

$$P\left[n \mid \text{succ}\right](L,\gamma,m) = \frac{P_{\text{good\_cycle}}(L,\gamma,m)\cdot\prod_{i=1}^{n}\left[1 - P_{\text{good\_cycle}}(L,\gamma,m)\right]}{P_{\text{succ}}(L,\gamma,m)} \tag{4.15}$$

The average transmission cycle for a packet with *L*–byte payload, given that the transmission is not successful with the retransmission limit *R*, can be obtained as follows:

$$D_{\text{av,fail}}(L,R) = \sum_{i=0}^{R} T_{\text{bad},i}(L) \tag{4.16}$$

Now, the average transmission cycle for a packet with *L*–byte payload and with a retransmit limit of *R* is given by

$$D_{\text{av}}(L,R) = \frac{1 - P_{\text{succ}}(L_a,\gamma,m)}{P_{\text{succ}}(L_a,\gamma,m)}\cdot\left[D_{\text{av,fail}}(L_a,R) + D_{\text{av,succ}}(L_a,R)\right] \tag{4.17}$$

Therefore, the effective throughput can then be calculated by

$$\begin{aligned} E_{\text{RS}}(L_a,\gamma,m) &= \frac{8\cdot L_a\cdot\dfrac{K}{N}}{\dfrac{1 - P_{\text{succ}}(L_a,\gamma,m)}{P_{\text{succ}}(L_a,\gamma,m)}\cdot D_{\text{av,fail}}(L_a,R) + D_{\text{av,succ}}(L_a,R)} \\ &= \frac{8\cdot L_a\cdot\dfrac{K}{N}}{\left[1 - P_{\text{succ}}(L_a,\gamma,m)\right]\cdot D_{\text{av,fail}}(L_a,R) + P_{\text{succ}}(L_a,\gamma,m)\cdot D_{\text{av,succ}}(L_a,R)} \\ &= \frac{E[data](L_a,\gamma,m)}{E[D_{data}](L_a,\gamma,m)} \end{aligned} \tag{4.18}$$

4.3.2 Delay Analysis

The maximum transmission delay depends on the length of a packet and the

maximum retry limit. The worst-case delay for retransmissions is given by [32]

$$D_{\max}(DR, L) = (R+1)(T_{\text{data}}^{DR}(L) + T_{\text{ack}}^{DR} + 2\text{SIFSTime}) \tag{4.19}$$

Therefore, the maximum buffering delay at the decoder is $N \cdot D_{\max}(DR, L)$. Assuming a frame size of 2000 bytes, R = 5, and PHY mode 5, the value of $D_{\max}$ is 6.876 ms. This delay, on top of the video encoding and decoding delay, is well within the acceptable range for noninteractive video streaming applications. Note that for the most noninteractive video streaming applications, the acceptable delay ranges between 1–10s.

4.4 Combining AMC with MAC Mechanism

In this section, we develop our cross-layer design, which combines AMC at the physical layer with several protection strategies at the MAC layer. Since only finite delays and buffer sizes can be afforded in practice, and the maximum transmission delay depends on the length of a packet and the maximum number of retransmissions. Therefore, the maximum number of ARQ retransmissions has to be bounded. This number can be specified by dividing the maximum allowable system delay over the round trip delay required for each retransmission. Formally, we adopt the following delay constraint.

1. The maximum number of retransmissions allowed per packet is $R^{\max}$. If a packet is not received correctly after $R^{\max}$ retransmissions, we will drop it, and declare packet loss. On the other hand, the error packets can also be utilized if the receiver decides to do so. To maintain an acceptable packet stream, we impose the following performance constraint:
2. The transmission duration of packet after $R^{\max}$ retransmissions is no longer than maximum delay limit.

3. The probability of packet loss after $R^{\max}$ retransmissions is no larger than P_{loss}.

Hence, constraint 1, 2, and 3 can be derived from the required quality of service in the application at hand. The delay constraint 1 dictates that truncated ARQ with up to $R^{\max}$ retransmissions should be performed at the data link layer. Having specified ARQ at the data link layer, we next design the AMC at the physical layer. In other words, we address the following interesting question: with the aid of $R^{\max}$-truncated ARQ at the data link layer, how can we optimally design the AMC at the physical layer to maximize throughput, while guaranteeing the overall system performance dictated by the three constrain?

4.4.1 System Performance Requirement at Physical Layer

We first determine how reliable performance is needed at the physical layer to meet C2, given that $R^{\max}$-truncated ARQ is implemented at the data link layer. Notice that a packet is dropped if it is received incorrectly after a maximum number of ($R^{\max}$ + 1) transmissions; i.e., after $R^{\max}$ retransmissions. Let us suppose that the instantaneous packet error rate (PER) is guaranteed to be no greater than for each chosen AMC mode at the physical layer. Then, the packet loss probability at the data link layer is no greater than $P_0^{R^{\max}+1}$. To satisfy C2, we need to impose [26]

$$P_0^{R^{\max}+1} \le P_{\text{loss}} \tag{4.20}$$

From (4.20), we obtain

$$P_0 \le P_{\text{loss}}^{(1/R^{\max}+1)} = P_{\text{target}} \tag{4.21}$$

Therefore, if we design AMC to satisfy a PER upper-bound as in Equation 4.21 at the

physical layer, and implement a $R^{\max}$–truncated ARQ at the data link layer, both delay and performance requirements C1 and C2 will be satisfied. Our remaining problem is to design AMC to maximize spectral efficiency while maintaining Equation 4.21.

4.4.1.1 AMC Design at the Physical Layer

Our objective here is to maximize the data rate, while maintaining the required performance, through AMC at the physical layer. As we already mentioned, the transmission modes are arranged so that the rate is increasing as the mode index *n* creases. Let *N* note the total number of transmission modes available. We partition the total SNR range into *N* + 1 overlapping consecutive intervals, with boundary points denoted as $\{\gamma_n\}_{n=0}^{N+1}$. Specifically, [26] mode *n* is chosen, when

$$\gamma \in \left[\gamma_n, \gamma_{n+1}\right) \tag{4.22}$$

To avoid deep channel fades, no payload bits will be sent when $\gamma_0 \le \gamma < \gamma_1$. What remains now is to determine the boundary points $\{\gamma_n\}_{n=0}^{N+1}$.

4.4.3.1 Error Performances of PHY Modes

The instantaneous error probabilities of the BPSK and QPSK modulations can be given by

$$P_{BPSK}(\gamma) = Q\left(\sqrt{2\gamma}\right) \tag{4.23}$$

$$P_{QPSK}(\gamma) = 1 - \left(1 - Q(\gamma)\right)^2 \tag{4.24}$$

For the rectangular signal constellation in which $M = 2^k$ where k is even, the QAM

signal constellation is equivalent to two PAM signals on quadrature carriers, each having $\sqrt{M} = 2^{k/2}$ signal points. The probability of a correct decision for the M-ary QAM system is

$$P_c = \left(1 - P_{\sqrt{M}}\right)^2 \tag{4.25}$$

where $P_{\sqrt{M}}$ is the error probability of an $\sqrt{M}$-ary PAM with one-half the average power in each quadrature signal of the equivalent QAM system. The closed-form instantaneous symbol error probability of M-QAM is given by

$$P_{M-QAM}(\gamma) = 1 - \left[1 - 2\left(1 - \frac{1}{\sqrt{M}}\right)Q\left(\sqrt{\frac{3}{M-1}\gamma}\right)\right]^2 \tag{4.26}$$

Obviously, the error performance of a modulation scheme varies with different SNR values. The probability of error after RS decoding is given by

$$P_{\mathrm{RS}}(N,K) = 1 - \sum_{i=0}^{(N-K)/2} \binom{N}{i} P_r^i \left[1 - P_r\right]^{N-i}$$

where $P_r = \int_0^\infty P_\Gamma(\gamma) P_e(\gamma) d\gamma$ is the bit error probability for the modulation scheme selected in PHY mode *m* under Rayleigh fading channel ($P_\Gamma(\gamma) = \frac{1}{\Gamma}\exp(-\frac{\gamma}{\Gamma})$). BER is not easily determined from PER, and vice versa, especially for coded transmissions. Furthermore, since our system uses packets as processing units, we will henceforth specify the boundary points to meet the required PER. To simplify the AMC design, we will rely on the following approximate PER expression:

$$\mathrm{PER}_n(\gamma) \approx \begin{cases} 1, & \text{if } 0 < \gamma < \gamma_{pn} \\ a_n \exp(-g_n \gamma), & \text{if } \gamma \geq \gamma_{pn} \end{cases} \tag{4.27}$$

where n is the mode index and γ is the received SNR. Parameters a_n, g_n, and γ_{pn} in Equation 4.27 are mode-dependent, and are obtained by fitting Equation 4.27 to the

exact PER, where the accuracy of this PER approximation is also verified. Using the approximate yet simple expression Equation 4.27 facilitates the mode selection. We set the region boundary (or the switching threshold) γ_n for the transmission mode n to be the minimum SNR required to achieve P_{target}. In general, the required PER in Equation 4.21 satisfies $P_{\text{target}} < 1$. Inverting the PER expression in Equation 4.27, we obtain

$$\begin{aligned} \gamma_0 &= 0 \\ \gamma_n &= \frac{1}{g_n} \ln\left(\frac{a_n}{P_{\text{target}}}\right), n = 1,2,\ldots,N \\ \gamma_{N+1} &= +\infty \end{aligned} \tag{4.28}$$

With the γ_n specified by Equation 4.28, one can verify that the AMC in Equation 4.26 guarantees Equation 4.25.

4.4.2 Adaptive Packet Length Selection at MAC Layer

In this section we have taken a general look at throughput by considering its definition for a packet-based scheme and how it is maximized for a given RS code and retransmission limit based on the channel model being used. As an initial step in a theoretical study, we examine the influence of transmission rate and packet size in a noise-limited transmission environment. Each packet contains L_a bits including a payload of L bits and a cyclic redundancy check error-detecting code with C bits. A forward error correction encoder produces the remaining $L_a - L - C$ bits in each packet. The optimal packet size is obtained from Equation 4.29 as follows: [31][32]

$$L_a^* = \arg_{L_a} \max E_{\text{RS}}(L_a, \gamma, m) \tag{4.29}$$

$$E_{\text{RS}}(L_a, \gamma, m) = \frac{8 \cdot L_a \cdot \frac{K}{N}}{\frac{1 - P_{\text{succ}}(L_a, \gamma, m)}{P_{\text{succ}}(L_a, \gamma, m)} \cdot D_{\text{av,fail}}(L_a, R) + D_{\text{av,succ}}(L_a, R)} \tag{4.30}$$

The above equation can be solved by evaluating the function for all possible values of L_a. In a practical implementation, we can use a lookup table by pre-computing the values. As expected, the optimal packet size increases with increasing SNR, with a corresponding increase in efficiency. For low SNRs, using the maximum allowed number of link layer retransmissions makes the link more reliable and, hence, allows the use of larger packet sizes. As the SNR improves, the optimal packet size corresponding to the case of increases rapidly. This is due to the fact that as the underlying link becomes more reliable at higher SNRs, the resultant packet erasures can be handled by the error control coding even in the absence of any retransmissions. Maintaining the target performance, the proposed cross layer design AMC with Equations 4.28 and 4.29 then maximizes the spectral efficiency, with the given finite transmission modes.

4.4.3 Physical/MAC Cross-Layer AMC Design

Based on the above analysis, the run-time optimal cross layer bit allocation algorithm can be summarized as follows:

1. Estimate the channel condition (various methods exist to estimate the channel condition based on the receiver feedback; these are not discussed here)
2. For the estimated channel SNR and given QoS parameters, determine the target packet error probability P_{target} from Equation 4.21.
3. Choose RS code and maximum retransmission number $R_{\max}$ to obtain the packet error probability to lower than the target packet error probability P_{target}
4. Base on the parameters selected by the previous step, construct SNR threshold table $\{\gamma_n\}_{n=0}^{N+1}$ by Equation 4.28.
5. Use Equation 4.29 to find the optimal packet length L_a. This combination of error

control coding, modulation order, MAC retransmission limit and the packet size will maximize the throughput.

Before presenting the experimental results, we summarize our run-time adaptation procedure based on what we described thus far.

1. Estimate the channel SNR.
2. Update the modulation order per frame by using the AMC scheme at physical layer as in Equation 4.22.
3. Optimal adaptive packet size selection based on estimated channel SNR for the packet sizes L_a ranging from 500 to 8100 bytes. The initial packet size is fixed at 2000 bytes.
4. Retransmit the error packets by truncated ARQ.
5. Cross-layer adaptive application-layer FEC + MAC ARQ.

4.5 Computer Simulations

In this section, computer simulations are conducted to evaluate the performance of the proposed V-BLAST based cross layer design AMC system. Throughout the simulation, we only deal with discrete time signal processing in the baseband, hence pulse-shaping and matched-filtering are removed from consideration for simulation simplicity. Also, channel estimation and timing synchronization are assumed to be perfect. Table 4.1 lists all parameters used in our simulation. The configuration we consider here is a MIMO-OFDM system with a bandwidth of 20 MHz and 64 subcarriers. The set of QAM constellation used in the simulation is {0, 2, 4, 16, and 64}. Each link in MIMO is modeled as an exponential decay Rayleigh fading channel with $\tau_{rms} = 50\ n\text{s}$.

Firstly, a look-up table that contains the SNR threshold values of each modulation

mode should be established. These threshold values could be obtained by dynamically evaluating each PER curve to find the corresponding SNR value that meets the PER requirement (10^{-2} in our simulations).

Figure 4.11 shows the selection probability of each modulation mode at different SNRs. It's obvious that higher order modulation modes are preferred as the average channel SNR increases. In the low SNR scenario, our cross layer design AMC forces some of transmit antennas to be blocked frequently to avoid inefficient or unreliable transmission in order to meet the target PER requirement.

In Figure 4.11 and Figure 4.12, we compare the modulation mode selection probability at different SNRs for the two cases: adaptive modulation (without combining of MAC protection mechanism) and cross layer design AMC (with combining of MAC protection mechanism). It is obvious that the cross layer design AMC will reach a higher peak in each modulation type. Besides, with the aid of channel coding, the cross layer design AMC has a higher probability to select the higher modulation order, which leads to a rate enhancement. In Figure 4.13 and Figure 4.14, we can see a significant PER improvement under the prescribed PER constraint (10^{-2} and 5×10^{-3} in our computer simulation).

Figures 4.15 and 4.16 show the throughput of the system for different packet lengths and for the basic DCF access and the RTS / CTS access scheme respectively. We can see that the throughput is packet length dependent, especially for the higher modes. This can be explained by the fact that the MAC overheads are considerably longer compared with the data transmission cycle if packets are small. Applications requiring high bit rates are therefore likely to use longer packets. For example, in Figure 4.16, the 500 byte long packets offers a throughput of 12 Mbits / s whereas 8136 byte packets lead to a throughput of 102 Mbits / s. However, longer packets are more likely to be corrupted.

By comparing Figures 4.15 and 4.16, we can see that the basic scheme offers better throughput than the RTS/CTS access technique. The RTS/CTS scheme decreases the efficiency since it transmits two additional frames without payload and two SIFS are introduced. This is only true under the assumption that each station has access to the medium after the first attempt. This is not the case any more when the number of users increases.

Finally, we simulate the proposed system in a realistic TDD system. In TDD, the estimation of the channel quality prior to transmission is used to select the appropriate modulation mode for the next transmission, hence a channel quality estimation delay is incurred in this scheme. During this delay, the fading channel quality varies according to the Doppler frequency and consequently, the channel quality estimates perceived prior to transmission may become obsolete. This makes the chosen modulation mode non-optimum with regards to the actual channel quality and hence degrades the performance.

In our experiment in Figure 4.17, we assume a delay time of one packet (0.48 *m*s). We observe that the degradation is dependent on the rate at which the fading channel quality fluctuates, as quantified by its Doppler frequency. In lower Doppler frequency scenarios ($f_d < 15$ Hz, or a speed < 1 m/s), the proposed system works well in meeting the target PER (10^{-2}) constraint. However, when the user end moves with a high mobility ($f_d > 50$ Hz, or a speed > 3 m/s), obvious degradation occurs at high SNRs. This is because that in the proposed adaptive procedure, higher order modulations, characterized by lower immunity against interference, are preferred at high SNRs. Such an impairment could be somewhat mitigated by either a channel predictor or an adjustment in the SNR thresholds.

4.6 Summary

Maximizing throughput in a wireless channel is a very important issue in the quality of voice or data transmission. In this chapter, we have shown that factors such as the optimum packet length and optimum transmission rate are functions of the signal to noise ratio. These equations can be used to find the optimum transmission parameters that the system should be operated with in order to achieve the maximum throughput. The employment of error correction coding gives us a significant increase in throughput. Too much coding, however, can lead to degradation because the amount of overhead necessary will begin to overshadow the data throughput effect.

The key concept behind this research is that for each particular channel and transmission scheme, there exists a specific value for each of the transmission parameters to maximize the throughput. Once the probability of error is known, these parameters can be obtained.

(a)

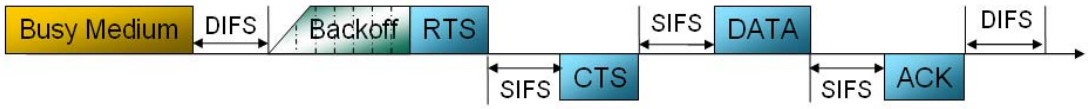

(b)

(c)

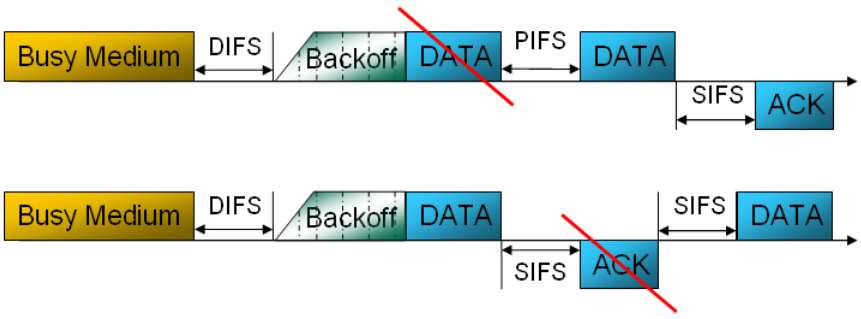

(d)

Figure 4.1 (a): DCF Basic Access Mechanism (b): DCF RTS/CTS Access Mechanism (c): Successful downlink frame transmission and associated timing (assume basic scheme) (d): Retransmission due to frame or ACK transmission error

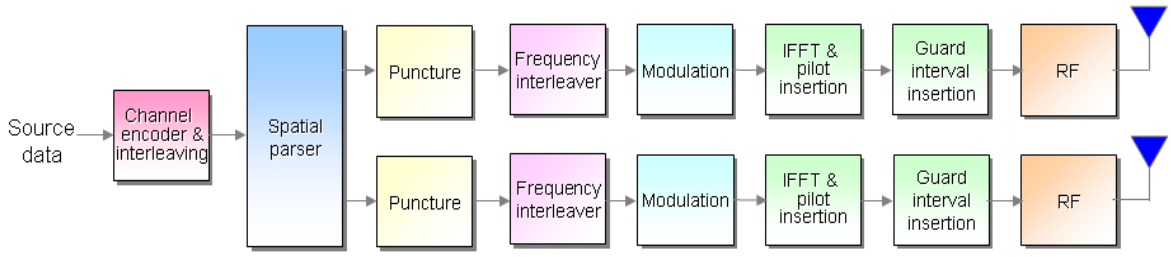

Figure 4.2: Transmitter datapath for 2-antenna MIMO in 20MHz

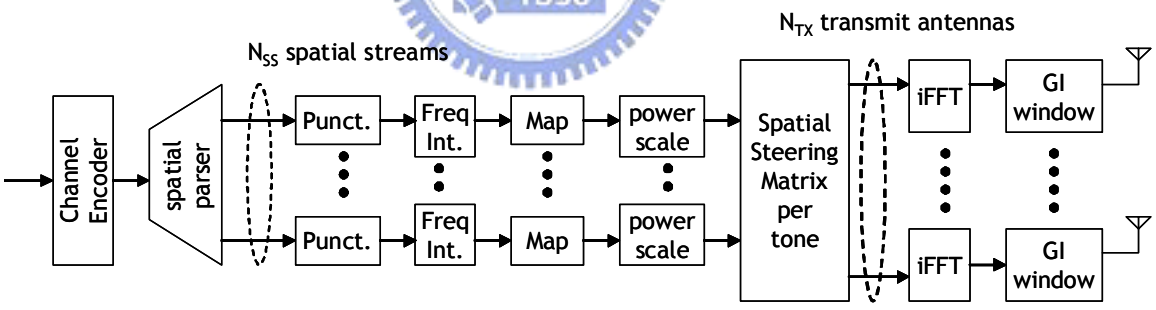

Figure 4.3: Transmitter datapath with option to perform spatial shaping

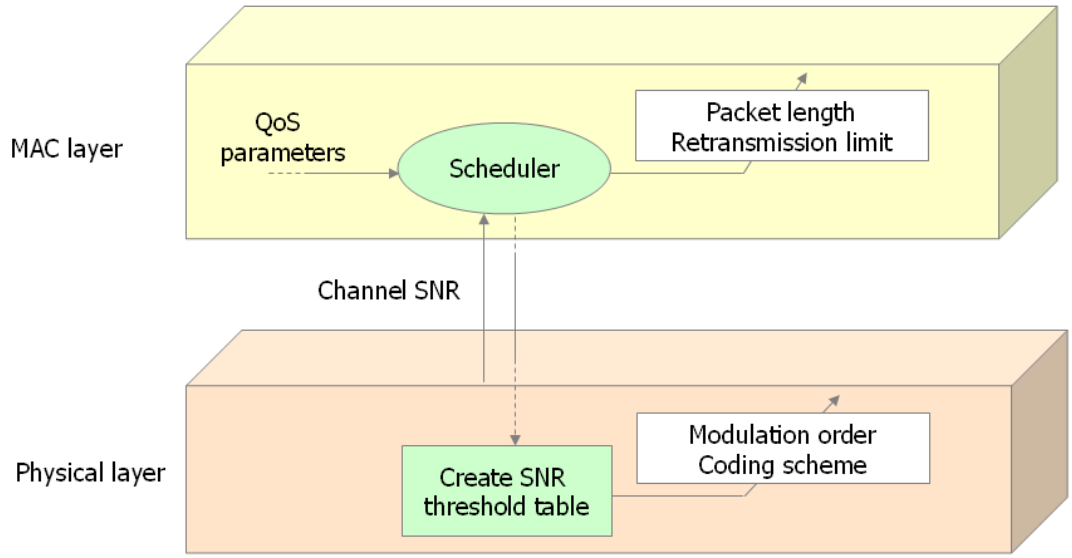

Figure 4.4: System architecture of the proposed V-BLAST based adaptive MIMO-OFDM system

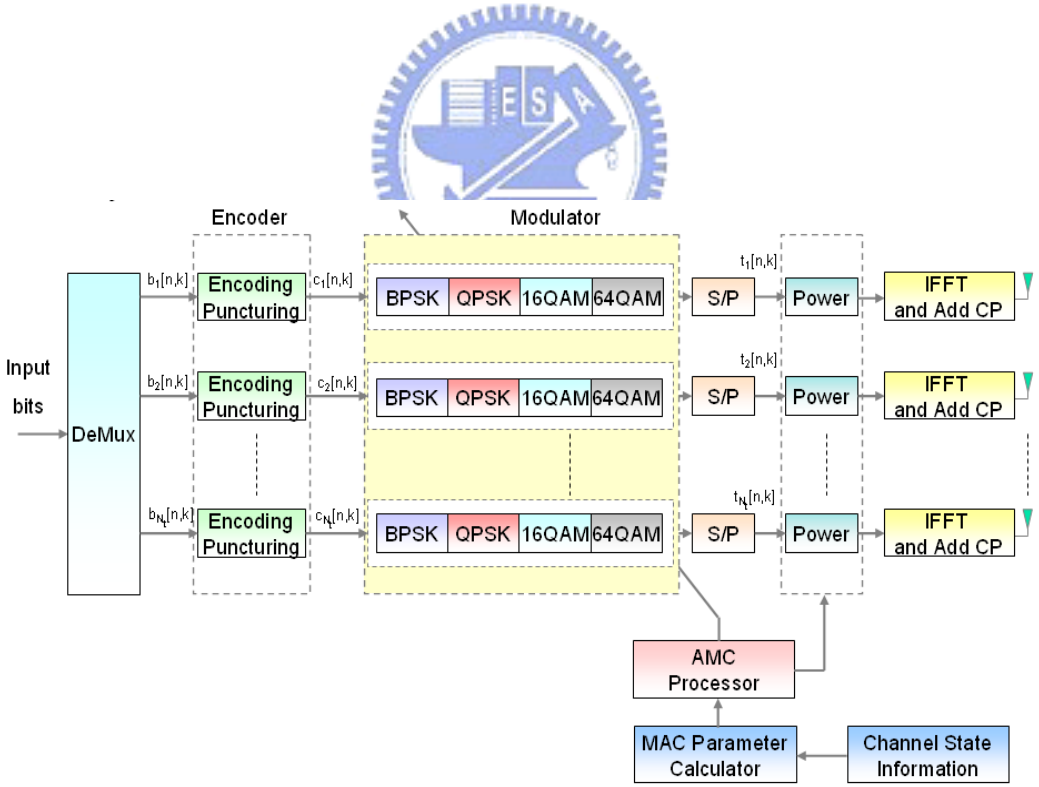

Figure 4.5: System architecture of the proposed V-BLAST based adaptive MIMO-OFDM system

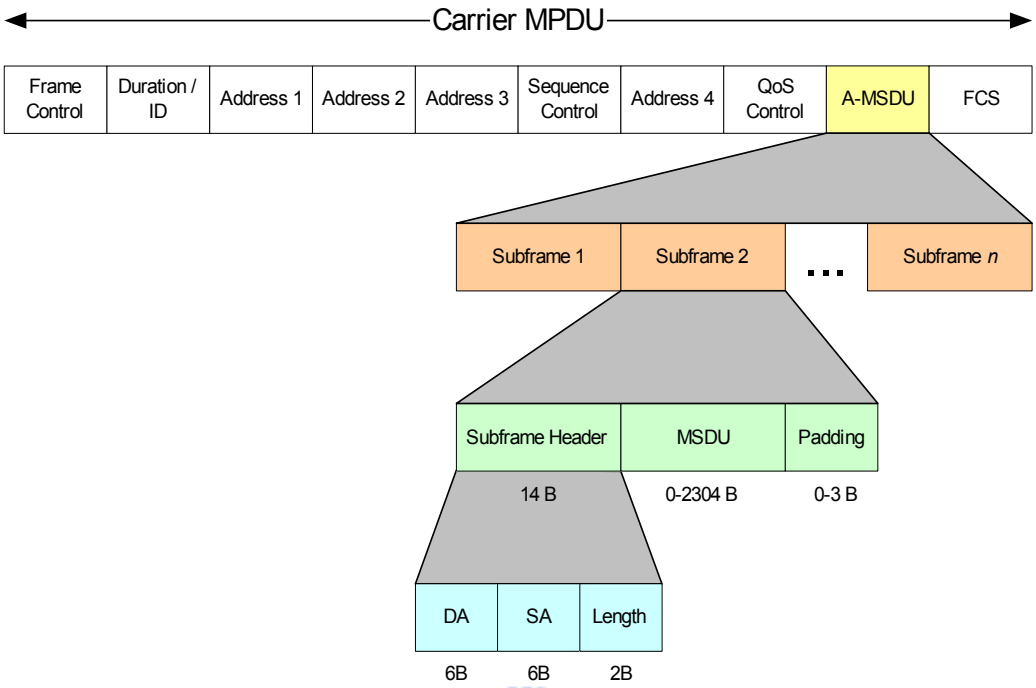

Figure 4.6: Frame Structure

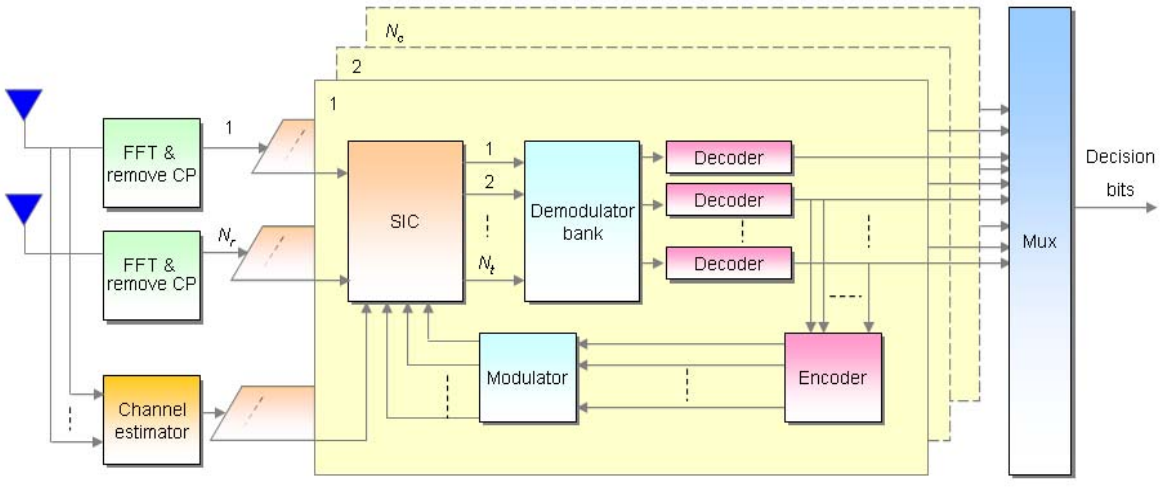

Figure 4.7: V-BLAST based adaptive MIMO-OFDM system receiver architecture.

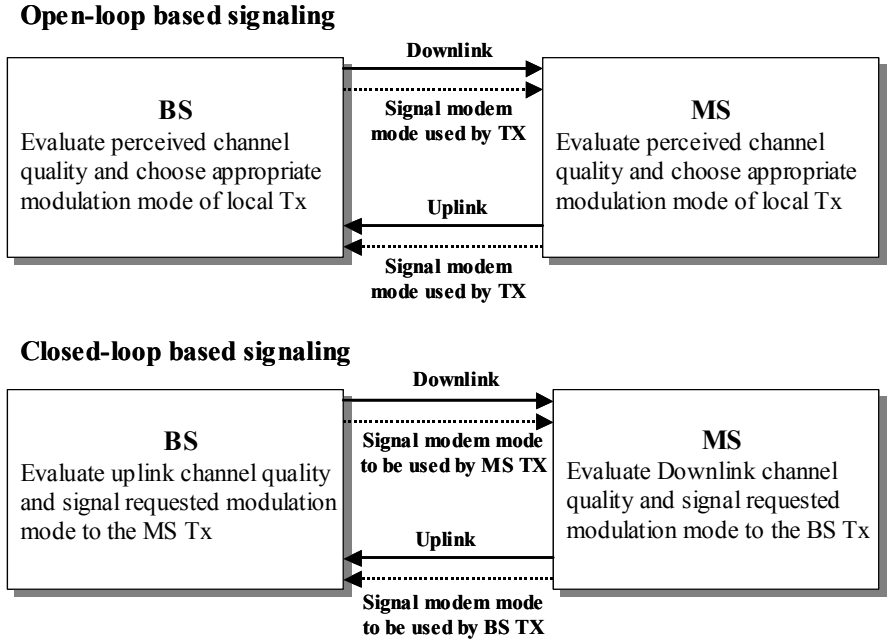

Figure 4.8: Closed-loop and open-loop signaling regimes for a typical adaptive modulation system, where BS represents the Base Station, MS denotes the Mobile Station and the transmitter is represented by TX.

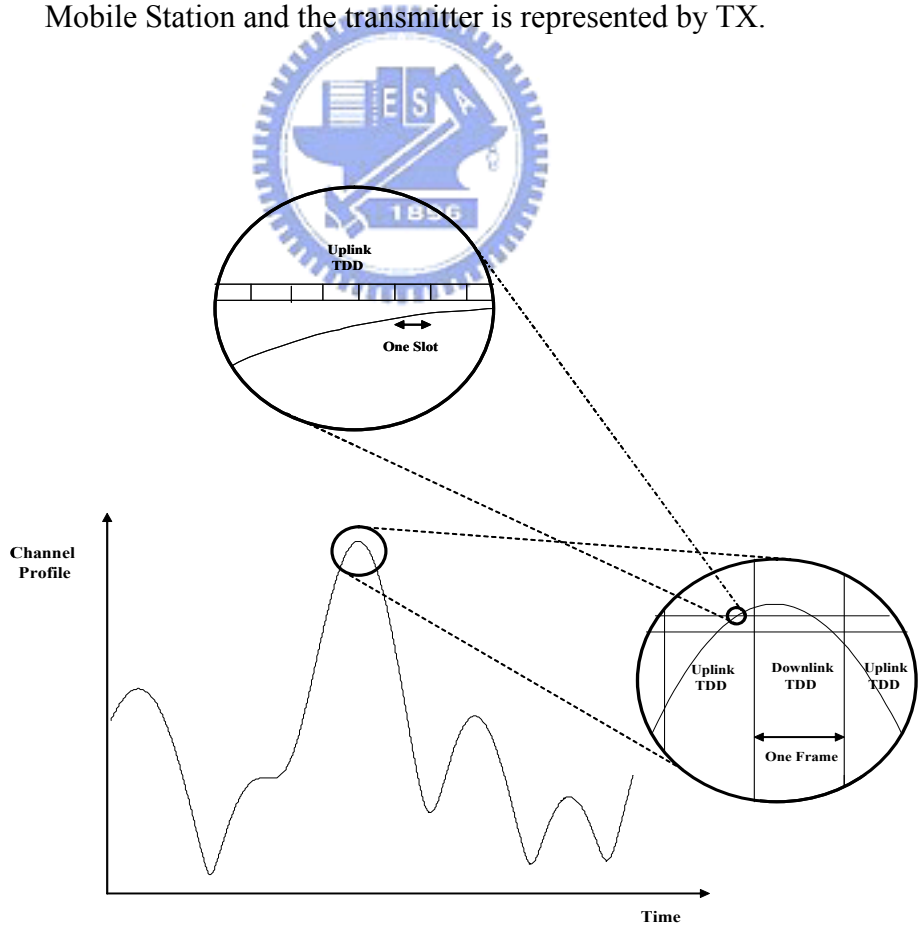

Figure 4.9: Received power fluctuation over the duration of one Time Division Duplex (TDD) slot.

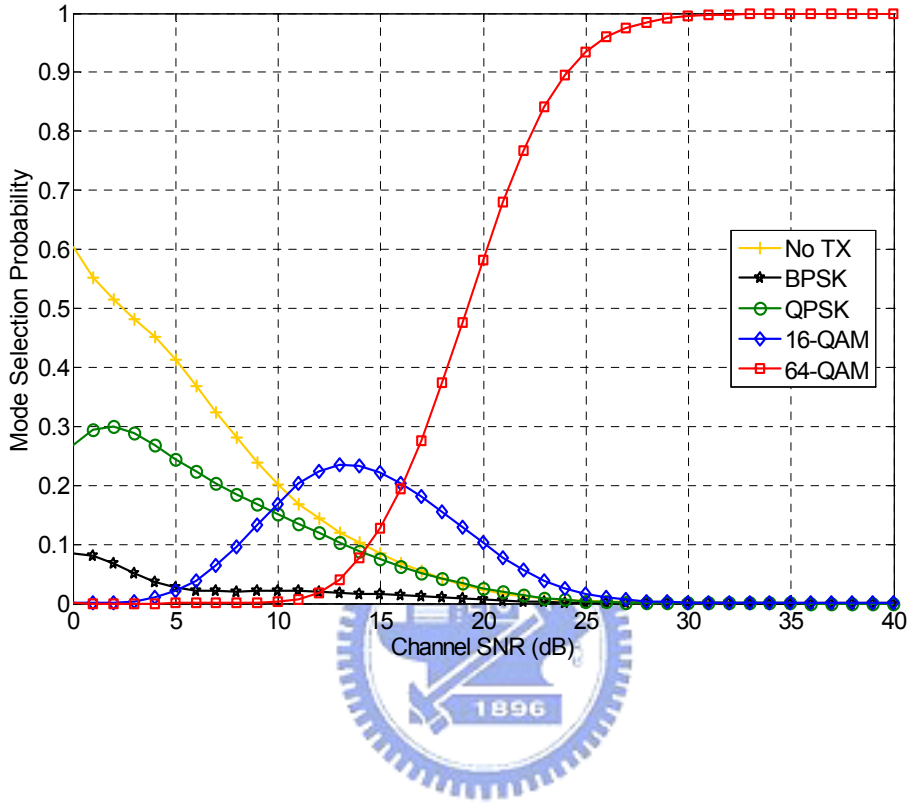

Figure 4.11: Simulated probabilities of each modulation mode utilized by the ZF V-BLAST based cross layer design AMC system in the exponentially decay Rayleigh fading channel with τ_{rms} =50 *n*s. $f_d = 0$ Hz . $(N_t, N_r) = (2,2)$. Other simulation parameters are listed in Table 4.1.

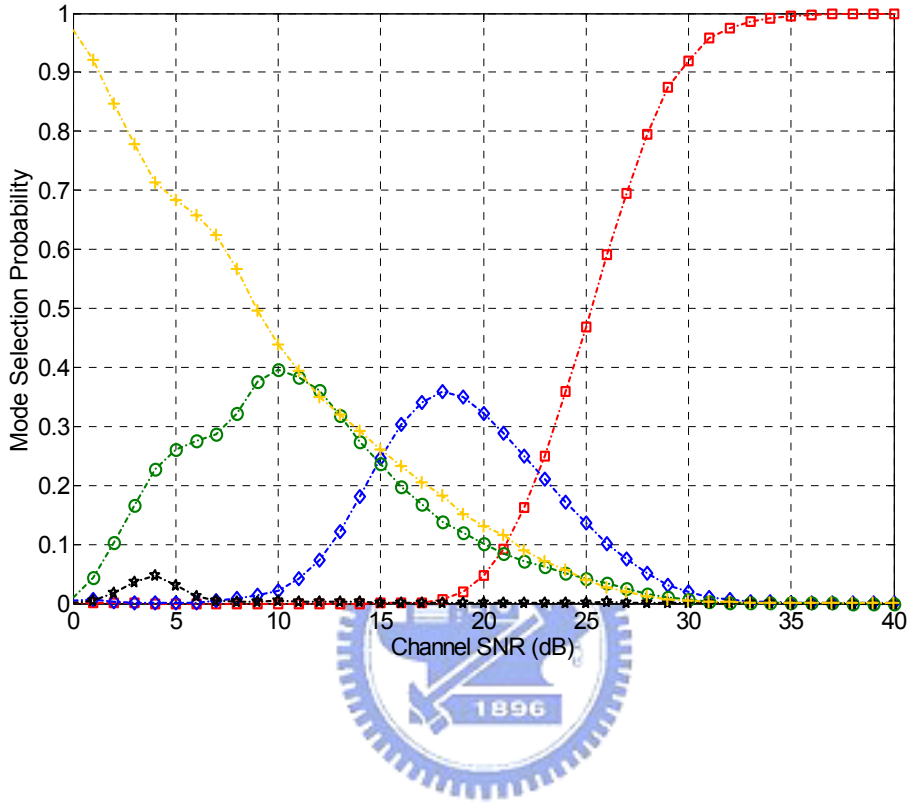

Figure 4.12: Simulated probabilities of each modulation mode utilized by the ZF V-BLAST based cross layer design AMC system in the exponentially decay Rayleigh fading channel with τ_{rms} =50 *n*s. $f_d = 0$ Hz . $(N_t, N_r) = (2,2)$. Other simulation parameters are listed in Table 4.1

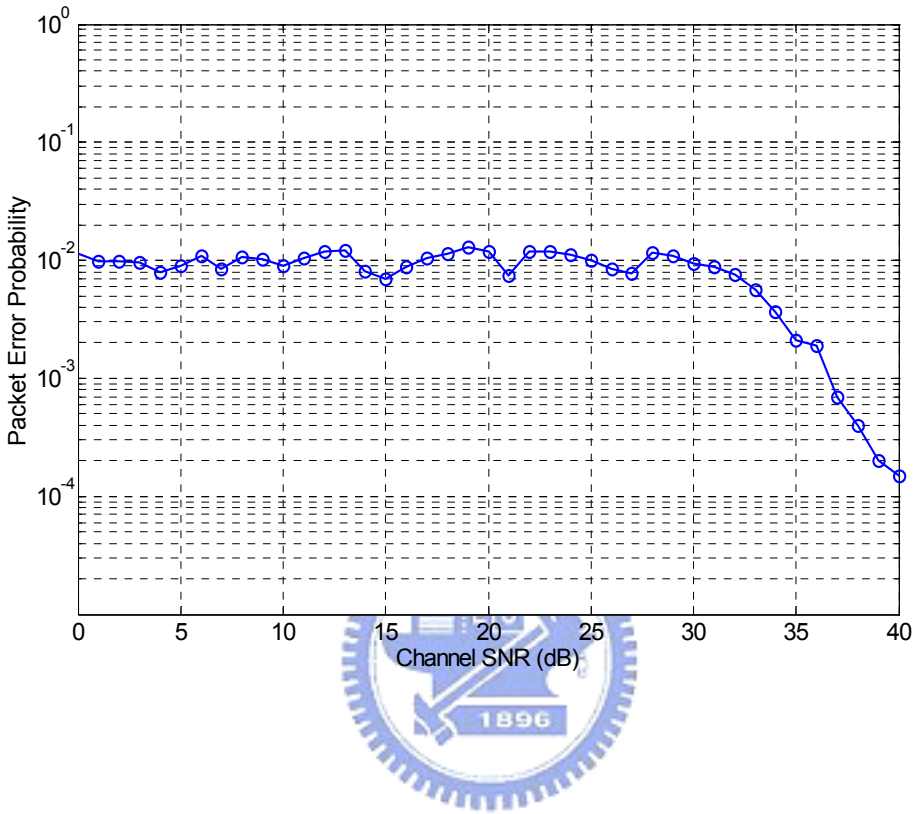

Figure 4.13: PER versus average channel SNR for the ZF V-BLAST based cross layer design AMC system (require PER = 10^{-2}) in an exponential decay Rayleigh fading channel with $\tau_{rms} = 50\ ns$. $f_d = 0$ Hz . Other parameters are listed in Table 4.1

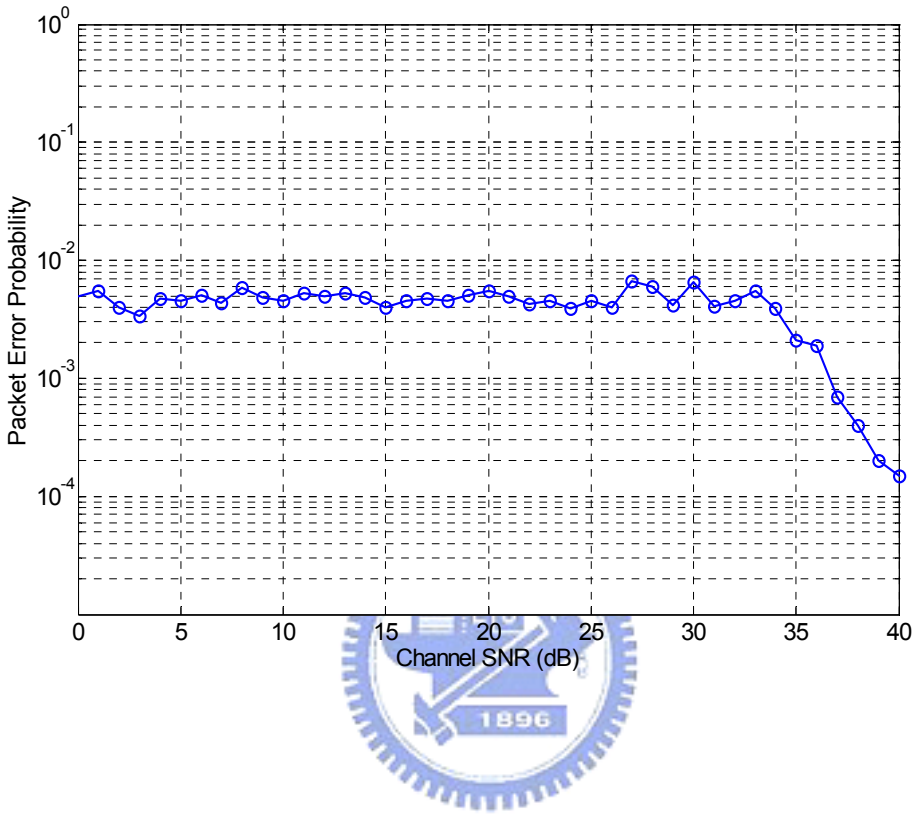

Figure 4.14: PER versus average channel SNR for the ZF V-BLAST based cross layer design AMC system (require PER = 0.005) in an exponential decay Rayleigh fading channel with $\tau_{rms} = 50\ ns$. $f_d = 0$ Hz . Other parameters are listed in Table 4.1

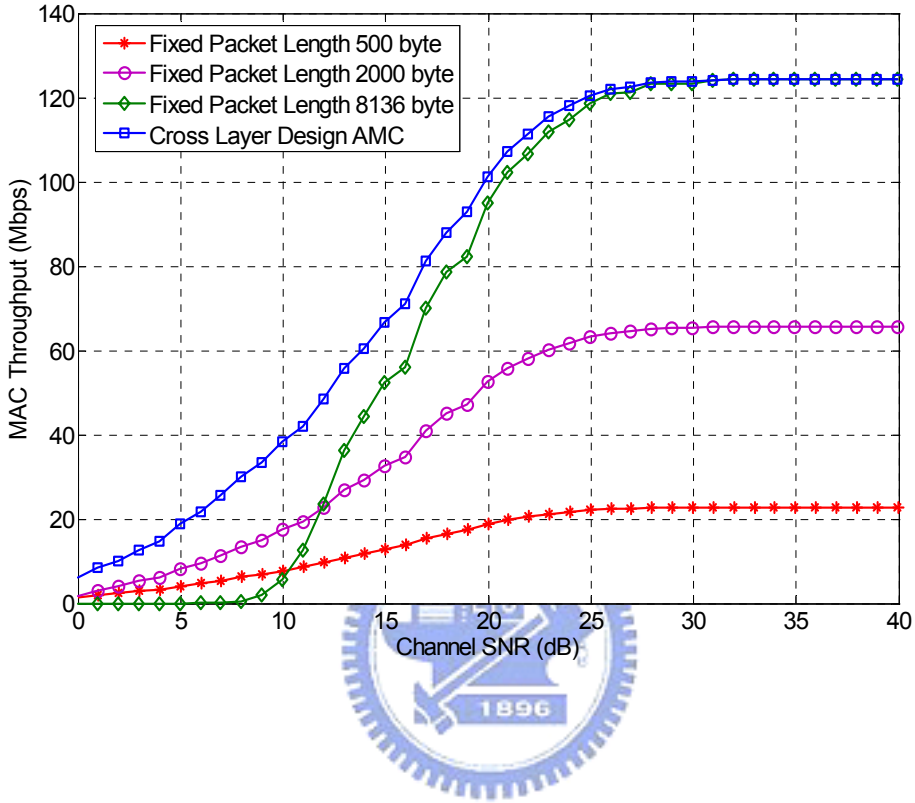

Figure 4.15: MAC Throughput for the ZF V-BLAST based cross layer design AMC system (with two way hand shaking) at different SNRs. Exponential decay Rayleigh fading channel is assumed with $\tau_{rms} = 50ns$. $f_d = 0$ Hz. Other parameters are listed in Table 4.1.

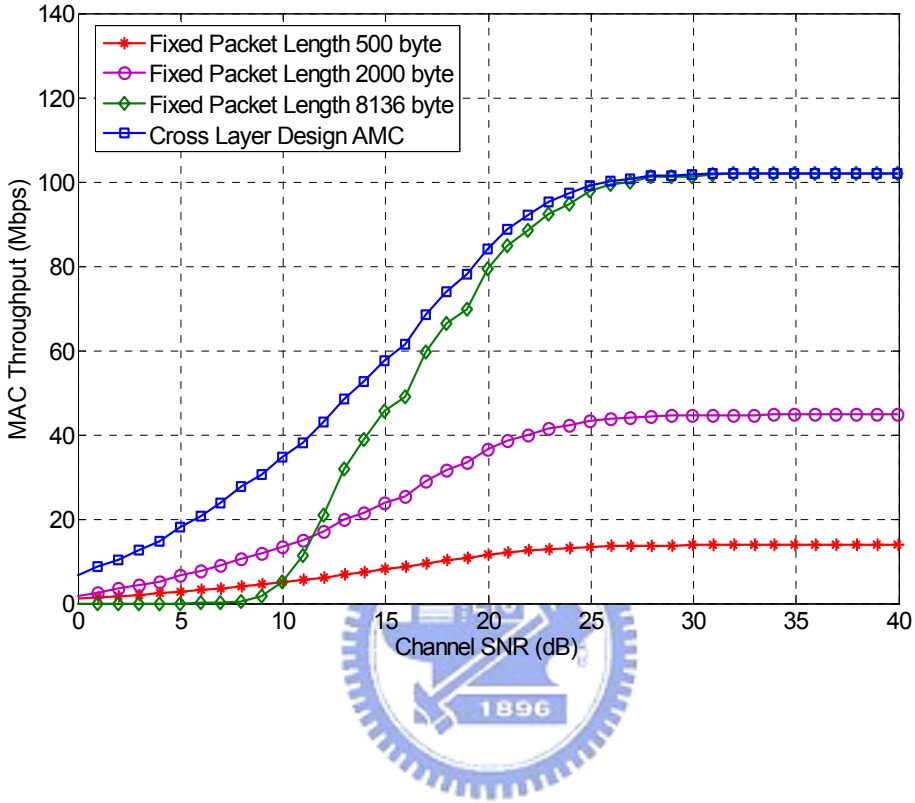

Figure 4.16: MAC Throughput for the ZF V-BLAST based cross layer design AMC system (with four way hand shaking) at different SNRs. Exponential decay Rayleigh fading channel is assumed with $\tau_{rms} = 50ns$. $f_d = 0$ Hz. Other parameters are listed in Table 4.1.

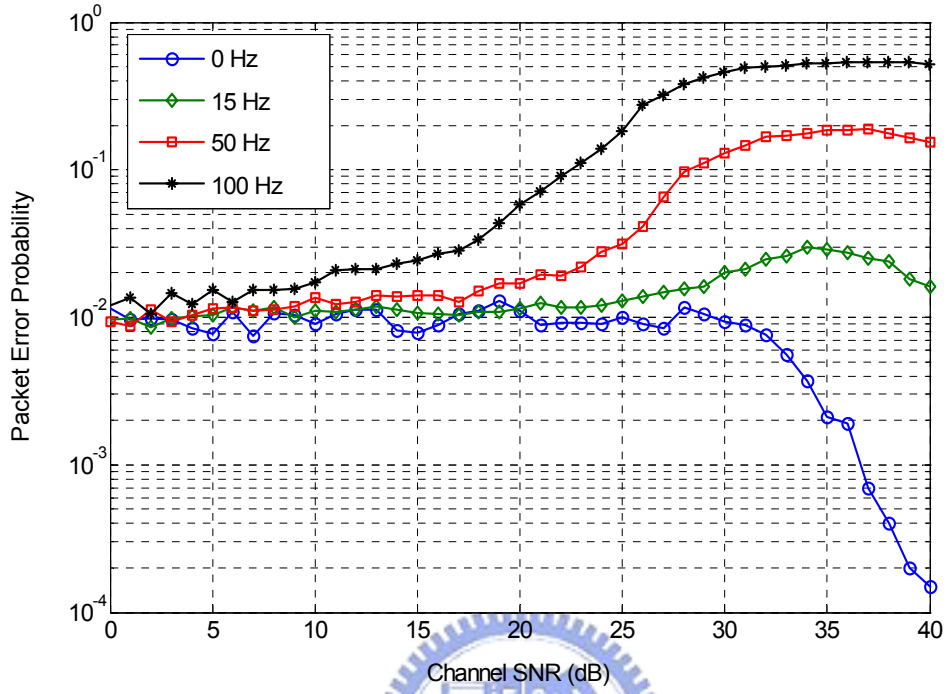

Figure 4.17: BER versus average channel SNR for the cross layer design AMC system in an exponential decay Rayleigh fading channel. τ_{rms} = 50 *n*s. $(N_t, N_r) = (4,4)$. f_d = 100, 50, 15, and 0 Hz. Other parameters are listed in Table 4.1.

Chapter 5

MIMO Channel Condition and Transmission Strategies

Now, the major challenge in mobile communications system is to design effective techniques to alleviate the effects of the wireless channels. The transmitted signal scattered by various environmental objects (buildings, trees, mountains, etc.) will cause both constructive and destructive interference, typically referred to as the multipath fading effect, and significantly degrade the system performance. As a remedy, multiple-input multiple-output (MIMO) techniques are used to combat the multipath fading and suppress the interference. Recent research has shown that the MIMO system can provide significant performance improvement and capacity gains over conventional uni-antenna systems.

The development of the MIMO schemes will depend on the fading channels. A classification of MIMO fading channels will be investigated below [45]:

- Uncorrelated high-rank (UHR, a.k.a., i.i.d.) model: The elements of $\mathbf{H}$ are i.i.d. $\mathcal{CN}(0,1)$.

- Correlated low-rank (CLR) model: $\mathbf{H} = g_{rx} g_{tx}^{*} \mathbf{u}_{rx} \mathbf{u}_{tx}^{H}$, where $g_{rx} \sim \mathcal{CN}(0,1)$ and

$g_{tx} \sim \mathcal{CN}(0,1)$ are independent random variables, and $\mathbf{u}_{rx}$ and $\mathbf{u}_{tx}$ are fixed deterministic vectors of size $M_R \times 1$ and $M_T \times 1$, respectively, with unit modulus entries. This model yields no diversity or multiplexing gain whatever, just receive array gain.

According to the MIMO channel models mentioned previously, the largest space-time gains will lead to the significant enhancement of the MIMO system capacity and the effective data throughput. Figure 5.1 illustrates these points graphically.

- Under UHR channel conditions, spatial multiplexing works well on full rank channel and can increase capacity and data rate.
- Under CLR channel conditions, beamforming can provide array gain and interference suppression, leading to increment in coverage, capacity, and link quality.

While beamforming systems tend to use a large number of closely spaced antennas, MIMO operates with typically fewer antennas. MIMO antennas use much space that can be afforded to try and realize decorrelation between the elements. However, the directional-based beamforming operation imposes stringent limits on spacing. Moreover, most MIMO algorithms focus on diversity or data rate maximization rather than just increasing the average SNR at the receiver or reducing interference. Finally beamforming systems thrive in near line of sight (LOS) environments because the beams can be more easily optimized to match one or two multipaths than a hundred of them. In contrast, MIMO systems turn a rich multi-path environment into an advantage and lose their multiplexing benefits in line of sight cases. Because of these differences, the optimal way of using multiple antenna systems depends on the situation or environment. In adaptive techniques, there will be able to pick the best possible solution at all times through the tracking of

environment/propagation characteristics.

In this chapter, we use a set of antennas equally spaced by a half wavelength ($\lambda/2$), where λ denotes the wavelength. A switching scheme is constructed based on the pre-determined channel condition. In the case of UHR channel, we will turn off some antennas and adapt these MIMO algorithms to achieve diversity gain or data rate maximization. On the contrary, beamforming technique will be applied the received signal to increase the average SNR over a CLR channel.

5.1 MIMO Channel Model for IEEE 802.11n

5.1.1 MIMO Channel Model

Consider a communication link comprising N_t transmit antennas and N_r receive antennas that contributes to a MIMO channel. Some important assumptions are made firstly:

1. The channel fading is frequency-flat. It means that what we deal with is the case of narrowband transmission, and constant fading over the bandwidth is thereby deserved. It also means that the channel gain can be represented as a complex number.
2. The communication is carried out in packets that are of shorter time-span then the coherence time of the channel. This means the channel is constant during the transmission of a packet.
3. There is only a single user transmitting at any given time, so the received signal is corrupted by AWGN only.

With these assumptions, it is common to formulate the MIMO channel model by the complex baseband vector notation

$$\mathbf{r}_t = \mathbf{H}_t \mathbf{s}_t + \boldsymbol{\eta}_t \tag{5.1}$$

where $\mathbf{s}_t = \left[s_t^1, s_t^2, \cdots s_t^{N_t} \right]^T$ is the sent signal vector, $\mathbf{r}_t = \left[r_t^1, r_t^2, \cdots r_t^{N_r} \right]^T$ is the received datum vector, and $\boldsymbol{\eta}_t = \left[\eta_t^1, \eta_t^2, \ldots, \eta_t^{N_r} \right]^T$ is the additive white Gaussian noise (AWGN) vector at a given time instant t. The $N_r \times N_t$ channel matrix $\mathbf{H}_t$ is made up of elements $h_t^{i,j}$ as follows

$$\mathbf{H}_t = \begin{bmatrix} h_t^{1,1} & \cdots & h_t^{1,N_t} \\ \vdots & \ddots & \vdots \\ h_t^{N_r,1} & \cdots & h_t^{N_r,N_t} \end{bmatrix} \tag{5.2}$$

where

$$\begin{aligned} h_t^{i,j} &= \alpha_t^{i,j} + j\beta_t^{i,j} = \sqrt{\alpha_t^{i,j^2} + \beta_t^{i,j^2}}\, e^{-j \arctan \frac{\beta_t^{i,j}}{\alpha_t^{i,j}}} \\ &= |h_t^{i,j}| \cdot e^{j\phi_t^{i,j}} \end{aligned} \tag{5.3}$$

denotes the complex channel gain between the jth transmit antenna and ith receive antenna. The $h_t^{i,j}$ coefficients stand for transmission properties of the medium, usually Rayleigh distributed in a rich scattering environment with no line-of-sight (LOS), and of course are unknown. In fact, they are likely to change over time and be subject to varying degrees of fading. But if all these coefficients are known, there will be sufficient information for the receiver to eliminate interference from the other transmitters operating at the same frequency. Hence, an essential aspect of MIMO processing is the determination of the channel matrix $\mathbf{H}_t$. This matrix is initially estimated using a well-designed preamble training sequences sent ahead of the payload. The matrix is subsequently refined dynamically using pilot tones that are sent in conjunction with the payload. Some MIMO channel estimation methods are proposed, which can be found in [46] and [47]. Moreover, when comparing systems equipped with different N_t and N_r, we need to normalize $\mathbf{H}$. $\mathbf{H}$ is normalized such that

$\|\mathbf{H}\|_F^2 = N_t \cdot N_r$, where $\|\cdot\cdot\|_F^2$ represents the Frobenius norm. This normalization removes the influence of the variation in time and frequency but keeps the spatial characteristics.

5.1.2 MIMO Channel Model for IEEE 802.11n

The MIMO channel matrix **H** for each tap, at one instance of time, in the A-F delay profile models can be separated into a fixed (constant, LOS) matrix and a Rayleigh (variable, NLOS) matrix [48]. The well-known Ricean model is used to demonstrate the different degrees of scattering richness. The channel possesses two distinct components:

- A specular component that illuminates the entire array and is thus spatially deterministic from antenna to antenna
- A scattered Rayleigh-distributed component which varies randomly from antenna to antenna

In the case of a rich-scattering environment, the deterministic component vanishes, while in the case of a pure specular environment, the channel response is totally contributed by the deterministic component. Note that the Ricean model comprising both the rich-scattering and specular is a particular case. Assume that the scattering terms on different antennas as full uncorrelated and only source of correlation among the array antennas is the deterministic component. The Ricean channel model is given by [26]

$$\mathbf{H} = \sqrt{\frac{K}{K+1}}\mathbf{H}^{sp} + \sqrt{\frac{1}{K+1}}\mathbf{H}^{sc} \tag{5.4}$$

where K denotes the Ricean K-factor, defined as the power ratio of deterministic-to-scattered, and

$$\mathbf{H}^{sc} = \sqrt{G}\tilde{\mathbf{H}}^{sc} \tag{5.5}$$

with G being the (local average) large-scale path gain encompassing distance-dependent as well as shadow fading. The elements of the scattering component $\tilde{\mathbf{H}}^{sc}$ are statistically independent unit variance complex Gaussian random variables. The specular component is given by

$$\mathbf{H}^{sp} = \sqrt{G}\tilde{\mathbf{H}}^{sp} \tag{5.6}$$

where $\tilde{\mathbf{H}}^{sp} = \mathbf{a}\left(\theta_r\right)\mathbf{a}^H\left(\theta_t\right)$, with $\mathbf{a}(\theta_t)$ and $\mathbf{a}(\theta_r)$ being the specular array responses of the transmitter and receiver, respectively. Note that the array response $\mathbf{a}(\theta)$ associated with an N-element linear array is given by $\left[1, e^{j2\pi d\cos(\theta)}, \ldots, e^{j2\pi d(N-1)\cos(\theta)}\right]^T$, where θ is the angle of arrival or departure of the specular component, and d is the antenna spacing in wavelength. The Ricean channel model can be simplified to a UHR channel as the value of K is close to zero, while as K approaches to an infinite number, the Ricean channel model is equivalent to a CLR channel.

The cluster model was introduced first by Saleh and Valenzuela [49] and later verified, extended, and elaborated upon by many other researchers in [39]-[44]. The received signal amplitude β_{kl} is a Rayleigh-distributed random variable with a mean-square value that obeys a double exponential decay law

$$\overline{\beta_{kl}^{\ 2}} = \overline{\beta^2(0,0)}e^{-T_l/\Gamma}e^{-\tau_{kl}/\gamma} \tag{5.7}$$

where $\overline{\beta^2(0,0)}$ represents the average power of the first arrival of the first cluster, T_l represents the arrival time of the l^{th} cluster, and τ_{kl} is the arrival time of the k^{th} arrival within the l^{th} cluster, relative to T_l. The parameters Γ and γ determine the inter-cluster signal level rate of decay and the intra-cluster rate of decay, respectively. The rates of

the cluster and ray arrivals can be determined using exponential rate laws

$$p(T_l \mid T_{l-1}) = \Lambda e^{-\Lambda(T_l - T_{l-1})} \tag{5.8}$$

$$p(\tau_{kl} \mid \tau_{k-1,l}) = \lambda e^{-\lambda(T_l - T_{l-1})} \tag{5.9}$$

where Λ is the cluster arrival rate and λ is the ray arrival rate.

The number of clusters found in different indoor environments varies between 1 and 7. Figure 5.2 shows Model D delay profile with clusters outlined by exponential decay. Clearly, three clusters can be identified. For Models B, C, D, E, and F we identified 2, 2, 3, 4 and 6 clusters, respectively. The number of clusters in each of the models B-F agrees well with the results reported in the literature. We recall that the model A consists of only one tap. Next, we extend each cluster in B-F models so that they overlap. We use a straight-line extrapolation function on the first few visible taps of each cluster. The powers of overlapping taps were calculated so that the total sum of the powers of overlapping taps corresponding to different clusters equals to the powers of the original B-F power delay profiles. In Table Ia we summarize the channel model parameters, and in Table Ib we provide model to environment mapping.

5.2 Determination of Channel Condition

In this section, we first determine the channel characteristic of UHR and CLR channels. The corresponding results are then used to select the optimal space-time processing technique. The condition number, defined as a ratio of the largest and smallest singular values of the channel matrix **H,** can be an indicator about the quality of the channel [33]. Since a CLR channel is a rank deficient channel, the condition number of the channel matrix will be very large. On the other hand, the condition number associated with a UHR channel is moderate due to that a UHR channel is a

full rank channel. Specifically, a CLR channel is determined as the condition number of the channel matrix is very larger. Contrarily, the channel is considered a UHR channel.

An example obtained by a 4 × 4 MIMO system is used to investigate the relationship between the condition number and the channel types (CLR and UHR channels). The number of samples is ten thousand. Figures 5.3 shown the condition numbers of CLR and UHR channels, respectively, obviously indicate that the condition number of a CLR channel (minimum value is equal to 2×10^{16}) is much larger than that of the a channel (maximum and mean values are equal to 6×10^{2} and 10.87).

5.3 Transmission Mode Selection Strategies

After the determination of channel condition, the optimal space-time processing technique is then selected for the given channel. In this section, the selection strategy of proper transmission mode is discussed from the point-of-view of the ergodic capacity.

5.3.1 Link-Optimal Space-Time Processing Based on Ergodic Capacity

The link-optimal space-time processing is chosen in the sense of maximum link spectral efficiency [37]-[38]. The capacities of V-BLAST and adaptive array over different channels are discussed as follows:

1. Capacity of V-BLAST

When the channel or interference information cannot be obtained by the transmitter preliminarily, the capacity of V-BLAST is given by [57]

$$C = \log_2 \det\left(\mathbf{I}_{M_R} + \frac{P_T}{M_T}\mathbf{H}\mathbf{H}^H\left(\mathbf{K}_n\right)^{-1}\right) \tag{5.10}$$

where P_T is total transmit power and $\mathbf{K}_n$ is an interference-plus-noise covariance matrix. In a noise-dominated situation, we have $\mathbf{K}_n = \sigma^2\mathbf{I}_{M_R}$ such that the capacity can be reduced to

$$C = \log_2 \det\left(\mathbf{I}_{M_R} + \frac{P_T}{\sigma^2 M_T}\mathbf{H}\mathbf{H}^H\right) \tag{5.11}$$

2. Capacity of adaptive array

With channel and interference information known at the transmitter and application of beamforming, a single data stream is transmitted by multiple antennas with proper weight vector **w**. The received signal can be expressed by $\mathbf{y} = \mathbf{H}\mathbf{w}s + \mathbf{n}$, where s is the transmitted signal. The corresponding capacity is given by [57]

$$\begin{aligned} C &= \log_2 \det\left(\mathbf{I}_{M_R} + P_T\mathbf{H}\mathbf{w}\mathbf{w}^H\mathbf{H}^H\left(\mathbf{K}_n\right)^{-1}\right) \\ &= \log_2\left(1 + P_T\mathbf{w}^H\mathbf{H}^H\left(\mathbf{K}_n\right)^{-1}\mathbf{H}\mathbf{w}\right) \end{aligned} \tag{5.12}$$

Note the Equation 5.12 holds when the fact $\det\left(\mathbf{I}_m + \mathbf{A}\mathbf{B}\right) = \det\left(\mathbf{I}_n + \mathbf{B}\mathbf{A}\right)$ for matrices $\mathbf{A}_{(\mathrm{m}\times\mathrm{n})}$ and $\mathbf{B}_{(\mathrm{n}\times\mathrm{m})}$. The weights of optimal beamformer is obtained by maximizing the system capacity in Equation 5.12 with the constraint that the total transmit power is limited to P_T.

$$\mathbf{w} = \arg\max_{\|\mathbf{w}\|^2=1}\left(P_T\mathbf{w}^H\mathbf{H}^H\left(\mathbf{K}_n\right)^{-1}\mathbf{H}\mathbf{w}\right) \tag{5.13}$$

whose solution is given by the dominant eigenvector of $\mathbf{H}^H(\mathbf{K}_n)^{-1}\mathbf{H}$ with norm set to

one. If the interference covariance matrix is not available at the transmitter, the signaling process is the same as when the noise covariance matrix is diagonal and the optimization problem becomes

$$\mathbf{w} = \arg\max_{\|\mathbf{w}\|^2=1} \left(P_T \mathbf{w}^H \mathbf{H}^H \mathbf{H} \mathbf{w} \right) \tag{5.14}$$

Simulation results are demonstrated to confirm the performance of MIMO systems. Each simulation result is obtained by the average from 500 independent trials. In the first simulation, the effect of the Ricean K-factor K is examined for a 2×2 MIMO system with SNR =10 dB, i.e., $P_T G/\sigma^2 = 10$. Figure 5.4 (a) shows the ergodic capacity versus the values of K. The results indicate that the ergodic capacity of V-BLAST is much larger than adaptive array as K is close to zero. That is, V-BLAST outperforms adaptive array over a UHR channel. On the contrary, as K is infinite, the ergodic capacity of adaptive array is higher than that of V-BLAST. The simulation was repeated with a 4×4 MIMO system. Figure 5.4 (b) shows the ergodic capacity plot for two types of the space-time processing techniques corresponding to Figure 5.4 (a). The same trend as in the previous case is observed. Obviously, adaptive array works better over the CLR channel. Similarly, Figure 5.4 (b) has the same trend as in the previous case of Figure 5.4 (b).

In the third simulation, the performance of various algorithms is investigated for a 4×4 MIMO system over a UHR channel ($K = 10^{-1}$). The corresponding ergodic capacity plots are shown in Figure 5.5 (a) with SNR varied. Obviously, the capacities of all types increase as the values of SNR increase. V-BLAST achieves the better performance. This implies that V-BLAST is the optimal space-time processing over a UHR channel. The simulation was repeated with a CLR channel ($K = 10^4$) used. The

capacities for all types corresponding to Figure 5.5 (a) shown in Figure 5.5 (b) indicate the same trend as in the previous case. However, beamforming performs best and provides an optimal space-time processing technique over a CLR channel. Consequently, V-BLAST and beamforming are the optimal space-time processing techniques over a UHR channel and a CLR channel, respectively.

5.3.2 Analysis of IEEE 802.11n Channel Model

In this section we determine some of the important properties of the 802.11n channel model. The time-domain MIMO channel matrix can be obtained from the Matlab program in [50], with proper antenna correlation properties. For the TGn channel model, there may be only several significant eigen channels available. Hence, in the following simulations, we use the information theoretic criterion [50] such as the AIC (Akaike Information Criterion) [50] or the MDL (Minimum Description Length) [50] to decide the number of effective eigen channels for the beamforming mode. The two popular information criteria are given as follows:

$$\mathrm{AIC}(N_s) = -\ln f\left(\mathbf{x}(1),\cdots,\mathbf{x}(i) \mid \hat{\xi}_{ML}\right) + N_s(2M - N_s + 1)$$

$$\mathrm{MDL}(N_s) = -\ln f\left(\mathbf{x}(1),\cdots,\mathbf{x}(i) \mid \hat{\xi}_{ML}\right) + \frac{1}{2}N_s(2M - N_s + 1)\ln(i)$$

where N_s is the number of effective eigen channels and M is the number of antenna elements. The effective eigen channel number estimates are given by

$$\widehat{N_s} = \arg\min_{N_s} \ \mathrm{AIC}(N_s)$$

$$\widehat{N_s} = \arg\min_{N_s} \ \mathrm{MDL}(N_s)$$

Figures 5.6 (a)-5.11 (a) show the ergodic capacity for Models A-F assuming a 4x4 MIMO system and the LOS conditions. Each simulation result is obtained by the average from 10000 independent trials. The results indicate that the ergodic capacity of V-BLAST is much larger than adaptive array in model A. In the other models, the

ergodic capacities of adaptive array are higher than that of V-BLAST.

The same simulations are repeated for the NLOS conditions. Figures 5.6 (b)-5.11 (b) show the ergodic capacity plot for two types of the space-time processing techniques corresponding to the LOS conditions. The results indicate that the ergodic capacity of V-BLAST is much larger than adaptive array in models A, D, E, and F. In models B and C, the ergodic capacity of adaptive array is higher than that of V-BLAST. For models D, E and F, it is expected that the capacity is higher because of more clusters present with wider angular spread when compared to models A, B, and C.

5.4 Summary

In this chapter, we first use the condition number to classify channels. The channel with a larger condition number is considered as a CLR channel; otherwise, it will be classified into a UHR channel. Optimal space-time processing is then determined based on the channel condition. Further, in the case of UHR channel, we will select V-BLAST. In addition, over a CLR channel, we will select beamforming with adaptive modulation.

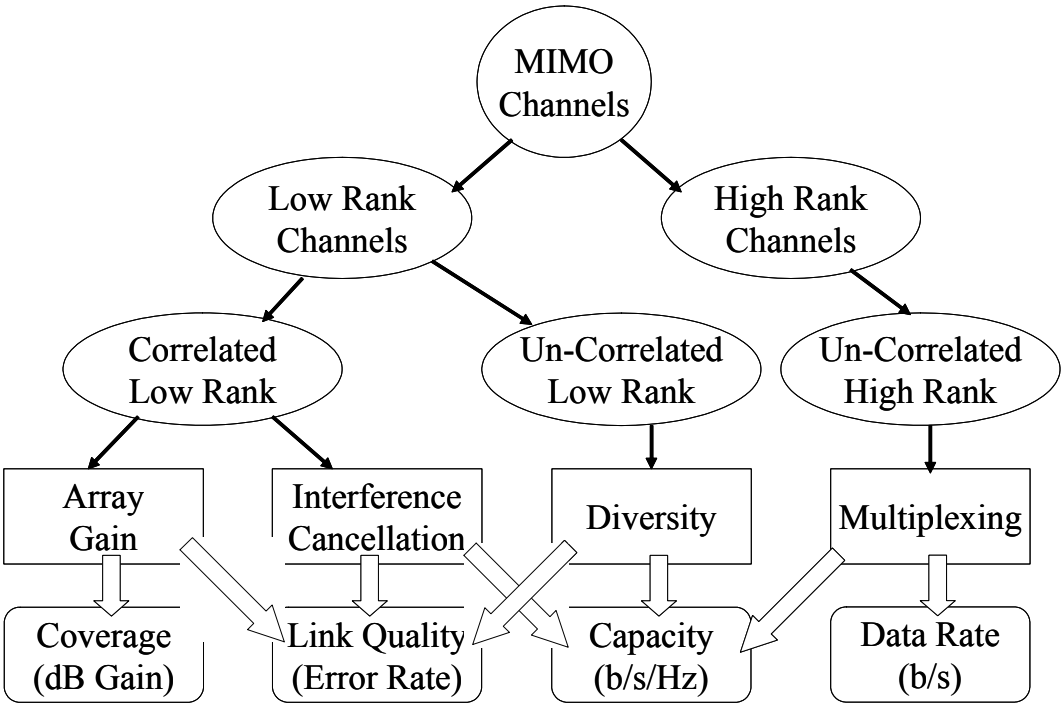

Figure 5.1: MIMO techniques and their benefits.

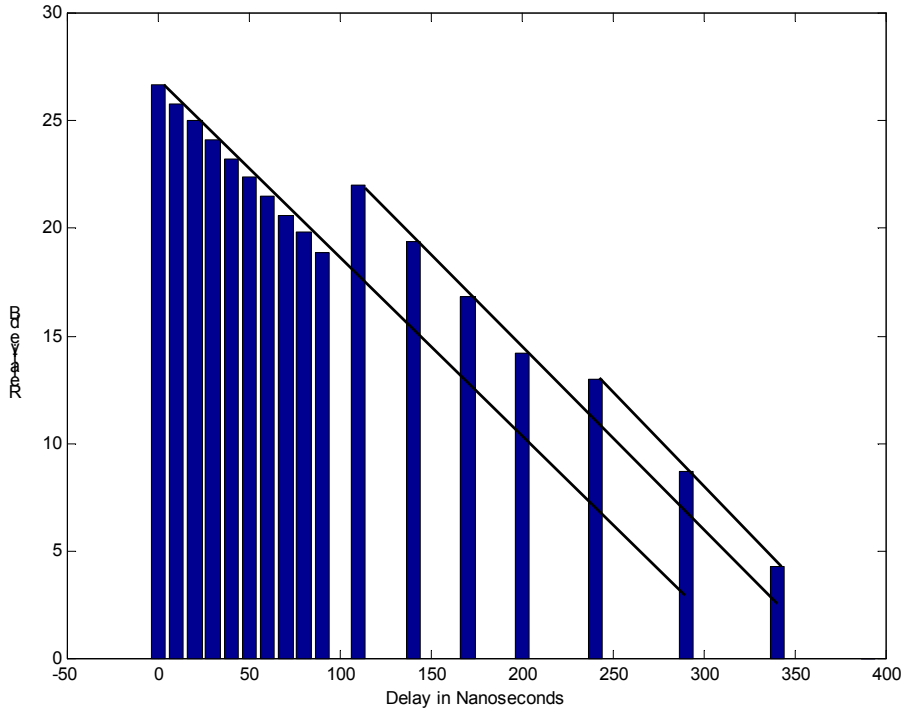

Figure 5.2: Model D delay profile with cluster extension (overlapping clusters).

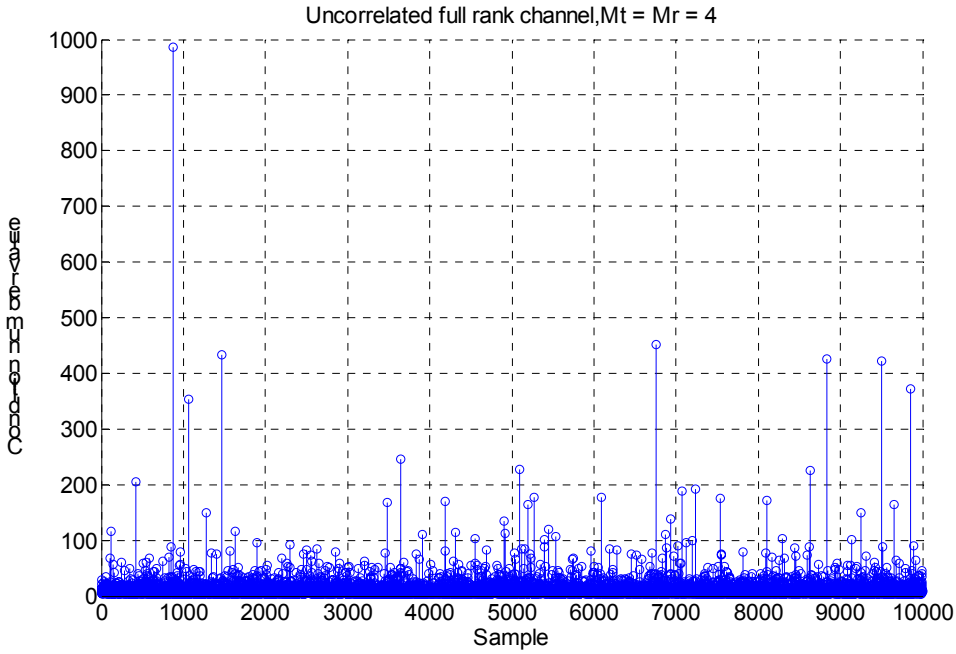

(a)

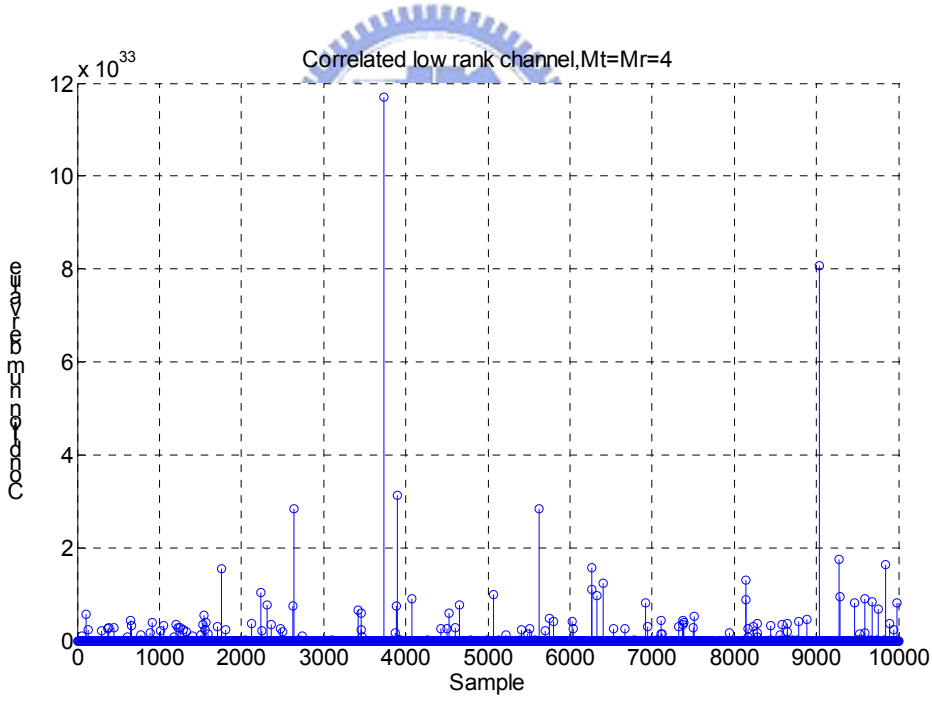

(b)

Figure 5.3: Condition number with $M_T = M_R = 4$. (a) Maximum condition number = 603.0125 and mean = 10.8683 over UHR channel. (b) Minimum condition number = 1.9585 × 1016 over CLR channel.

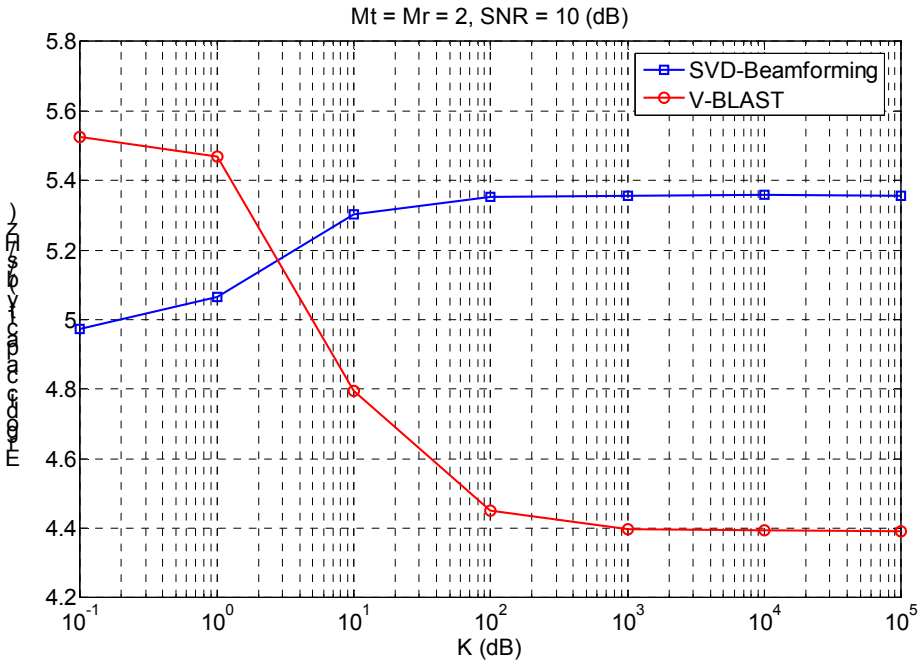

(a)

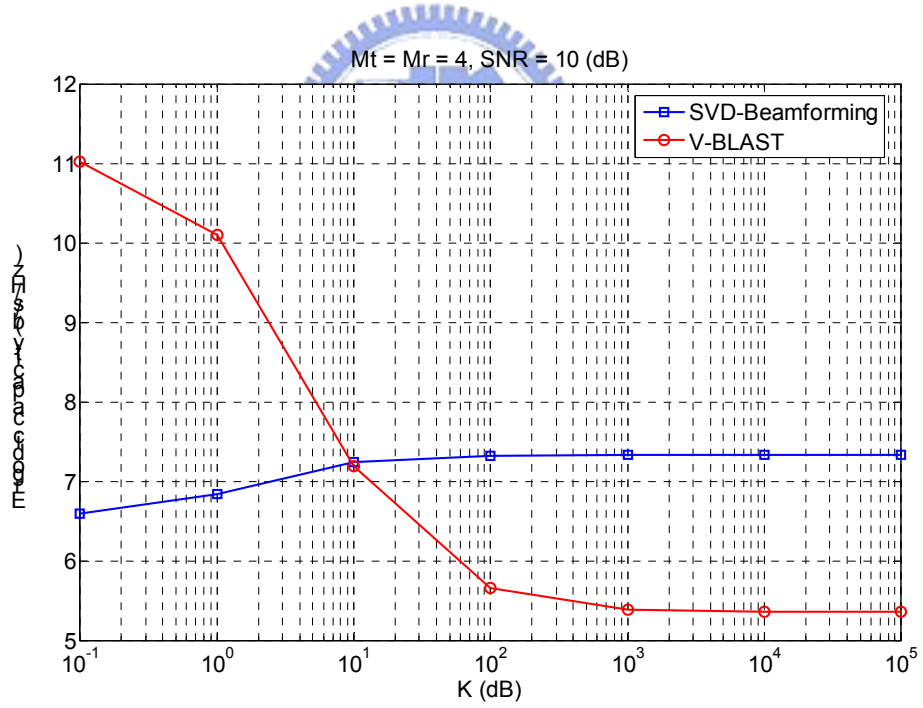

(b)

Figure 5.4: Ergodic capacity versus Ricean K–factor of various transmission techniques and average SNR = 10 dB. (a) $M_T = M_R = 2$. (b) $M_T = M_R = 4$.

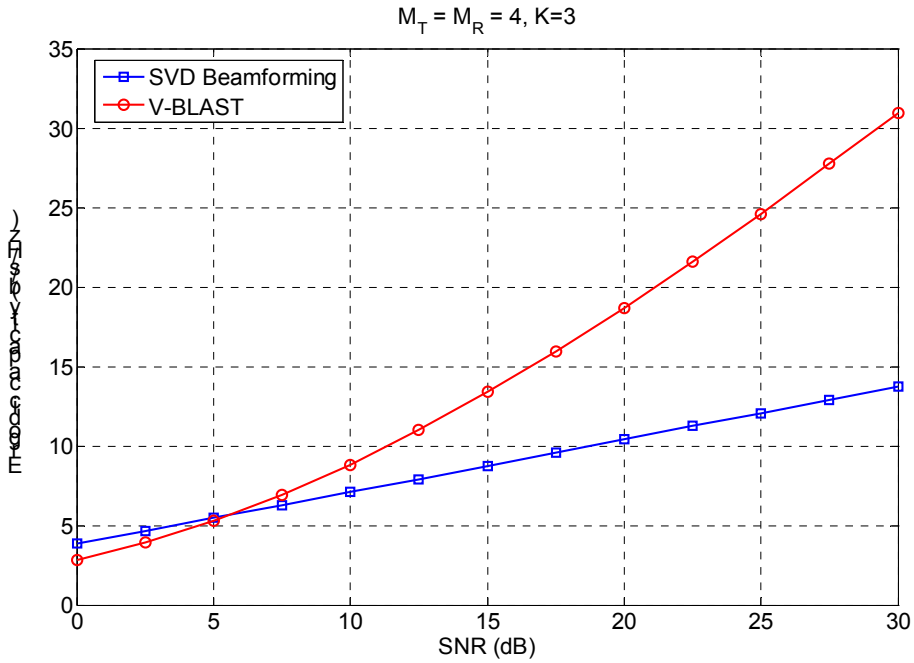

(a)

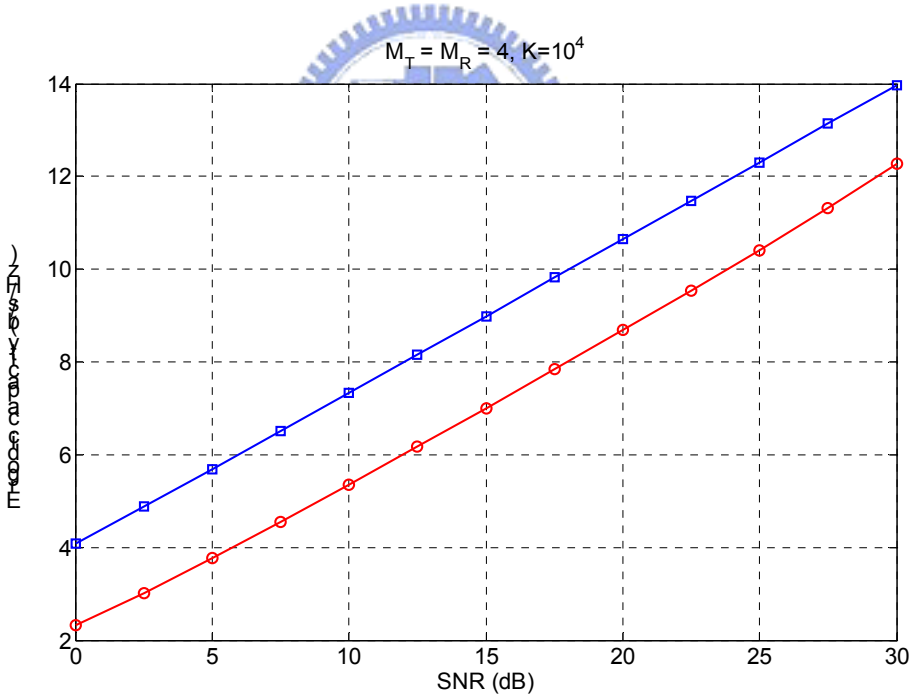

(b)

Figure 5.5: Ergodic capacity versus SNR of various transmission techniques with $M_T = M_R = 4$. (a) UHR channel. ($K = 10^{-1}$) (b) CLR channel. ($K = 10^4$)

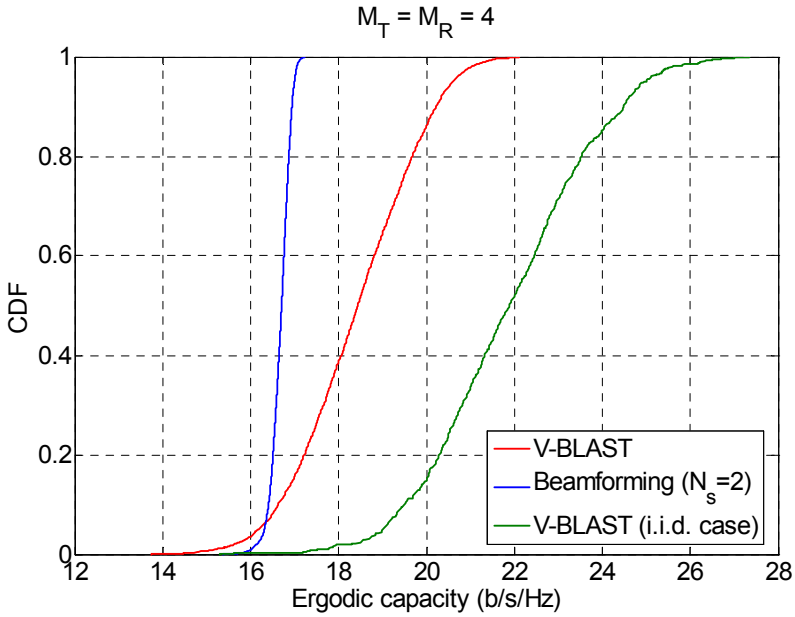

(a)

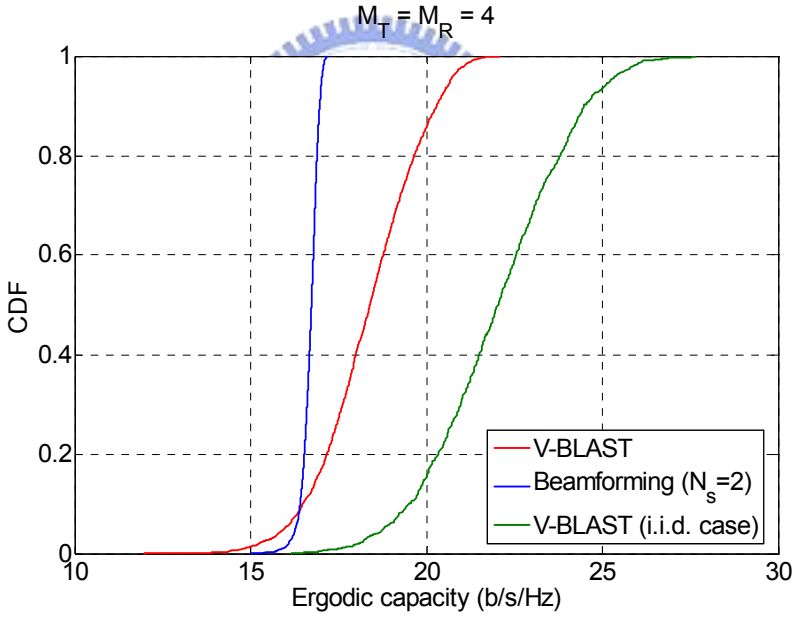

(b)

Figure 5.6: Ergodic capacity CDFs of various transmission techniques with $M_T = M_R = 4$. (a) IEEE 802.11n channel. (Model A, LOS condition) (b) IEEE 802.11n channel. (Model A, NLOS condition)

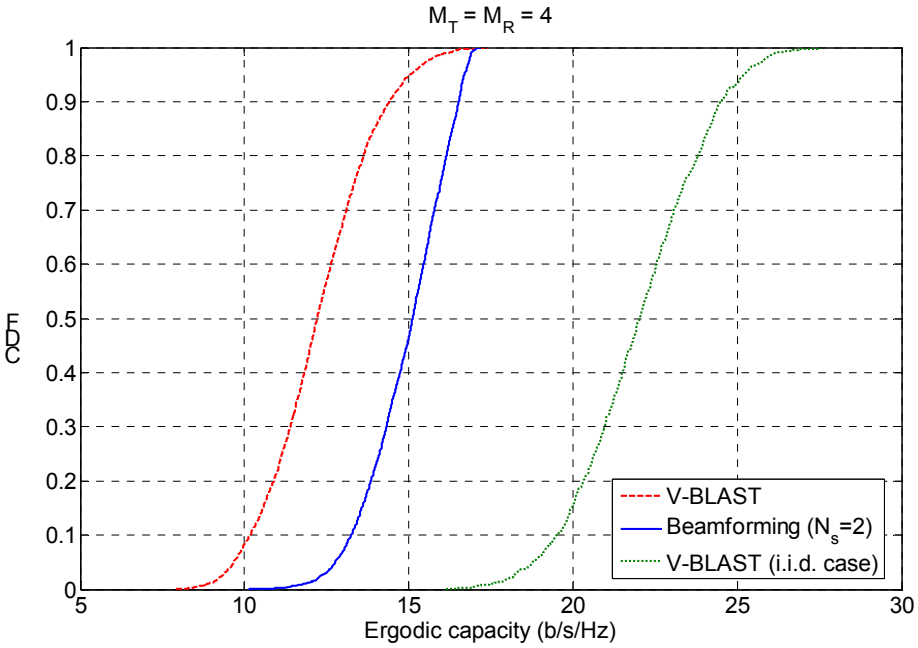

(a)

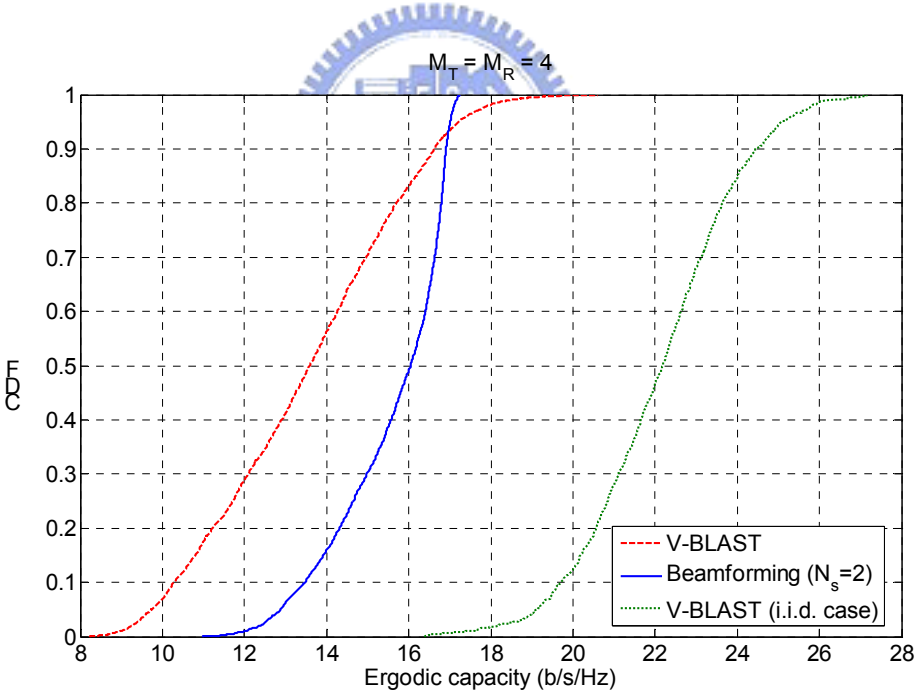

(b)

Figure 5.7: Ergodic capacity CDFs of various transmission techniques with $M_T = M_R = 4$. (a) IEEE 802.11n channel. (Model B, LOS condition) (b) IEEE 802.11n channel. (Model B, NLOS condition)

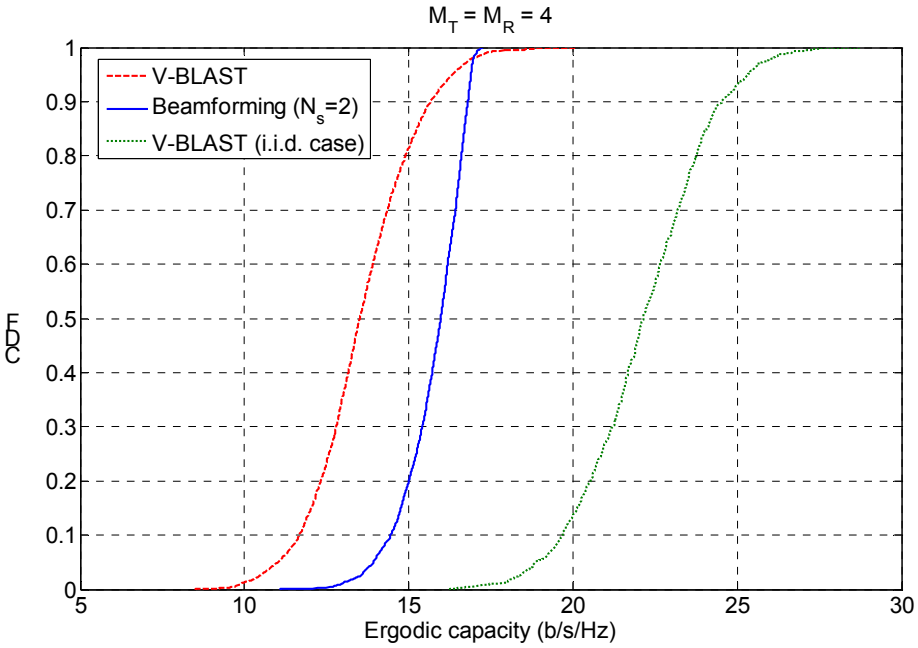

(a)

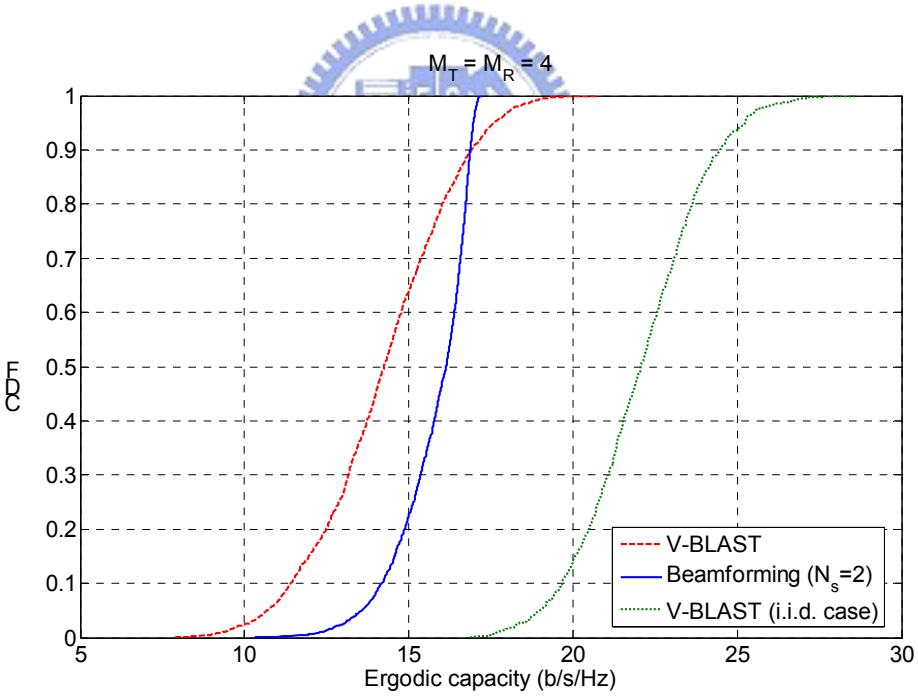

(b)

Figure 5.8: Ergodic capacity CDFs of various transmission techniques with $M_T = M_R = 4$. (a) IEEE 802.11n channel. (Model C, LOS condition) (b) IEEE 802.11n channel. (Model C, NLOS condition)

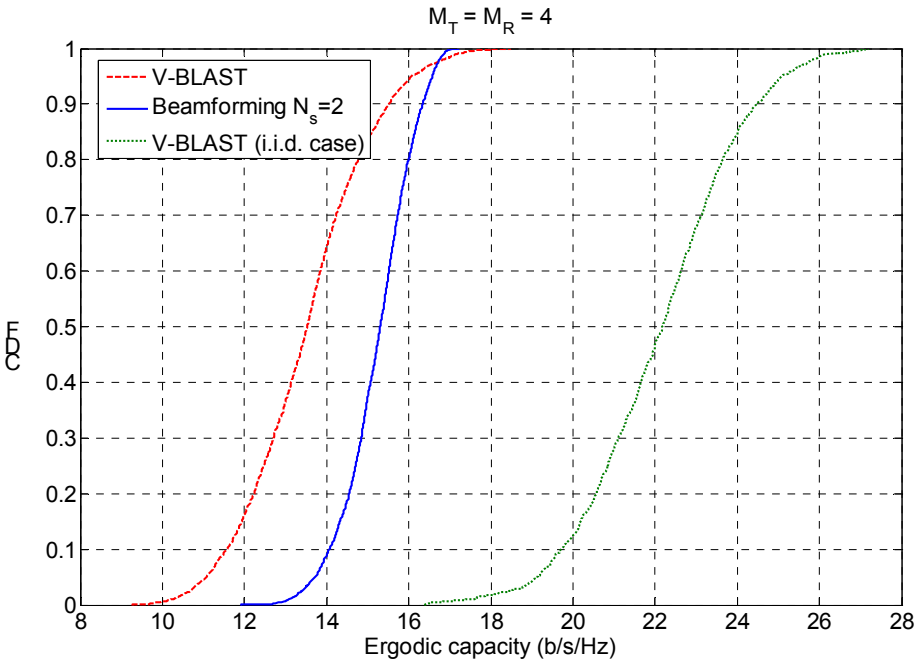

(a)

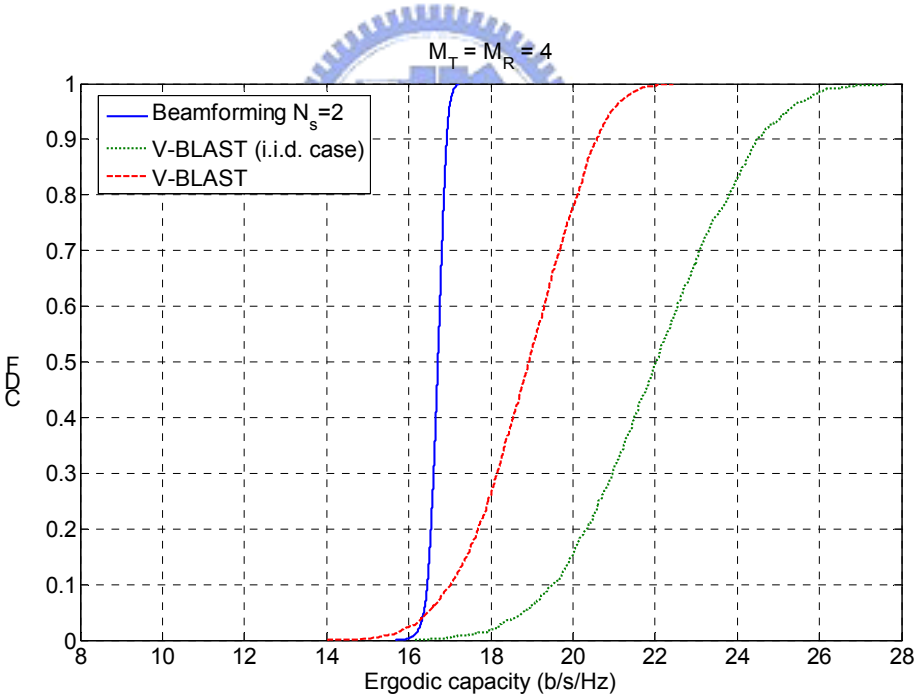

(b)

Figure 5.9: Ergodic capacity CDFs of various transmission techniques with $M_T = M_R = 4$. (a) IEEE 802.11n channel. (Model D, LOS condition) (b) IEEE 802.11n channel. (Model D, NLOS condition)

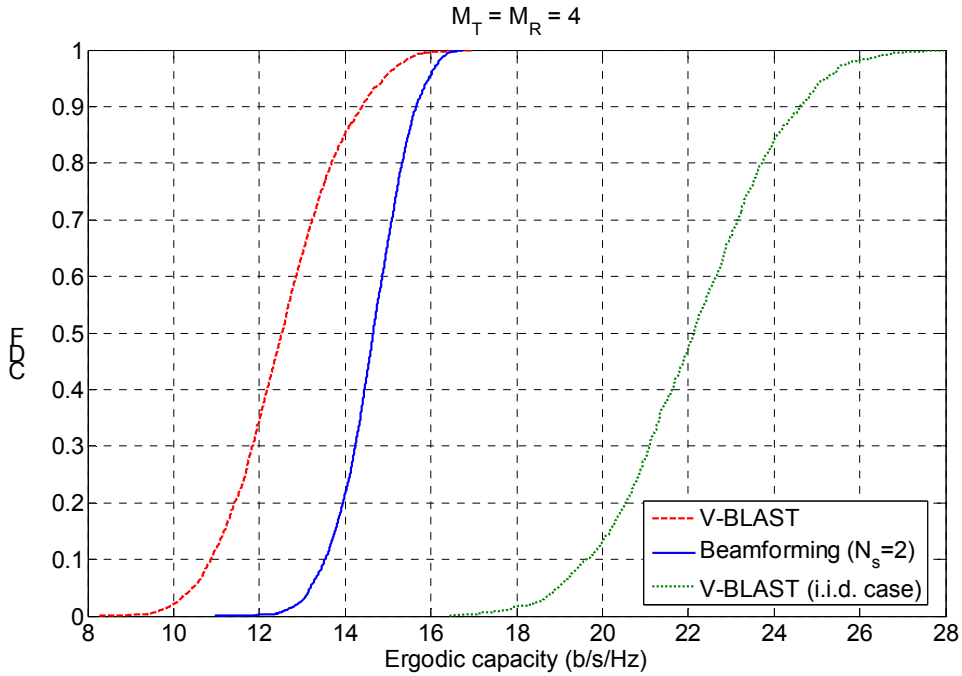

(a)

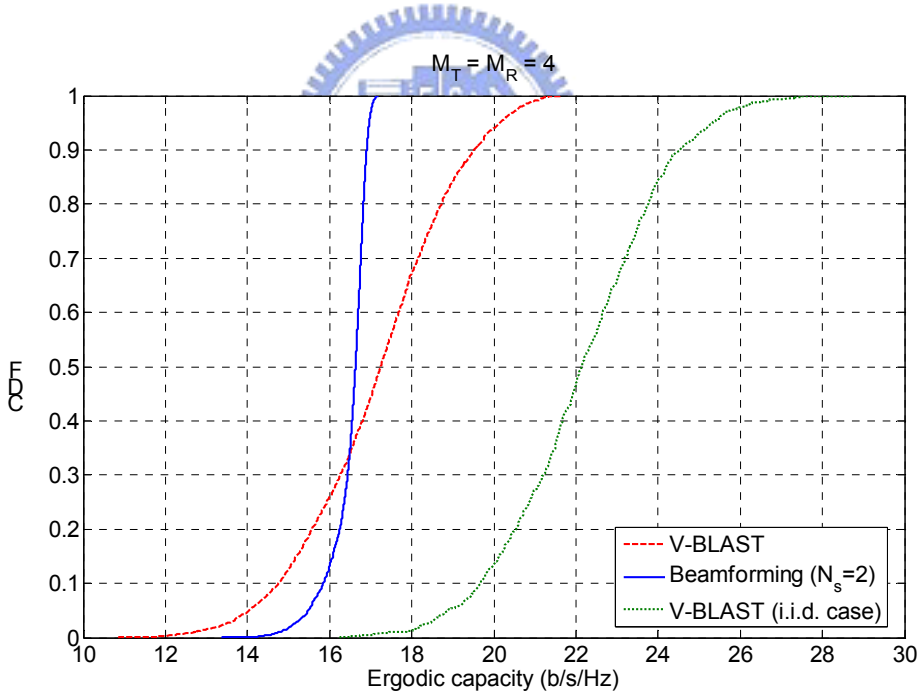

(b)

Figure 5.10: Ergodic capacity CDFs of various transmission techniques with $M_T = M_R = 4$. (a) IEEE 802.11n channel. (Model E, LOS condition) (b) IEEE 802.11n channel. (Model E, NLOS condition)

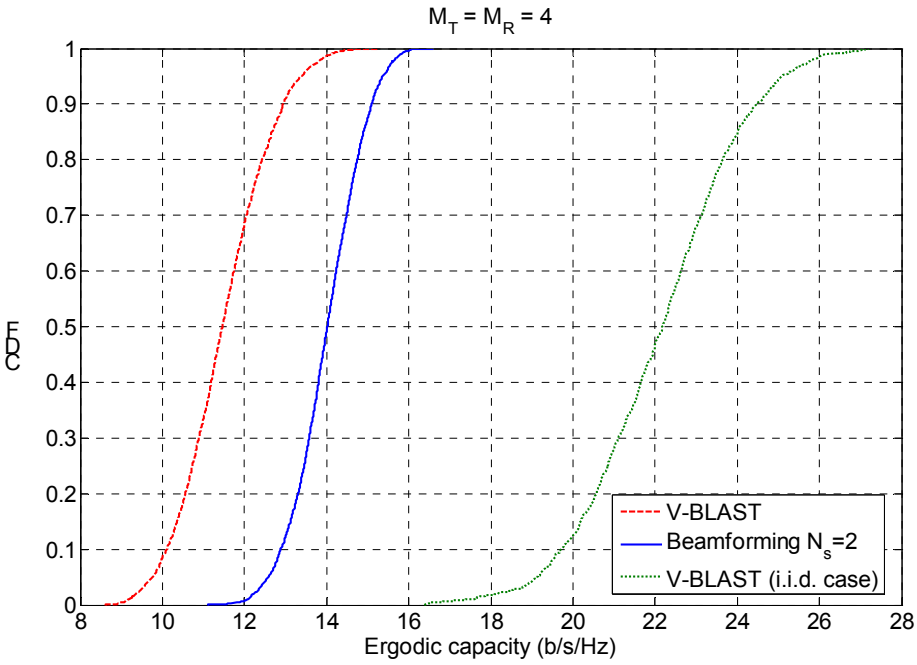

(a)

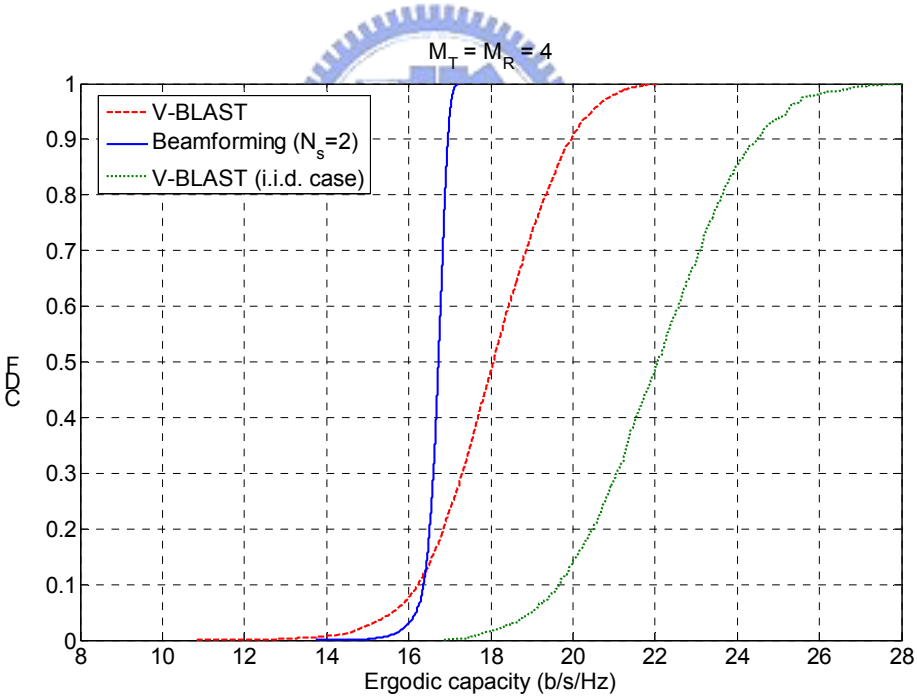

(b)

Figure 5.11: Ergodic capacity CDFs of various transmission techniques with $M_T = M_R = 4$. (a) IEEE 802.11n channel. (Model F, LOS condition) (b) IEEE 802.11n channel. (Model F, NLOS condition)

Table 5.1: Summary of model parameters for LOS/NLOS conditions. *K*-factor for LOS conditions applies only to the first tap, for all other taps $K = -\infty$ dB.

A (optional)	LOS/NLOS	0/ -∞	0	1 tap
B	LOS/NLOS	0 / -∞	15	2
C	LOS/NLOS	0 / -∞	30	2
D	LOS/NLOS	3 / -∞	50	3
E	LOS/NLOS	6 / -∞	100	4
F	LOS/NLOS	6 / -∞	150	6

Table 5.2: Model to environment mapping.

Environment	**Condition**	**Model**
Residential	LOS	B – LOS
	NLOS	B - NLOS
Residential/ Small Office	LOS	B - LOS
	NLOS	C - NLOS
Typical Office	LOS	C - LOS
	NLOS	D - NLOS
Large Office	LOS	D - LOS
	NLOS	E - NLOS
Large Space (Indoors and Outdoors)	LOS	E - LOS
	NLOS	F - NLOS

Chapter 6

Conclusion

In this thesis, we survey the MIMO techniques and explore their applications in the OFDM systems. With the aid of OFDM, we show that MIMO can find a feasible way in extending itself to wideband transmission based on the flat fading channels introduced by OFDM tones. In Chapter 2, we present two possible MIMO-OFDM architectures: one is beamforming based OFDM, aimed to provide high quality communication link and the other is targeted at high spectral efficiency.

In Chapter 3, we compare several configurations with different modulation orders and conclude that the best scheme with respect to BER performance differs in different channel conditions in the adaptive MIMO-OFDM systems. Although the adaptive MIMO-OFDM systems can enjoy both the diversity and multiplexing gains in a flexible manner, it does not consider the requirement of higher layer. By analytical throughput computation, the adaptive MIMO-OFDM systems at physical layer will not lead to a significant throughput increase at higher layers.

Observing that the network performance in mobile wireless applications is determined significantly by a complex interaction between PHY, medium access (MAC), link layer, and transmission control protocol (TCP), a joint design of these layers was proposed in Chapter 4. The cross layer design AMC system combines adaptive modulation and coding scheme at the physical layer and MAC protection

strategies at the MAC layer to maximize the system throughput under prescribed delay and performance constrains. It presents a new point of view in which SM and SD are complementary rather than competing approaches. We also derived a closed-form expression of the average throughput for packets transmission. This expression can be used to find the optimum packet length for a given channel condition to achieve the maximum throughput. Besides, the expression has shown that factors such as the optimum packet length and optimum transmission rate are both functions of the signal to noise ratio. These equations can be used to find the optimum transmission parameters that the system should be operated with in order to achieve the maximum throughput. By adjusting the transmission parameters to prevent ill-conditioned sub-channels from dominating the system performance, an indirect form of diversity is also drawn. Computer simulation result demonstrated the throughput and PER performance improvement of the cross-layer design AMC.

In chapter 5, we consider a wireless communications system with smart antenna and MIMO techniques incorporated. It can select effective techniques to cope with the problems associated with the wireless environment. The condition number is used to determine the channel type. Moreover, from the point-of-view of ergodic capacity, the link-optimal space-time processing technique for a specific channel condition is then discussed. Consequently, in the case of UHR channel, V-BLAST is the primary modes to be considered. With the aid of the information criterion, we can find the effective eigen channel and select beamforming mode over a CLR channel. The simulation results indicate that the ergodic capacity of V-BLAST is much larger than the adaptive array in model A. In the other models, the ergodic capacities of the adaptive array are higher than that of V-BLAST. The ergodic capacity of models D, E, F, are higher because of the more clusters present with wider angular spread when compared to the models A, B, and C.

As a remark for addressing the ability of system extension, the proposed adaptive MIMO transceiver is an example of link adaptation which can be achieved by adjusting the transmission parameters. It is noted that the proposed adaptive MIMO transceiver is essentially an adaptive modulation and coding scheme at the physical layer, and integrated with several protection strategies at the MAC layer to achieve the QoS demands under prescribed delay and error performance constraints. Finally, the assumptions that perfect CSI is available at the receiver, and the feedback channel has zero delay and is error free, may not always hold true. One possible extension of this work is to design and analyze the cross layer design with imperfect CSI at the transmitter. Besides, the impact of cross layer design on other parameters at the physical and higher layers is also worth investigating.

Bibliography

[1] G. J. Foschini, "Layered space-time architecture for wireless communication in a fading environment when using multiple antennas," *Bell Labs Syst. Tech. J.*, vol. 1, pp. 41-59, Autumn 1996.

[2] G. J. Foschini and M. J. Gans, "On limits of wireless communications in a fading environment when using multiple antennas," *Wireless Personal Commun.*, vol. 6, no. 3, pp. 311-335, 1998.

[3] P. W. Wolniansky, G. J. Foschini, G. D. Golden, R. A. Valenzuela, "V-BLAST: an 1rchitecture for realizing very high data rates over the rich-scattering wireless channel," *URSI International Symposium*, pp. 295-300, 29 Sep. -2 Oct. 1998.

[4] X. Li, H. Huang, G. J. Foschini, and R. A. Valenzuela, "Effects of iterative detection and decoding on the performance of BLAST," *IEEE GLOBECOM*, vol. 2, pp. 1061-1066, 2000.

[5] E. Biglieri, G. Taricco and A. Tulino, "Decoding space-time codes with BLAST architectures," *IEEE Trans. Signal Processing*, vol. 50, no. 10, pp. 2547-2552, Oct. 2002.

[6] Y. Li, J. H. Winters, N. R. Sollenberger, "MIMO-OFDM for wireless communications: signal detection with enhanced channel estimation," *IEEE Trans. Commu.*, vol. 50, no. 9, pp. 1471-1477, Sept. 2002.

[7] S. Catreux, D. Gesbert, V. Ercge, "Adaptive modulation and MIMO coding for broadband wireless data networks," *IEEE Communications Magazine*, June 2002.

[8] S. Shim, J. S. Choi, C. Lee, D. H. Youn, "Rank adaptive transmission to improve the detection performance of the BLAST in spatially correlated MIMO channel," *IEEE VTC 2002-Fall*, vol. 1, pp. 195-198, Sept. 2002.

[9] A. Goldsmith and S. Chua, "Variable-rate variable-power MQAM for fading channels," *IEEE Trans. Commu.*, vol. 45, pp. 1218-1230, Oct. 1997.

[10] W. T. Webb and R. Steele, “Variable rate QAM for mobile radio,” *IEEE Trans. Commu.*, vol. 43, no. 7, pp. 2223-2230, July 1995.

[11] S. M. Alamouti, “A simple transmitter diversity technique for wireless communications,” *IEEE J. Select. Areas Commun.*, vol. 16, no. 8, pp. 1451-1458, Oct. 1998.

[12] V. Tarokh, N. Seshadri, and A. R. Calderbank, “Space-time codes for high data rate wireless communication: performance analysis and code construction,” *IEEE Trans. Inform. Theory*, vol. 44, no. 2, pp. 744-765, Mar. 1998.

[13] V. Tarokh, H. Jafarkhani, and A. R. Calderbank, “Space-time block codes from orthogonal designs,” *IEEE Trans. Inform. Theory*, vol. 45, no. 5, pp. 1456-1467, July 1999.

[14] V. Tarokh, H. Jafarkhani, and A. R. Calderbank, “Space-time block coding for wireless communications: performance results,” *IEEE J. Select. Areas Commun.*, vol. 17, no. 3, pp. 451-460, Mar. 1999

[15] D. Qiao, S. Choi, and K. G. Shin, “Goodput Analysis and Link Adaptation for IEEE 802.11a Wireless LANs,” *IEEE Trans. Mobile Comp.*, vol. 1, no. 4, 2002, pp. 278 – 92.

[16] P. Ferre, A. Doufexi, A. Nix, D. Bull, “Throughput Analysis of IEEE 802.11 and IEEE 802.11e MAC,” *WCNC*, 2004.

[17] H. Sampath, S. Talwar, J. Tellado, V. Erceg and A. Paulraj, “A fourth-generation MIMO-OFDM broadband wireless systems: design, performance, and field trial results,” *IEEE Communications Magazine*, vol. 40, no. 9, pp. 143-149, Sep. 2002.

[18] N. Al-Dhahir, C. Fragouli, A. Stamoulis, W. Younis, and R. Calderbank, “Space-time processing for broadband wireless access,” *IEEE Communications Magazine*, vol. 40, no. 9, pp. 136-142, Sep. 2002.

[19] T. H. Liew and L. Hanzo, “Space-time block coded adaptive modulation aided OFDM,” *IEEE GLOBECOM*, vol. l, pp. 136-140, Nov. 2001.

[20] D. Gesbert, L. Haumonte, H. Bölcskei, R. Krishnamoorthy, A J. Paulraj, “Technologies and performance for non-line-of-sight broadband wireless access networks,” *IEEE Communications Magazine*, vol. 40, no. 4, pp. 86-95, Apr. 2002.

[21] A. F. Naguib, N. Seshadri, A. R. Calderbank, ”Increasing data rate over wireless channels,” *IEEE Signal Processing Magazine*, vol. 17, no. 3, pp. 76-92, May 2000.

[22] A. N. Barreto, “Antenna transmit diversity for wireless OFDM systems,” *IEEE VTC 2002-Spring*, vol. 2, pp. 757-761, May 2002.

[23] A. J. Paulraj and C. B. Papadias, “Space-time processing for wireless communications,” *IEEE Signal Processing Magazine*, vol. 14, pp. 49-83, Nov. 1997.

[24] Helmut Bölcskei, A. J. Paulraj, et al, “Fixed broadband wireless access: state of the art, challenges, and future directions,” *IEEE Communication Magazine*, vol. 39, no. 1, pp. 100-108, Jan. 2001.

[25] D. Dardari, “Ordered Subcarrier Selection Algorithm for OFDM-Based High-Speed WLANs,” *IEEE Trans. Wireless Commu.*, vol. 3, no. 5, pp. 1452-1458, Sep. 2004.

[26] Q. Liu, S. Zhou, G. B. Giannakis, “Cross-Layer Combining of Adaptive Modulation and Coding with Truncated ARQ over Wireless Links,” *IEEE Trans. Wireless Commun.*, vol. 3, pp. 1746 – 1755, Sept. 2004.

[27] J. Campello De Souza, “Discrete bit loading for multicarrier modulation systems,” PhD. Dissertation, Stanford University, 1999.

[28] V. Erceg, L. Schumacher, P. Kyristsi, “IEEE 802.11 Wireless LANs TGn Channel Models,” *IEEE 802.11-03/940r4*, May, 2004.

[29] B. Bangerter, E. Jacobsen, M. Ho, A. Stephens, “High Throughput Wireless LAN Air Interface,” *Intel Technology Journal*, vol. 7, Aug., 2003.

[30] P. Lettieri, M. B. Srivastava, “Adaptive Frame Length Control for Improving Wireless Link Throughput, Range, and Energy Efficiency,” *IEEE,* 1998.

[31] J. Yin, X. Wang and D. P. Agrawal, “Optimal Packet Size in Error-prone Channel for IEEE 802.11 Distributed Coordination Function,” *Wireless Communications and Networking Conference*, vol.3, pp.1654 – 1659, March, 2004.

[32] M. van der Schaar, S. Krishnamachari, Sunghyun Choi, Xiaofeng Xu, “Adaptive cross-layer protection strategies for robust scalable video transmission over 802.11 WLANs,” *IEEE Journal on Selected Areas in Communications,* vol. 21, NO.10, pp. 1752-1763, Dec. 2003.

[33] V. Erceg, P. Soma, D. S. Baum, and A. J. Paulraj, “Capacity obtained from multiple-input multiple-output channel measurements in fixed wireless environments at 2.5 GHz,” *Communications, ICC 2002. IEEE International Conference on*, vol. 1, pp. 396-400, May 2002.

[34] I. E. Telatar, "Capacity of multi-antenna Gaussian channels," *European Transactions on Communications*, vol. 10, no. 6, pp. 585-595, 1999.

[35] G. G. Raleigh and J. M. Cioffi, "Spatial-temporal coding for wireless communications," *Proc. IEEE 1996 Global Communications Conference,* pp. 1809-1814, Nov. 1996.

[36] A. Alexiou, M. Haardt, "Smart Antenna Technologies for Future Wireless Systems: Trends and Challenges," IEEE Commun. *Magazine*, 2004.

[37] F. R. Farrokhi, G. J. Foschini, A. Lozano, and R. A. Valenzuela, "Link-optimal space-time processing with multiple transmit and receive antennas," *IEEE Commun. Letters*, vol. 5, no. 3, March 2001.

[38] F. R. Farrokhi, G. J. Foschini, A. Lozano, and R. A. Valenzuela, "Link-optimal BLAST processing with multiple-access interference," in *VTC'2000*, Boston, MA, 2000.

[39] X. Li, H. Huang, G. J. Foschini, and R. A. Valenzuela, "Effects of iterative detection and decoding on the performance of BLAST," *IEEE GLOBECOM*, vol. 2, pp. 1061-1066, 2000.

[40] E. Biglieri, G. Taricco and A. Tulino, "Decoding space-time codes with BLAST architectures," *IEEE Trans. Signal Processing*, vol. 50, no. 10, pp. 2547-2552, Oct. 2002.

[41] Siavash M. Alamouti, "A simple transmitter diversity technique for wireless communications," *IEEE J. Select. Areas Commun.*, vol. 16, no. 8, pp. 1451-1458, Oct. 1998.

[42] V. Tarokh, N. Seshadri, and A. R. Calderbank, "Space-time codes for high data rate wireless communication: performance analysis and code construction," *IEEE Trans. Inform. Theory*, vol. 44, no. 2, pp. 744-765, Mar. 1998.

[43] V. Tarokh, H. Jafarkhani, and A. R. Calderbank, "Space-time block codes from orthogonal designs," *IEEE Trans. Inform. Theory*, vol. 45, no. 5, pp. 1456-1467, July 1999.

[44] V. Tarokh, H. Jafarkhani, and A. R. Calderbank, "Space-time block coding for wireless communications: performance results," *IEEE J. Select. Areas Commun.*, vol. 17, no. 3, pp. 451-460, Mar. 1999.

[45] D. Gesbert, H. Bölcskei, D. A. Gore, and A. Paulraj, "Outdoor MIMO Wireless Channels: Models and Performance Prediction," *IEEE Trans. on Comm.*, vol. 50,

no. 12, Dece. 2002.

[46] H. Zhang, “The capacity and error probability analysis for high data rate IEEE 802.11 handbook: A designer’s companion,” New York: *IEEE Press*, 1999.

[47] S. Sandhu and A. Paulraj, “Space-time block codes: A capacity perspective,” *IEEE Commun. Letters*. Vol. 4, no. 12, pp.384-386, Dec, 2000.

[48] Spatial Channel Model AHG, “Spatial channel model text description,” Tech. Rep. (File No: SCM-095-SCM Text v2.1b), 3GPP & 3GPP2, Jan. 2003.

[49] P. W. Wolniansky, G. J. Foschini, G. D. Golden, and R. A. Valenzuela, “V-BLAST: an 1rchitecture for realizing very high data rates over the rich-scattering wireless channel,” *URSI International Symposium*, pp. 295-300, 29 Sep. -2 Oct. 1998.

[50] L. Schumacher “WLAN MIMO Channel Matlab program,” download information: http://www.info.fundp.ac.be/~lsc/Research/IEEE_80211_HTSG_CMSC/distribution_terms.html